Universidad del Valle

Bosonización en un sistema de bosones reticulares de espín-1 fuertemente interactuantes

Bosonization in a strongly interacting spin-1 lattice boson system

Presentado por
Felipe Reyes Osorio

Dirigido por
Dr. rer. Nat Karem Rodríguez Ramírez

Facultad de Ciencias Naturales y Exactas
Departamento de Física

2022

Resumen

Desarrollos teóricos y experimentales en el siglo XX han llevado a la realización experimental del condensado de Bose-Einstein, lo cual ha sido un importante logro dentro del área de la materia condensada. A partir de ahí, en el siglo XXI su estudio se ha expandido al de sistemas de muchos cuerpos desde supernovas hasta ultra bajas energías, como lo es el análisis de gases cuánticos sujetos a redes ópticas. Más aún, el alto grado de control que proporcionan las técnicas experimentales de átomos ultra-fríos ha traído a los sistemas unidimensionales a la realidad experimental. En una dimensión, las fluctuaciones tienden a ser colectivas y a propagarse a través de largas distancias debido a la inevitabilidad de las colisiones. Por ende, se han desarrollado teorías que se valen de esto para lograr describir estos sistemas. En el presente trabajo derivamos pedagógicamente el formalismo de la bosonización, y lo aplicamos a un gas bosónico unidimensional de espín-1 sujeto a una red óptica. Calculamos el espectro del sistema a bajas energías para mostrar la existencia de una transición de fase entre el superfluido y el aislante de Mott. Enfocándonos en este último, consideramos a la energía cinética como una perturbación para formular el modelo bilineal-bicuadrático de Heisenberg que describe al aislante. Discutimos aspectos generales de la física de espín-1, proponemos varios hamiltonianos efectivos con los que describimos diferentes sectores del espacio de fases y determinamos las transiciones entre los mismos.

Palabras claves: átomos ultrafríos, bosonización, cuadrupolo, espín-1, fases magnéticas

Abstract

Developements throughout the XX century have led to the experimental observation of a Bose-Einstein condensate, which constitutes an important achievement within condensed matter physics. This has sparked the expansion of the area into the study of many body systems ranging from supernovas to ultra low energies, such as quantum gases subjected to optical lattices. Moreover, the fine control permitted by these ultracold atomic techniques has made one-dimensional systems an experimental reality. In one dimension, the inevitability of collisions leads to collective fluctuations that propagate for long distances. As such, analytical approaches that exploit this collectivity have been developed. In the present body of work, we pedagogically review and derive one of these formalisms, bosonization, and apply it to a gas of spin-1 bosons subject to an optical lattice. We retrieve the low-energy spectrum of the system and show the existence of a phase transition between the gapless superfluid and the gapped Mott insulator. Focusing on the latter, we treat the kinetic energy as a perturbation to formulate the bilinear-biquadratic Heisenberg model to describe the Mott insulator phase. Then, after discussing the general and fundamental aspects of spin-1 physics, we propose different effective Hamiltonians that stem from the Heisenberg chain in order to describe through bosonization different areas of phase space and determine the transitions between them.

Agradecimientos

Durante el desarrollo de mi trabajo de grado aprendí mucha física, y, gradualmente, buenos hábitos de investigación. Pero más que nada, fortalecí una lección que fui aprendiendo a lo largo de la carrera: ningún logro se obtiene solo, menos aún un proyecto largo y envolvente como este. Estoy en deuda con muchas personas que de múltiples maneras hicieron esto posible. Primero, quiero agradecer a mis padres por mostrarme el valor del conocimiento desde pequeño. A mi mamá, quien me mostró que las grandes cosas se logran con esfuerzo y dedicación, le debo muchas oportunidades que me llenaron de confianza para emprender la carrera. A María Camila Salamanca, gracias por el apoyo y la comprensión durante este trabajo, y por alegrarme en los momentos difíciles. Gracias a toda mi familia, quienes me han acompañado en mi proceso educativo; en particular gracias a mi abuelita y a mi tío por su entusiasmo, interés, y apoyo en mis estudios. Agradezco también a Valentina Restrepo por su duradera amistad, y al Prof. Andrés Lara, ya que sin su motivación quizás habría entrado a otra carrera, perdiéndome de lo apasionante de la física.

Agradezco a la Prof. Karem Rodríguez, por darme la oportunidad de entrar a la investigación, por su dedicada ayuda y supervisión durante el proyecto, por los consejos, y por la confianza puesta en mí. Agradezco a mis amigos y compañeros de grupo, Jalil Varela y Diego Velasco por las discusiones y colaboración durante este último año. También agradezco a todos los amigos que hice durante la carrera por los buenos tiempos, y a los que terminaron conmigo por vivir esta etapa de investigación juntos. Gracias también a todos los profesores que me dieron clase los últimos 5 años por su dedicación y conocimiento.

Es imposible no mencionar los cuatro meses del proyecto que invertí en la pasantía de investigación de la Universidad de Delaware (UD). Allí reforcé la tenacidad y perseverancia que requiere un buen proyecto de investigación. Agradezco al Prof. Branislav Nikolic, por dirigir mi investigación en UD y por importantes lecciones. Agradezco a mis compañeros de grupo en UD, Akshat Mishra y Abhin Suresh, por compartir la experiencia conmigo y por la ayuda brindada. A Sasiri Vargas y a Jalil, amigos y compañeros de carrera, gracias por la ayuda al llegar a Newark y por el tiempo que pasamos juntos en EE. UU. También agradezco a todos los amigos que hice en la pasantía, una genial generación de jóvenes científicos colombianos cuya amistad valoro mucho. Mi estadía en UD fue financiada mayormente por la Fundación Nacional de Ciencia (NSF) de EE. UU. y parcialmente por la Universidad del Valle, a través de la subvención NSF No. ECCS 1922689 y el proyecto interno Cl. 71270, otorgados al Prof. Nikolic y la Prof. Rodríguez respectivamente.

Agradezco al Ministerio de Educación Nacional por el premio Andrés Bello a los mejores puntajes en las Pruebas Saber 11 realizadas en el 2016, cuya correspondiente beca cubrió los gastos de matrícula durante los semestres 2 a 10 de mi carrera, junto con un estipendio semestral. Finalmente, le doy las gracias a la Universidad del Valle, la cuál llevo en el corazón, por todas las experiencias, enseñanzas, y logros que me permitió; por la excelente educación a la cuál me dio acceso; y por financiar mayoritariamente la investigación de mi proyecto de grado a través del proyecto interno Cl. 71270.

Publications

The following is a list of publications and writings produced during the developement of this project:

- F. Reyes Osorio and K. Rodríguez Ramirez,"Deducing the phase transitions of interacting spin-1 bosons through bosonization," Under developement (2022)
- F. Reyes Osorio, J. Varela Manjarrés, D. L. Velasco Gonzalez, S. Figueroa Manrique, and K. Rodríguez Ramirez, "Ultracold spin-1 systems: a constructive approach from the fundamentals," Under developement (2022)

[1] F. Reyes Osorio and B. K. Nikolić, *Wide ferromagnetic domain walls can host both adiabatic reflectionless spin transport and finite nonadiabatic spin torque: a time-dependent quantum transport picture*, 2021, arXiv:`2112.08356 [cond-mat.mes-hall]` Submitted and in peer review at Phys. Rev. B

Other publications by the author:

[2] F. Reyes Osorio, J. M. Scarpetta Ramirez, and K. Rodriguez Ramirez, "Computational relaxation method for modeling electrostatic systems with non-trivial geometries," European Journal of Physics **41**, 025201 (2020)

Contents

1 Introduction

At the turn of the 20th century, quantum mechanics redefined the way we looked at the physical world. The continuum became discrete, first for light and soon for atoms and their energy levels. A rich new scale of reality unfolded in front of physicist's eyes, and allowed for the formal description of phenomena old and new; from magnetism to waves of matter, the success of quantum mechanics as a theory only grew as the years and decades passed. However, as is often the case in the modern day, theory advanced faster than technology, and many astounding predictions were left in the waiting room for the next landmark experiment to confirm or disprove them. This is a consequence of the extreme conditions required for the manifestation of the quantum properties of matter; only the very small and the very cold exhibits the surprising qualities described so well by quantum mechanics, and observing these systems proved to be a great challenge.

At the turn of the 21st century, physicists were finally able to achieve these extreme temperatures, building upon decades of experimental developement and effort, and allowing the direct observation of the quantum world. One of the most impressive leaps, which served as the seed for a new field of research, is undoubtedly the confirmation of one of quantum mechanic's oldest predictions: the Bose-Einstein condensate [4, 5]. Due to the indistiguishability of particles, one must consider different statistics when dealing with many-body quantum systems. In the case of particles symmetric under permutations, denominated bosons [6], statistics dictate that below a critical temperature all particles fall to the ground state [7], allowing the system to behave as a macroscopic body obeying quantum mechanics [8]. For most atomic gases, the critical temperature is of the order of nanokelvin, millions of times colder than interstellar space. The existence of the condensate remained a theoretical prediction from 1924 to 1995, when Cornell and Wiemann, and Ketterle [4, 5] independently realized it in the lab, winning the 2001 Nobel prize for their efforts. Their achievement was possible thanks to the developement of innovative laser cooling techniques [9–11], which were themselves subject of the 1997 Nobel prize. Illuminating the bosonic gas with wavelengths tuned to the natural frequency of the atoms, these lose momentum and energy to exothermic spontaneus emmissions, lowering the temperature in the process [12]. Once this is done, atoms that remain excited are removed through magnetic evaporation [13], causing the remaining particles to drop below the critical temperature. At this point, the Bose-Einstein condensate is reached, and it exhibits exotic properties, such as superfluidity [14, 15] and abnormally high refraction indeces [16, 17].

The technology and experimental skill that was needed for the realization of the condensate developed alongside other similar techniques for atomic control. Among those, optical lattices [18, 19] stand out for their surprising nature, and wide range of applications [20, 21]. In an optical lattice, counter-propagating lasers form standing waves of light which can be superposed to form grid-like patterns. Then, ultracold gases achieved with methods like the ones mentioned for the Bose-Einstein condensate can be suspended on top of the beams of light and finely controlled and tuned [22]. This phenomenon, which borders on science ficition, can be explained with a simple semiclassical model of the atom [23]. Consider an alkali nucleus with a single valence electron susceptible to external fields: when shined upon with a laser beam, the electron can be seen as a forced harmonic oscillator, moving according to $x(\mathbf{r},t) = \alpha E \cos(\omega t - \mathbf{k}\cdot\mathbf{r})$, where $x(\mathbf{r},t)$ is the spatially-dependent position of the electron with respect to the nucleus, ω is the frequency of the laser, E is the amplitude of the field, and α is the resonance factor given by

$$|\alpha| \propto \frac{1}{\sqrt{\left(\omega_0^2 - \omega^2\right)^2 + \omega^2\Gamma^2}}, \tag{1.1}$$

where ω_0 is the natural frequency of the atom, and Γ is a damping factor. The oscillating movement of the electron induces an electric dipole $\mu = ex(\mathbf{r},t)$ in the atom, and has a phase ϕ given by

$$\tan\phi = \frac{\Gamma\omega}{\omega_0^2 - \omega^2}. \tag{1.2}$$

Without loss of generality, let us consider red-detuned light, that is, a laser with a frequency below the natural one of the atom; in this case, the dipole is in phase with the field. Moreover, the induced dipole is still free to interact with the field, being subject to a force $\mathbf{F} = \frac{1}{2}\nabla(\mu E)$, or an equivalent averaged-over-time potential

$$U \propto -\alpha E^2 \cos^2(\mathbf{k}\cdot\mathbf{r}). \tag{1.3}$$

We have retrieved the periodic potential proportional to the intensity profile $I = |\mathbf{E}(\mathbf{r})|^2$ that is the basic building block of an optical lattice. The polarized atom is attracted to the maxima of the intensity as shown in Fig. 1.1(b). In the complementary case of blue-detuned light, the dipole is out of phase with the laser, which changes the sign of the potential, and thus attracts the atoms to the minima of I.

The fine control provided by optical lattices allows for quantum simulation [24], a concept that originates with Feynman [25] and considers exploring and understanding quantum systems through the realization and study of other, different but equivalent ones [26]. For instance, by analyzing ultracold gases in a deep optical lattice so that each atom is confined to the lowest energy level of a site, the Hubbard model can be flawlessly rendered on a grid thousands of times larger than conventional crystals [22]. Thus, the phenomena that occurs at and below the

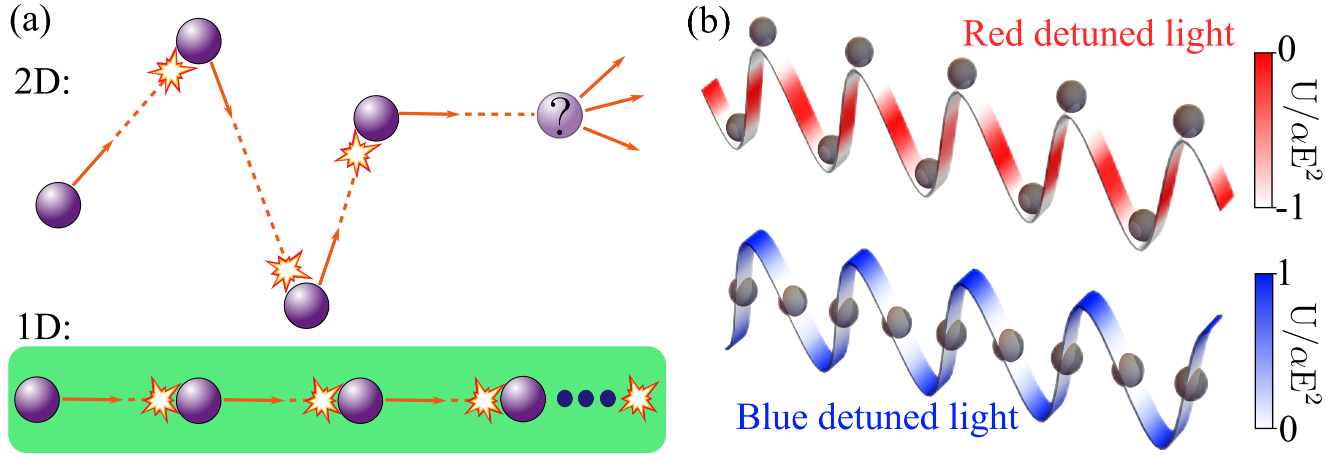

Figure 1.1: (a) Cartoon showing how in one dimension, particles have no choice but to collide with their neighbors, causing fluctuations to easily propagate across the system over long distances. In higher dimensions, this is not the case and particles can travel a long distance without interacting along the way, leading to a dissipation of fluctuations. (b) Schematic diagram of the optical potential of red (blue) detuned light. Since the potential follows the intensity profile, the particles find stable minima at the nodes (antinodes) of the light.

nanoscale in real materials can be observed in bigger, impurity-free, tunable lattices. In particular, the empirical observation of the superfluid-Mott insulator phase transition represents a landmark triumph of quantum simulation and optical lattices [24]. Since then, the ability of fine-tuning lattice and interaction parameters has spurred research on the phase space of spinor systems [27], the simulation of complex geometries and models [28, 29], and even the development of ever more accurate clocks [20].

Optical lattices also allow for the experimental realization of one-dimensional systems [30], which had been previously reduced to theorist's playthings due to their simplicity, and disposition for closed solutions [31]. Now, direct observations confirm decades-old predictions [32], and open the door to reinvigorated research in multiple areas of theoretical physics, such as quantum magnetism [33], conformal field theory [34], and integrable systems [31].

One-dimensional systems exhibit a range of interesting properties, due in large part to the strong correlations that stem from the repulsive interactions between particles. As opposed to higher dimensions where particles can easily avoid each other, a one-dimensional body has no choice but to eventually collide with it's neighbors. These, in turn, bump into their neighbors and so on, leading to perturbations propagating for long distances [35, 36], as shown schematically in Fig. 1.1(a). These perturbations are clearly collective in nature, leading to global excitations that can be identified as quasi-particles at low energies. The first objective of this work is to include the simplest internal degree of freedom available for bosons, spin 1, and study its low-energy behavior in one dimension. Furthermore, the emergence of quasi-particles leads to an interesting theoretical approach known as bosonization [37]. It consists of formulating an effective field theory in terms of the collective excitations to describe the low-energy behavior of the system [38]. Therefore, the second objective of this work is to understand the bosonization formalism, while the third objective is to apply it to a system of one-dimensional spin-1 bosons on an optical lattice in order to extract physical information from the magnetic phases that unfold. This has been studied in the past with other methods [39], so we will lean on the rich literature to conduct our analysis. Our approach, however, intends to obtain analytical results that employ the least amount of approximations, in contrast to similar mean-field treatments.

The bosonization procedure is a powerful tool for dealing with a wide range of systems, from high energy physics [40] to condensed matter [41–43], and has strong connections to advanced topics in theoretical physics [44]. Unfortunately, the existing literature is dense and can appear impenetrable to a would-be interested learner. It is our intention for this work to serve as a pedagogical review of bosonization that is accessible to beginners, guiding them through the mathematical and physical framework up to where the technique meets more advanced theories. Thus, we hope that by the end of this work, the reader is not only capable to understand the literature, but is ready to pursue further interesting topics that are natural continuations of bosonization.

This work is organized as follows: in Chs. 2 and 3 we introduce bosonization through a pedagogical and historical example of free and interacting fermions, before applying the built theoretical framework to two toy models that are relevant to the main physical system of interest, that is, one-dimensional spin 1 bosons. This is studied in Ch. 4, where we formulate Hamiltonians that capture general and particular features of spin 1 systems and apply bosonization to study the different phases that emerge, emphasizing the physical aspects of the analysis. Finally, in Ch. 5 we give general conclusions of our work, while discussing perspectives regarding advanced topics that can be built upon our methods and results.

2
Bosonization

To begin, we explore a well-known system whose solution is straightforward to obtain using elementary methods of many-body quantum mechanics: the free fermion gas in one dimension. We will then include interactions, to show how this normally complicated addition can be easily dealt with. However, rather than limmiting ourselves to showing the solution using bosonization, we take care to transform and reformulate the system methodically. This way, every step is connected to the previous in a more-or-less intuitive manner, avoiding large leaps that presupose a more advanced understanding, as is often found in the literature on this topic. The result of our process will reveal a large portion of the underlying formalism, and yield a powerful result that makes succesive applications of bosonization much more streamlined.

2.1 Free fermions

Consider a system of a single species of free one-dimensional fermions with Hamiltonian

$$\hat{H}_0 = \sum_k \frac{k^2}{2m} \hat{c}^\dagger(k)\hat{c}(k). \tag{2.1}$$

We refer to this system as the *real* system, since it is the objective of our present study. It has a quadratic energy dispersion $\epsilon(k) = k^2/2\mathrm{m}$, where k is the wavenumber and m the mass. The occupation of states is full up to the Fermi energy ϵ_F, as shown in Fig. 2.1(a), and applying Born-von Karman periodic boundary conditions [45], allowed momenta are of the form $k = 2\pi n/L$, where n is an integer and L is the length of the system. At low energies, the only contributions to the dynamics of the system come from states close to the Fermi surface [45, 46], which in 1 dimension consists of two points, $\pm k_F$. Thus, if our interests lie in the low-energy properties of the system, we can restrict our scope to small intervals of size Λ arround $\pm k_F$. Every state within can be approximately taken into account by performing a Taylor expansion around the Fermi surface, so that the dispersion is

$$\epsilon(k) \approx \epsilon_F \pm (k \mp k_F)\, v_F, \tag{2.2}$$

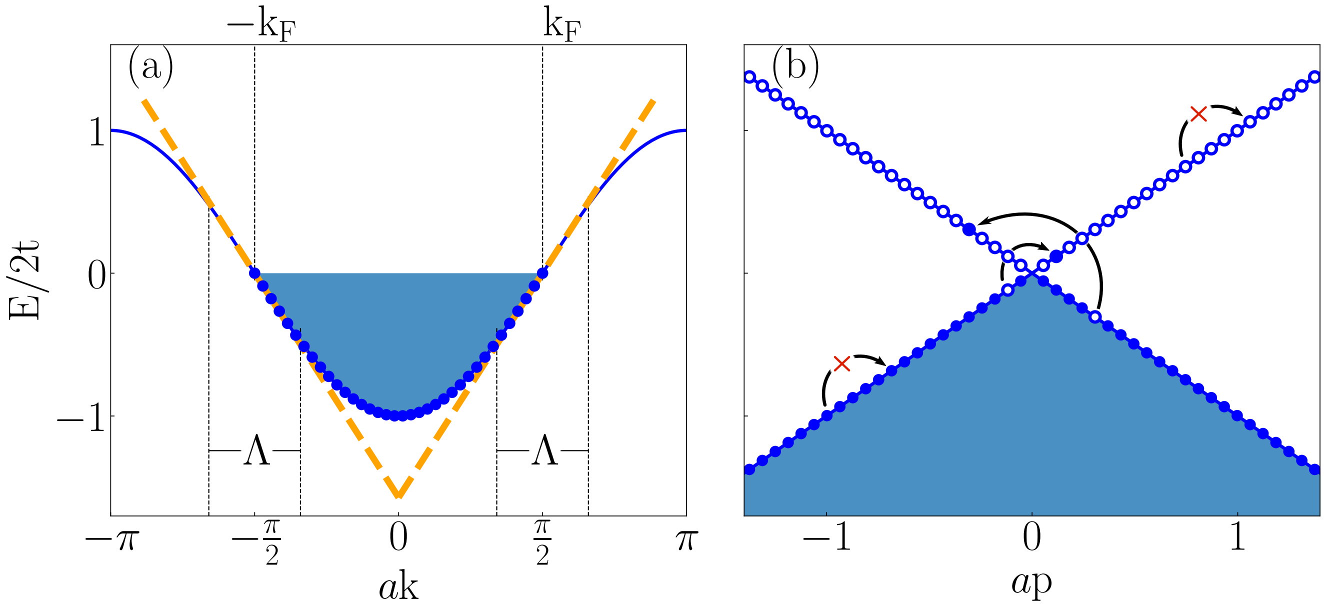

Figure 2.1: (a) Dispersion of a single species of free fermions on a lattice at half filling. Within an interval Λ around it's Fermi points $\pm k_F$ it resembles a system of two species with linear dispersion. (b) Linearized system, where p measures momenta with respect ot the Fermi points. The arrows show allowed excitations; in the right(left) branch positive(negative) p increases the energy.

where the Fermi velocity is $v_F = \frac{\partial}{\partial k}\epsilon(k_F)$. The linearization procedure maps the real system into a new, *chiral* system with two species of linear dispersion fermions characterized by a direction, right or left. Explicitely, the map between the real fermions $\hat{c}$ and the chiral particles $\hat{\psi}_{R/L}$ is given by

$$\hat{c}(k) = \theta(k)\hat{\psi}_R(k) + \theta(-k)\hat{\psi}_L(k), \tag{2.3}$$

where $\theta(k)$ is the Heaviside step function. This map takes particles with positive momentum to the right moving branch and viceversa; essentially, its image has the simpler low-energy behavior of the real system at every scale. Thus, measurements performed on the chiral system correspond to what would be obtained for the real system as long as the low-energy condition is satisfied.

To develop the simpler chiral system, first notice that any momentum k can be expressed as

$$k = \begin{cases} k_F + p_R, & \text{if } k > 0 \\ -k_F + p_L, & \text{if } k < 0, \end{cases} \tag{2.4}$$

where $p_{R/L}$ is the displacement away from the Fermi surface. Notice right states with a positive p_R have an energy above ϵ_F, while the opposite is true for left movers. With this in mind, and the map given by Eq. 2.3, we can rewrite $\hat{H}_0$ as

$$\begin{aligned} \hat{H}_0 &= \sum_{k>0} \left(\epsilon_F + v_F \left(k - k_F\right)\right) \hat{\psi}_R^\dagger(k)\hat{\psi}_R(k) + \sum_{k<0} \left(\epsilon_F - v_F \left(k + k_F\right)\right) \hat{\psi}_L^\dagger(k)\hat{\psi}_L(k) \\ &= \sum_{p_R} v_F p_R \hat{\psi}_R^\dagger(p)\hat{\psi}_R(p) - \sum_{p_L} v_F p_L \hat{\psi}_L^\dagger(p)\hat{\psi}_L(p) + (\text{vacuum energy}), \end{aligned} \tag{2.5}$$

where $\hat{\psi}_\alpha(p) = \hat{\psi}_{R/L}(\alpha k_F + p_{R/L})$, and $\alpha = \pm 1$ to represent the right and left brach respectively. Also, in Eq. 2.5 we can drop the subscript of the p's in favor of a simpler dispersion $\alpha v_F p$ where p runs from $-\infty$ to ∞. This emphasizes the fact that while the real system and the chiral system are different at high energies, their low-energy dynamics match. Aditionally, by working with p we implicitly shift the Fermi energy to zero, as seen in Fig. 2.1(b). Disregarding the constant terms as part of the vacuum energy, we get

$$\hat{H}_0 = v_F \sum_{\alpha,p} \alpha p \hat{\psi}_\alpha^\dagger(p)\hat{\psi}_\alpha(p). \tag{2.6}$$

In the future, we will look to move away from the free system and deal with interactions. However, the momentum creation/annihilation operators in the Hamiltonian of Eq. 2.6 are not adequate to deal with interactions. Interactions are local in space, so we need a position basis for the new system. To achieve this, let us perform a Fourier series expansion in terms of the momentum operators of the real system:

$$\begin{aligned} \hat{c}(x) &= \frac{1}{\sqrt{L}} \sum_k e^{ikx} \hat{c}(k) \\ &= \frac{1}{\sqrt{L}} \sum_k e^{ikx} \Big(\theta(k)\hat{\psi}_R(k) + \theta(-k)\hat{\psi}_L(k)\Big) \\ &= \frac{1}{\sqrt{L}} \sum_p e^{ik_F x} e^{ipx} \hat{\psi}_R(k) + \frac{1}{\sqrt{L}} \sum_{p>} e^{-ik_F x} e^{ipx} \hat{\psi}_L(k) \\ &= e^{ik_F x}\hat{\psi}_R(x) + e^{-ik_F x}\hat{\psi}_L(x), \end{aligned} \tag{2.7}$$

where we have introduced new chiral position field operators,

$$\hat{\psi}_\alpha(x) = \frac{1}{\sqrt{L}} \sum_p e^{ipx} \hat{\psi}_\alpha(p). \tag{2.8}$$

Again, the summation $\sum_p$ over all p's in the third line of Eqs. 2.7 is a very good approximation as long as we stay within Λ and k_F is far from the band edges. Notice that Eq. 2.7 is equivalent to the map in Eq. 2.3.

Now that we have both bases for the new system, we can apply the Heisenberg equations of motion to calculate their time evolution. First, in momentum,

$$\hat{\psi}_\alpha(p,t) = \hat{\psi}_\alpha(p,0) e^{-\alpha i v_F p t}. \tag{2.9}$$

As expected, the operators that create particles in the eigenstates of $\hat{H}_0$ have a time dependent phase. Before moving on to the evolution of the position operators, it is useful to introduce the moving variable $x_\alpha = v_F t - \alpha x$, in terms of which

$$\hat{\psi}_\alpha(x,t) = \frac{1}{\sqrt{L}} \sum_p e^{-\alpha i p x_\alpha} \hat{\psi}_\alpha(p,0), \tag{2.10}$$

by simply plugging in Eq. 2.9 into Eq. 2.8. Now, using the Heisenberg equation and the chain rule it is straightforward to show

$$\partial_{-\alpha} \hat{\psi}_\alpha(x_\alpha) = 0, \tag{2.11}$$

where $\partial_\alpha = \partial_t / v_F - \alpha \partial_x$. This shows that the chiral position basis operators are mutually independent, and that their time evolution is tied exclusively to the corresponding x_α.

It might be tempting to rewrite the Hamiltonian of Eq. 2.6 in terms of the new position basis. In fact, the relationship between the temporal and spatial derivatives of the position operators given by Eq. 2.11 suggests the existence of a first-quantized operator $\hat{p}_\alpha$ with coordinate representation $-i\partial_x \delta(x - x')$. Consequently,

$$\hat{H}_0 = -i v_F \int \mathrm{d}x \left(\hat{\psi}_R^\dagger(x) \partial_x \hat{\psi}_R(x) - \hat{\psi}_L^\dagger(x) \partial_x \hat{\psi}_L(x) \right). \tag{2.12}$$

From the literature we recognize a form of the Dirac Hamiltonian. There is, in fact, a close relationship between our low-energy theory and Dirac's relativistic formalism, and between systems with linear dispersions in general. However, bosonization deals with collective excitations so the microscopic formulation in terms of the individual chiral position operators is not adequate for our objective. In order to rewrite $\hat{H}_0$ with proper, well defined operators that represent collective degrees of freedom, let us address a surpisingly subtle nuance of a big aspect of bosonization.

2.2 Infinities

Linearizing the dispersion relationship might be a useful tool, but it comes with a very important caveat. In the real system, the Fermi surface is determined by the total number of particles N, each of which occupies an eigenstate. When we linearize and shift our attention to the new chiral system, the Fermi surface is no longer a function of the number of particles; instead, it is set to be equal to that of its real counterpart and becomes the reference energy level. Consequently, how many particles are there in the linearized system? Let us focus on the left branch: if ϵ_F is set, then every level below it must be occupied. But it is clear that a linear dispersion has no ground state of minimal energy. Therefore, in each branch of the chiral system there are infinite particles under the Fermi surface, as shown in Fig. 2.1(b). Operators such as the total number of particles $\sum_k \hat{\psi}^\dagger(k)\hat{\psi}(k)$ are no longer well defined and convergent in terms of chiral operators.

To get around this issue, we define a new vacuum state that will act as a ground state for the chiral system. We pick $|\varnothing\rangle$ such that every state below ϵ_F in each branch is occupied. Even though there are still infinite particles, by redefining the vacuum we are now measuring finite changes with respect to $|\varnothing\rangle$, and by sticking to low energy excitations, we ensure that the infinite sea of particles (Dirac sea) of the chiral system does not alter the dynamics in a noticeable way. Finally, in order for operators to take our new vacuum into account we introduce the normal ordering [47] operation

$$:\hat{A}: = \hat{A} - \langle \hat{A} \rangle. \tag{2.13}$$

The expected value in the previous equation, and henceforth unless specified otherwise, is taken with respect to $|\varnothing\rangle$. By normal ordering an operator, we substract its expected value in the vaccum, effectively getting rid of the infinite particles and focusing only on the fluctuations around the surface.

2.3 Densities and Currents

Now that infinities have been dealt with, let us start looking at meaningful operators. We define the chiral current densities as

$$\hat{J}_\alpha = :\hat{\psi}^\dagger_\alpha(x)\hat{\psi}_\alpha(x):, \tag{2.14}$$

which are normal ordered, indicating that they measure a quantity with respect to $|\varnothing\rangle$. Although this operator looks like a particle density, we call it a current for the directionality inherited from the chiral branches. In terms of these currents, we also define

$$\hat{\rho}(x) = \hat{J}_R(x) + \hat{J}_L(x), \quad \text{and} \quad \hat{J}(x) = v_F\Big(\hat{J}_R(x) - \hat{J}_L(x)\Big), \tag{2.15}$$

which are the total density and current of the chiral system, respectively. With the Heisenberg equation of motion in Eq. 2.11 it is straightforward to show that $\hat{\rho}$ and $\hat{J}$ satisfy the conservation equations

$$\begin{aligned} \partial_t\hat{\rho} + \partial_x\hat{J} &= 0 \\ \partial_x\hat{\rho} + \frac{1}{v_F^2}\partial_t\hat{J} &= 0. \end{aligned} \tag{2.16}$$

The first equation shows regular continuity, whereas the second one implies the conservation of the individual chiral currents. The latter is valid as long as there are no interactions that can send a particle to the opposite branch.

It turns out [31] that the operators $\hat{J}^2_\alpha(x)$ are of great importance; however, composite operators on the same point have divergences, as can be seen in Eq. 2.21. These divergences are common in relativistic Dirac systems [48] and need to be regularized, using a point-splitting scheme [35, 48], which we revisit in Sec. 3.1.1. Thus, we make sense of this product as

$$\begin{aligned} \hat{J}^2_\alpha(x) &= \lim_{\epsilon\to 0}\hat{J}_\alpha(x-\epsilon)\hat{J}_\alpha(x+\epsilon) \\ &= \lim_{\epsilon\to 0} :\hat{\psi}^\dagger_\alpha(x-\epsilon)\hat{\psi}_\alpha(x-\epsilon)::\hat{\psi}^\dagger_\alpha(x+\epsilon)\hat{\psi}_\alpha(x+\epsilon): \end{aligned} \tag{2.17}$$

To calculate the product of two normal ordered operators, we use the identity

$$
\begin{aligned}
:\hat{A}\hat{A}'::\hat{B}\hat{B}': \;&=\; :\hat{A}\hat{A}'\hat{B}\hat{B}': \\
&+\; \langle\hat{A}\hat{B}\rangle :\hat{A}'\hat{B}': + \langle\hat{A}'\hat{B}'\rangle :\hat{A}\hat{B}: + \langle\hat{A}\hat{B}'\rangle :\hat{A}'\hat{B}: + \langle\hat{A}'\hat{B}\rangle :\hat{A}\hat{B}': \\
&+\; \langle\hat{A}\hat{B}\rangle\langle\hat{A}'\hat{B}'\rangle + \langle\hat{A}\hat{B}'\rangle\langle\hat{A}'\hat{B}\rangle,
\end{aligned} \tag{2.18}
$$

which is based on nested applications of Wick's theorem [47]. Therefore, we need to first determine the correlations between the chiral creation/annihilation operators, beginning with

$$
\begin{aligned}
\left\langle \hat{\psi}^\dagger_\alpha(p)\hat{\psi}_\alpha(p')\right\rangle &= \theta(-\alpha p)\delta_{pp'} \\
\left\langle \hat{\psi}_\alpha(p)\hat{\psi}^\dagger_\alpha(p')\right\rangle &= \theta(\alpha p)\delta_{pp'},
\end{aligned} \tag{2.19}
$$

which is evident from the fact that, in the branch α, only particles with $\alpha p < 0$ can be annihilated from the vacuum, as shown in Fig. 2.1(b). Next, the correlations in the position basis are given by

$$
\begin{aligned}
\left\langle \hat{\psi}^\dagger_\alpha(x)\,\hat{\psi}_\alpha(y)\right\rangle &= \frac{1}{L}\sum_{pp'} e^{-ipx}e^{ipy}\left\langle \hat{\psi}^\dagger_\alpha(p)\hat{\psi}_\alpha(p')\right\rangle \\
&= \frac{1}{L}\sum_{p} e^{-ip(x-y)}\theta(-\alpha p) \\
&= \frac{1}{2\pi}\int \mathrm{d}p\, e^{-ip(x-y)}\theta(-\alpha p),
\end{aligned} \tag{2.20}
$$

where in the last line we applied the continuum limit $\sum_p \to (L/2\pi)\int \mathrm{d}p$. This is the Fourier transform of the step function [49], yielding

$$
\left\langle \hat{\psi}^\dagger_\alpha(x)\,\hat{\psi}_\alpha(y)\right\rangle = \frac{1}{2}\delta(x-y) + \frac{\alpha i}{x-y}, \tag{2.21}
$$

$$
\left\langle \hat{\psi}^\dagger_\alpha(x)\,\hat{\psi}_\alpha(y)\right\rangle = -\left\langle \hat{\psi}_\alpha(y)\,\hat{\psi}^\dagger_\alpha(x)\right\rangle. \tag{2.22}
$$

Notice that these correlations satisfy the fermionic anticommutation relations. With all this, we can finally calculate $\hat{J}^2_\alpha(x)$: the first line of the identity in Eq. 2.18 is negligible to first order, while the last can be lumped in with the vacuum energy. Plugging in the correlations of Eq. 2.21 we get

$$
\begin{aligned}
\hat{J}^2_\alpha(x): &= \frac{-\alpha i}{2\pi 2\epsilon}\Big(:\hat{\psi}_\alpha(x-\epsilon)\hat{\psi}^\dagger_\alpha(x+\epsilon): + :\hat{\psi}^\dagger_\alpha(x-\epsilon)\hat{\psi}_\alpha(x+\epsilon):\Big) \\
&= \frac{-\alpha i}{2\pi}\left(:\hat{\psi}^\dagger_\alpha(x-\epsilon)\left(\frac{\hat{\psi}_\alpha(x+\epsilon)-\hat{\psi}_\alpha(x-\epsilon)}{2\epsilon}\right): -\mathrm{h.c}\right) \\
&= \frac{-\alpha i}{2\pi}\Big(:\hat{\psi}^\dagger_\alpha(x)\partial_x\hat{\psi}_\alpha(x): -\mathrm{h.c}\Big).
\end{aligned} \tag{2.23}
$$

This expression is suspiciously akin to the Dirac Hamiltonian of Eq. 2.12, suggesting that the Hamiltonian in the position basis should be

$$\hat{H}_0 = \pi v_F \int \mathrm{d}x \left(\hat{J}_R^2(x) + \hat{J}_L^2(x)\right). \tag{2.24}$$

This Hamiltonian corresponds to a symmetrized form of the Dirac Hamiltonian, and shows us, not only the correct formulation for our new system, but also that the currents are the appropriate operators for it. In fact, Hamiltonians that are quadratic in conserved currents are a staple of more general and advanced methods of bosonization, like non-Abelian bosonization [38].

Finally, although Eq. 2.21 is correct, there is a divergence when $x = y$. Therefore, it will be useful to introduce a smooth cutoff that regularizes the infinity and ensures that we stay within the small momentum interval Λ by eliminating the high energy contributions that cause this divergence in the first place. With this in mind, we get

$$\left\langle \hat{\psi}_\alpha^\dagger(x)\, \hat{\psi}_\alpha(y) \right\rangle = \frac{1}{2\pi} \int \mathrm{d}p\, e^{-\delta|p|} e^{-ip(x-y)} \theta(-\alpha p), \tag{2.25}$$

where δ is the cutoff length. This recurring integral, denominated $\mathcal{I}_{-\alpha}$, is calculated in Eq. A.1, yielding

$$\left\langle \hat{\psi}_\alpha^\dagger(x)\, \hat{\psi}_\alpha(y) \right\rangle = \frac{\alpha i}{2\pi((x-y) + i\alpha\delta)}, \tag{2.26}$$

and the relations of Eq. 2.22 still hold.

2.4 Bosonic fluctuations

The chiral currents provide an appropriate formulation for the chiral system. However, this is not the end of the road, for we now need their reciprocal space counterparts. We get these by expanding in a Fourier series, yielding

$$\begin{aligned} \hat{J}_\alpha(p) &= \frac{1}{\sqrt{L}} \sum_q :\hat{\psi}_\alpha^\dagger(q - \alpha p) \hat{\psi}_\alpha(q):, \\ \hat{J}_\alpha^\dagger(p) &= \hat{J}_\alpha(-p). \end{aligned} \tag{2.27}$$

We see that the Fourier components of the chiral currents are operators that create and annihilate a superposition of particle-hole excitations, which collectively can be thought of as a fluctuation of momentum p. In the previous expression, we are adopting a convention which makes $\hat{J}_\alpha^\dagger(p)$ create a fluctuation for $p > 0$. Hence, the current densities according to this convention are

$$\hat{J}_\alpha(x) = \frac{1}{\sqrt{L}} \sum e^{\alpha i p x} \hat{J}_\alpha(p). \tag{2.28}$$

Now consider the commutator

$$\begin{aligned}\left[\hat{J}_\alpha(p), \hat{J}_\alpha^\dagger(p)\right] &= \frac{1}{L}\sum_{q,q'}\left[\hat{\psi}_\alpha^\dagger(q-\alpha p)\hat{\psi}_\alpha(q), \hat{\psi}_\alpha^\dagger(q'-\alpha p)\hat{\psi}_\alpha(q')\right] \\ &= \frac{1}{L}\sum_{q}\hat{\psi}_\alpha^\dagger(q-\alpha p)\hat{\psi}_\alpha(q-\alpha p) - \hat{\psi}_\alpha^\dagger(q)\hat{\psi}_\alpha(q),\end{aligned} \tag{2.29}$$

where in the last line we used standard algebraic identities. Normally, those two terms would cancel out after relabeling the indices, but since in the chiral system they represent infinite quantities, we must proceed with caution and replace the operators with their normal ordered counterpart as such:

$$\begin{aligned}\left[\hat{J}_\alpha(p), \hat{J}_\alpha^\dagger(p)\right] &= \frac{1}{L}\sum_{q} :\hat{\psi}_\alpha^\dagger(q-\alpha p)\hat{\psi}_\alpha(q-\alpha p): - :\hat{\psi}_\alpha^\dagger(q)\hat{\psi}_\alpha(q): \\ &+ \left\langle\hat{\psi}_\alpha^\dagger(q-\alpha p)\hat{\psi}_\alpha(q-\alpha p)\right\rangle - \left\langle\hat{\psi}_\alpha^\dagger(q)\hat{\psi}_\alpha(q)\right\rangle \\ &= \frac{1}{L}\sum_{q}\theta(p-\alpha q) - \theta(-\alpha q) \\ &= \frac{p}{2\pi}.\end{aligned} \tag{2.30}$$

In the first line, the normal ordered terms are finite, so the indices can be relabeled and the terms canceled without issue. Then, notice that the correlations in the third line would have vanished had we started with the commutator of diferent wavenumbers, say p and p'. Finally, the result of the last line is retrieved after switching the summation for an integral. By inspecting the allowed excitations shown in Fig. 2.1(b), further shown schematically in Fig. 2.3, it can be seen that only some terms in the summation of Eq. 2.30 are different than zero.

With these commutation relations in mind, we can define the following rescaled operators:

$$\hat{b}(p) = A\Big(\hat{J}_R(p)\theta(p) \pm \hat{J}_L(-p)\theta(-p)\Big), \tag{2.31}$$

where A is a complex number allowing us to arbitrarily set a global phase, as well as a relative phase indicated by the $\pm$. A convenient choice is

$$\begin{aligned}\hat{b}(p) &= -i\sqrt{\frac{2\pi}{|p|}}\Big(\hat{J}_R(p)\theta(p) - \hat{J}_L(-p)\theta(-p)\Big), \\ \hat{b}^\dagger(p) &= i\sqrt{\frac{2\pi}{|p|}}\Big(\hat{J}_R^\dagger(p)\theta(p) - \hat{J}_L^\dagger(-p)\theta(-p)\Big),\end{aligned} \tag{2.32}$$

although regardless of the decision, these operators satisfy $[\hat{b}(p), \hat{b}^\dagger(q)] = \delta_{pq}$. The inverses of these relationships are

$$\begin{aligned}\hat{J}_R(p) &= i\sqrt{\frac{|p|}{2\pi}}\Big(\theta(p)\hat{b}_p - \theta(-p)\hat{b}^\dagger_{-p}\Big), \\ \hat{J}_L(p) &= -i\sqrt{\frac{|p|}{2\pi}}\Big(\theta(p)\hat{b}_{-p} - \theta(-p)\hat{b}^\dagger_{p}\Big).\end{aligned} \tag{2.33}$$

What do these new operators do? According to our convention, $\hat{b}^\dagger(p)$ creates a fluctuation of momentum $|p|$ in the R branch if $p > 0$ or in the L branch if $p < 0$. Remarkably, this results shows that the collective excitations of the chiral system are bosonic, which means that this is also true at low energies in the real system. In fact, we can show this correspondence with the real system by calculating the spectral function of the chiral system:

$$\begin{aligned}A(q,\omega) &= \int \mathrm{d}t\,\mathrm{d}x\, e^{i(\omega t - qx)} \left\langle \hat{J}_\alpha(x_\alpha)\hat{J}_\alpha(0)\right\rangle \\ &= \int \mathrm{d}t\,\mathrm{d}x\, e^{i(\omega t - qx)} \left\langle \hat{\psi}^\dagger_\alpha(x_\alpha)\hat{\psi}_\alpha(0)\right\rangle \left\langle \hat{\psi}_\alpha(x_\alpha)\hat{\psi}^\dagger(0)\right\rangle,\end{aligned} \tag{2.34}$$

where in the second line we used the nested Wick's theorem of Eq. 2.18, remembering that the expected value of normal ordered operators vanishes. To avoid divergences, we use the correlations with cutoff of Eq. 2.26 while taking into account the time evolution, yielding

$$\begin{aligned}A(q,\omega) &= \frac{-1}{4\pi^2}\int \mathrm{d}t\,\mathrm{d}x\, e^{i(\omega t - qx)} \frac{1}{(x_\alpha - i\delta)^2} \\ &= \frac{1}{4\pi^2}\int \mathrm{d}t\,\mathrm{d}x\, e^{i(\omega t - qx)} \partial_\alpha\Big(\frac{1}{x_\alpha - i\delta}\Big).\end{aligned} \tag{2.35}$$

Remembering the definition that $x_\alpha = v_F t - \alpha x$, we can calulate the integral and find that

$$A(q,\omega) \propto \delta(\omega - \alpha v_F q), \tag{2.36}$$

which corresponds to the low energy spectrum of the real system [35, 36, 50].

We have finally reformulated the fermionic system in terms of its bosonic fluctuations; all that remains is plugging the inverse relations of Eq. 2.33 into the Hamiltonian of Eq. 2.24, bringing us to

$$\begin{aligned}\hat{H}_0 &= \pi v_F \sum \Big(\hat{J}_R(p)\hat{J}_R(-p) + \hat{J}_L(p)\hat{J}_L(-p)\Big) \\ &= v_F \sum_{p\neq 0} |p|\hat{b}^\dagger(p)\hat{b}(p).\end{aligned} \tag{2.37}$$

Let us take a moment to appreciate this expression, which is ubiquitous in the literature [31, 35–38, 50–52]: in terms of the fluctuations, the chiral system (and as we saw earlier, the real system as well) is reformulated as infinite harmonically oscillating quantized modes with a linear dispersion. Incidentally, this is also the reason why we do not need to take the mode $p = 0$ into account: this is a null fluctuation that is best understood as a part of the vacuum. The form of the Hamiltonian of Eq. 2.37 allows us to link the quantized fluctuations to bosonic fields, a key aspect of the bosonization procedure that will be explored further in the next section.

2.5 Fields

In analogy to the mode expansions of a real scalar field [53], let us define the fields

$$\begin{aligned} \hat{\Phi}(x,t) &= \sum_{p\neq 0}\sqrt{\frac{1}{2L|p|}}\Big(e^{i(px-|p|v_F t)}\hat{b}_p + \text{h.c.}\Big), \\ \hat{\Pi}(x,t) &= -i\sum_{p\neq 0}\sqrt{\frac{|p|}{2L}}\Big(e^{i(px-|p|v_F t)}\hat{b}_p - \text{h.c.}\Big), \end{aligned} \tag{2.38}$$

satisfying the canonical commutation relations $[\hat{\Phi}(x), \hat{\Pi}(y)] = i\delta(x-y)$, and $\partial_t\hat{\Phi} = v_F\hat{\Pi}$. A few remarks about this definition: first, we omit the Fermi velocity, which is analogous to the speed of light c, from the definition; the reason behind this becomes clear in Sec. 2.7. Second, the use of $|p|$ in the exponent ensures that fluctuations on the right branch propagate to the right and viceversa. Third, based on the commutation relations, we can refer to the canonical operators $\hat{\Phi}$ and $\hat{\Pi}$ as the position and momentum fields, respectively. Finally, the sums in the definitions and henceforth exclude the mode $p = 0$, unless specified. This will seldom be a problem, since most calculations are done in the continuum limit, where a single point has no appreciable effect on an integral.

If we attempt to invert the definitions of Eq. 2.38, we find an interesting result:

$$\begin{aligned} \frac{1}{\sqrt{L}}\int \mathrm{d}x\, e^{-ipx}\partial_x\hat{\Phi} &= \operatorname{sgn}(p)i\sqrt{\frac{|p|}{2}}\Big(\hat{b}_p + \hat{b}^\dagger_{-p}\Big), \\ \frac{1}{\sqrt{L}}\int \mathrm{d}x\, e^{-ipx}\hat{\Pi} &= -i\sqrt{\frac{|p|}{2}}\Big(\hat{b}_p - \hat{b}^\dagger_{-p}\Big). \end{aligned} \tag{2.39}$$

Adding and substracting the previous expressions yields

$$\begin{aligned} \hat{b}_p &= \frac{-i}{\sqrt{2|p|L}}\int \mathrm{d}x\, e^{-ipx}\Big(\operatorname{sgn}(p)\partial_x\hat{\Phi} - \hat{\Pi}\Big), \\ \hat{b}^\dagger_p &= \frac{i}{\sqrt{2|p|L}}\int \mathrm{d}x\, e^{ipx}\Big(\operatorname{sgn}(p)\partial_x\hat{\Phi} - \hat{\Pi}\Big). \end{aligned} \tag{2.40}$$

Notice that this is a Fourier decomposition of the bosonic operators, which means that there is a direct relationship between these combinations of fields and the current operators. In fact, from

Eq. 2.40, it can be shown that

$$\hat{J}_\alpha(x) = \frac{1}{2\sqrt{\pi}}\Big(\partial_x\hat{\Phi} - \alpha\hat{\Pi}(x)\Big). \tag{2.41}$$

This is a crucial relationship as it allows us, not only to rewrite the Hamiltonian in terms of these bosonic fields, but also to give them a physical interpretation. On the one hand, the quadratic currents can now be easily determined, so that the Hamitonian of Eq. 2.24 becomes

$$\hat{H}_0 = \frac{v_F}{2}\int \mathrm{d}x\,\bigg(\Big(\partial_x\hat{\Phi}\Big)^2 + \hat{\Pi}^2\bigg), \tag{2.42}$$

which is the free scalar Hamiltonian, as expected from field theory [47, 53]. On the other hand, for the total density and current we get

$$\hat{\rho}(x) = \frac{1}{\sqrt{\pi}}\partial_x\hat{\Phi} \quad \text{and} \quad \hat{J}(x) = \frac{-v_F}{\sqrt{\pi}}\hat{\Pi}, \tag{2.43}$$

according to Eq. 2.15. These relationships show the, perhaps intuitive, link between the position field and the density, and the momentum field and the current. However, as done in the literature [35], we can go even further and realize that a particle distribution of almost localized particles would be represented by a $\langle\hat{\Phi}(x)\rangle$ like the one shown in Fig. 2.3: a stairwell-like graph that has a kink of height $\sqrt{\pi}$ every time it encounters a charge. Consequently, it would be more accurate to refer to $\hat{\Phi}$ as a counting field, that increases by a constant amount every time there is a full charge.

There are two additional, useful auxilliary fields that we can define. The first one is

$$\hat{\theta}(x,t) = -\sum \frac{\mathrm{sgn}(p)}{\sqrt{2L|p|}}\Big(e^{i(px - v_F|p|t)}\hat{b}_p + \text{h. c.}\Big), \tag{2.44}$$

which is defined to satisfy $\hat{\Pi} = \partial_x\hat{\theta}$. This field will later be interpreted as a phase and is immediately useful as it allows us to write the currents as $\hat{J}_\alpha(x) = (1/2\sqrt{\pi})\partial_x(\hat{\Phi} - \alpha\hat{\theta})$. Finally, we split the modes of $\hat{\Phi}$ into the contributions from each branch to define

$$\hat{\phi}_\alpha = \sum_{\alpha p>0}\sqrt{\frac{1}{2L|p|}}\Big(e^{i(px - |p|v_F t)}\hat{b}_p + \text{h.c.}\Big), \tag{2.45}$$

where we use the fact that, by Eq. 2.32, the sign of p determines the chirality of $\hat{b}_p$. Thus, the following identities are then satisfied:

$$\begin{aligned} \hat{\Phi} &= \hat{\phi}_R + \hat{\phi}_L \\ \hat{\phi}_\alpha &= \frac{1}{2}\Big(\hat{\Phi} - \alpha\hat{\theta}\Big) \\ \hat{J}_\alpha(x) &= \frac{1}{\sqrt{\pi}}\partial_x\hat{\phi}_\alpha. \end{aligned} \tag{2.46}$$

The relevant commutators between these fields are calculated and compiled in appendix A.

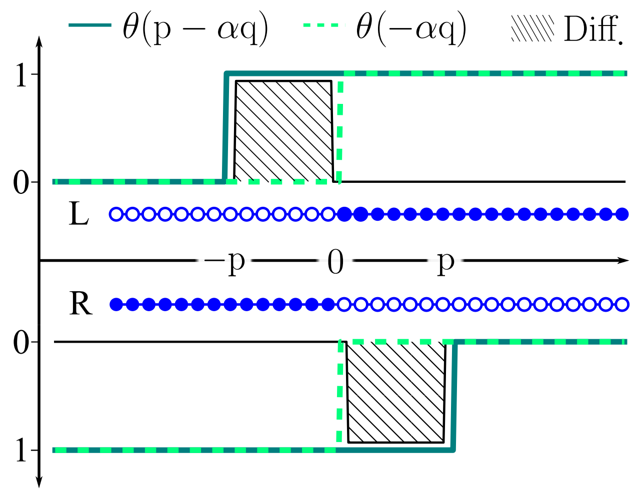

Figure 2.2: Diagram showing where the step functions that arise from the commutator of Eq. 2.30. The difference of what would be divergent integrals on their own, vanishes except for a small region that yields the finite result.

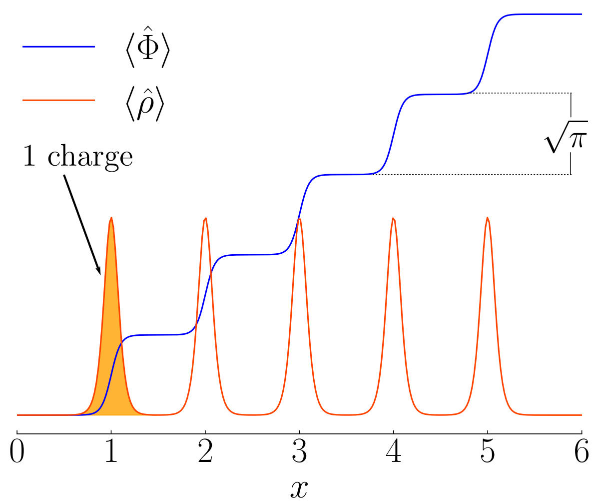

Figure 2.3: $\langle\hat{\Phi}\rangle$ has a kink of height $\sqrt{\pi}$ at every charge. It is important to note that the $\hat{\rho}$ shown is only an explanatory tool as it represents huge fluctuations that would not be seen at low energy.

2.6 The bosonization identity

Would it not be wonderful if we had a simple way to formulate our original chiral fermions in terms of the canonical fields? After all, these will prove to be a very powerful tool, and the process we used to obtain them is a lengthy one. Fear not, for all our work allows us to find a way to bosonize a system without the meticulous chain of steps we have performed so far.

Using the identity $[\hat{A}, e^{\hat{B}}] = [\hat{A}, \hat{B}]e^{\hat{B}}$, proven in Eq. B.5 and the commutator $[\hat{J}_\alpha(x), \hat{\phi}_\alpha(y)] \propto \delta(x-y)$, shown in Eq. A.20, we find that

$$\left[\hat{J}_\alpha(x), e^{\alpha i 2\sqrt{\pi}\hat{\phi}_\alpha(y)}\right] = -\delta(x-y)e^{\alpha i 2\sqrt{\phi}_\alpha(y)}. \tag{2.47}$$

This is, by construction, the same commutation relationship that there is between $\hat{J}_\alpha(x)$ and the original chiral fermion $\hat{\psi}_\alpha(x)$. This suggests that

$$\hat{\psi}_\alpha(x) \propto e^{\alpha i 2\sqrt{\pi}\hat{\phi}_\alpha(x)}, \tag{2.48}$$

up to some proportionality constant C. Let us check that this expression is physically reasonable. In the exponent we find a combination of fields $\alpha\hat{\Phi} - \hat{\theta}$. Taking each field on their own, we find that the part proportional to $\exp\,(-i\sqrt{\pi}\hat{\theta})$ can be seen as a translation operator that acts on the field $\hat{\Phi}$ at a point x creating a kink. This is accompanied by a factor proportional to $\exp\,(\sqrt{\pi}\hat{\Phi})$, which similarly creates a fluctuation on the momentum field, specifically affecting the current. This is important, because it guarantees that fluctuations conserve the number of particles N: we create a localized kink and at the same time change the currents so that this is dissipated throughout the system creating a localized fluctuation of the density. On the other hand, since $\hat{\psi}_\alpha(x)$ has a net effect on N, the creation or annihilation of global charge must be done by an operator contained in the proportionality constant. Therefore, we introduce the non-hermitian, unitary Klein factors $\hat{\eta}_\alpha$, which commute with the fields and are responsible for the global changes in the number of particles. For a detailed calculation of $\hat{\eta}_\alpha$ in terms of the fields, see Ref. [51].

To find the remaining scalar proportionality constant, let us calculate the correlation

$$\begin{aligned}\left\langle \hat{\psi}_R(x)\hat{\psi}_R^\dagger(y)\right\rangle &= |C|^2\left\langle \hat{\eta}_R\hat{\eta}_R^{-1}e^{i2\sqrt{\pi}\hat{\phi}_R(x)}e^{-i2\sqrt{\pi}\hat{\phi}_R(y)}\right\rangle \\ &= |C|^2\left\langle e^{i2\sqrt{\pi}(\hat{\phi}_R(x)-\hat{\phi}_R(y))}e^{i\frac{\pi}{2}\operatorname{sgn}(x-y)}\right\rangle \\ &= i\operatorname{sgn}(x-y)|C|^2\left\langle e^{\hat{B}}\right\rangle,\end{aligned} \tag{2.49}$$

where we used the commutator of Eq. A.15, and $\hat{B} = i2\sqrt{\pi}(\hat{\phi}_R(x) - \hat{\phi}_R(y))$. In order to use the identity $\langle \exp \hat{B}\rangle = \exp\Big(\langle \hat{B}^2\rangle/2\Big)$, proven in Eq. B.9, we need to determine

$$\frac{1}{2}\left\langle \hat{B}^2\right\rangle = -2\pi\left\langle \hat{\phi}_R^2(x) + \hat{\phi}_R^2(y) - 2\hat{\phi}_R(x)\hat{\phi}_R(y)\right\rangle - \frac{i\pi}{2}\operatorname{sgn}(x-y). \tag{2.50}$$

The expected values are calculated in Eq. A.7, and allow us to express

$$\frac{1}{2}\left\langle \hat{B}^2\right\rangle = \ln\left(\frac{i\delta}{(x-y)+i\delta}\right) - i\frac{\pi}{2}\operatorname{sgn}(x-y), \tag{2.51}$$

which finally yields the correlation we were interested in the first place:

$$\left\langle \hat{\psi}_R(x)\hat{\psi}_R^\dagger(y)\right\rangle = \frac{i\delta|C|^2}{(x-y)+i\delta}. \tag{2.52}$$

If we compare this result to the same correlation obtained in Eq. 2.26, we identify $C = 1/\sqrt{2\pi\delta}$. What we get for the functional relationship between the fermionic field and the bosonic ones is

$$\hat{\psi}_\alpha(x) = \frac{1}{\sqrt{2\pi\delta}}\hat{\eta}_\alpha e^{\alpha i2\sqrt{\pi}\hat{\phi}_\alpha(x)}, \tag{2.53}$$

which is the fundamental bosonization identity, a crucial tool in our analysis, and the main result of this chapter. With it, we can easily reformulate any suitable system in terms of the canonical fields, without going through the meticulous chain of replacements. Make no mistake, we had to do it the long way first, painstakingly showing and justifying the steps that lead to Eq. 2.53; now that we are here, we can skip it all if needed. We are ready to show the power of the bosonization identity by applying it to many-body interacting systems in the next section.

2.7 Interacting Fermion gas

In order to show the power and usefulness of bosonization, let us build upon the treatment of the free fermion gas developed in earlier sections by taking into account an interaction potential $\hat{V}$ so that

$$\hat{H} = \hat{H}_0 + \hat{V} = \hat{H}_0 + \frac{1}{2}\int \mathrm{d}x\,\mathrm{d}y\, g(x-y)\hat{\psi}^\dagger(x)\hat{\psi}^\dagger(y)\hat{\psi}(y)\hat{\psi}(x), \tag{2.54}$$

where $g(x-y)$ is the separation-dependent interaction strength, satisfying $g(x) = g(-x)$. Using the map introduced by Eq. 2.7, the interaction term is rewritten in terms of the chiral fermions as

$$\begin{aligned}
\hat{V} &= \frac{1}{2}\int \mathrm{d}x\,\mathrm{d}y\, g(x-y)\Big[\Big(\hat{\psi}^\dagger_R(x)\hat{\psi}^\dagger_R(y)\hat{\psi}_R(y)\hat{\psi}_R(x) + \hat{\psi}^\dagger_R(x)\hat{\psi}^\dagger_L(y)\hat{\psi}_L(y)\hat{\psi}_R(x) + (R\to L)\Big) \\
&+ \Big(e^{-i2k_F(x-y)}\hat{\psi}^\dagger_R(x)\hat{\psi}^\dagger_L(y)\hat{\psi}_R(y)\hat{\psi}_L(x) + e^{-i2k_F(x+y)}\hat{\psi}^\dagger_R(x)\hat{\psi}^\dagger_R(y)\hat{\psi}_L(y)\hat{\psi}_L(x) \\
&+ e^{-i2k_Fx}\hat{\psi}^\dagger_R(x)\hat{\psi}^\dagger_R(y)\hat{\psi}_R(y)\hat{\psi}_L(x) + e^{i2k_Fx}\hat{\psi}^\dagger_L(x)\hat{\psi}^\dagger_L(y)\hat{\psi}_L(y)\hat{\psi}_R(x) \\
&+ e^{-i2k_Fy}\hat{\psi}^\dagger_R(x)\hat{\psi}^\dagger_R(y)\hat{\psi}_L(y)\hat{\psi}_R(x) + e^{i2k_Fy}\hat{\psi}^\dagger_L(x)\hat{\psi}^\dagger_L(y)\hat{\psi}_R(y)\hat{\psi}_L(x) + \mathrm{h.\,c.}\Big)\Big].
\end{aligned} \tag{2.55}$$

For the present analysis we will neglect short-wavelength oscillations, following physical arguments discussed below, and yearning for pedagogical clarity [37]. This leaves us with the first line and after applying anticommutation relations we get for the first term

$$\begin{aligned}
\hat{\psi}^\dagger_R(x)\hat{\psi}^\dagger_R(y)\hat{\psi}_R(y)\hat{\psi}_R(x) &= \hat{\psi}^\dagger_R(x)\hat{\psi}_R(x)\hat{\psi}^\dagger_R(y)\hat{\psi}_R(y) - \delta(x-y)\hat{\psi}^\dagger_R(x)\hat{\psi}_R(y) \\
&= \Big(:\hat{\psi}^\dagger_R(x)\hat{\psi}_R(x): + \Big\langle\hat{\psi}^\dagger_R(x)\hat{\psi}_R(x)\Big\rangle\Big)\Big(:\hat{\psi}^\dagger_R(y)\hat{\psi}_R(y): + \Big\langle\hat{\psi}^\dagger_R(y)\hat{\psi}_R(y)\Big\rangle\Big) \\
&\quad -\delta(x-y)\hat{\psi}^\dagger_R(x)\hat{\psi}_R(y) \\
&= \hat{J}_R(x)\hat{J}_R(y) + \frac{1}{(2\pi\delta)^2} + \frac{1}{2\pi\delta}\Big(\hat{J}_R(x) + \hat{J}_R(y)\Big) - \delta(x-y)\hat{\psi}^\dagger_R(x)\hat{\psi}_R(y).
\end{aligned} \tag{2.56}$$

For the opposite chirality we proceed analogously to get

$$\begin{aligned}
\hat{\psi}^\dagger_L(x)\hat{\psi}^\dagger_L(y)\hat{\psi}_L(y)\hat{\psi}_L(x) &= \hat{J}_L(x)J_L(y) + \frac{1}{(2\pi\delta)^2} - \frac{1}{2\pi\delta}\Big(\hat{J}_L(x) + J_L(y)\Big) \\
&- \delta(x-y)\hat{\psi}^\dagger_L(x)\hat{\psi}_L(y).
\end{aligned} \tag{2.57}$$

Similarily, the second term and its chiral opposite become

$$\begin{aligned}
\hat{\psi}^\dagger_R(x)\hat{\psi}^\dagger_L(y)\hat{\psi}_L(y)\hat{\psi}_R(x) &= J_R(x)J_L(y) - \frac{1}{(2\pi\delta)^2} - \frac{1}{2\pi\delta}J_R(x) + \frac{1}{2\pi\delta}\hat{J}_L(y) \\
\hat{\psi}^\dagger_L(x)\hat{\psi}^\dagger_R(y)\hat{\psi}_R(y)\hat{\psi}_L(x) &= J_R(y)J_L(x) - \frac{1}{(2\pi\delta)^2} - \frac{1}{2\pi\delta}J_R(y) + \frac{1}{2\pi\delta}\hat{J}_L(x).
\end{aligned} \tag{2.58}$$

Notice that the terms proportional to $\delta(x-y)$ in Eqs. 2.56 and 2.57 make up the density operator $\hat{\rho}$. Therefore, they constitute a term proportional to the total number of particles, which is conserved and can be swept into the vacuum energy. Finally, we join everything together to get the interaction in terms of the chiral fermions

$$\begin{aligned} \hat{V} &= \int \mathrm{d}x\,\mathrm{d}y\,\Big(2g_2(x-y)J_L(x)\hat{J}_R(y) + g_4(x-y)\Big(\hat{J}_R(x)\hat{J}_R(y) + \hat{J}_L(x)\hat{J}_L(y)\Big)\Big) \\ &+ \text{(vacuum energy)}. \end{aligned} \tag{2.59}$$

Here we see that the potential is split into interactions between branches and within them, characterized by the couplings $g_2(x-y)$ and $g_4(x-y)$ respectively. Our notation for the couplings follows Ref. [46], which is now standard in the literature and known as g-ology. Consequently, each type of process has an independent coupling strength, and we keep only the forward-scattering g_2 and g_4. Backscaterring, commonly associated with g_1 has been neglected from Eq. 2.55 because of the large momentum transfer involved, whereas umklapp processes tied to g_3 are only slow oscillations in half-filled lattice systems due to the role of the reciprocal lattice.

Equation 2.59 is a first indication of the usefulness of bosonization: the interaction is quadratic in currents, just as the free Hamiltonian, suggesting a possible diagonalization of $\hat{H}$. For now, let us continue manipulating the expression by writing it in terms of operators from the reciprocal space. For the Fourier components of the currents, we use Eq. 2.28, whereas for the potential

$$g_i(x-y) = \frac{1}{\sqrt{L}}\sum e^{ik(x-y)}g_i(k), \tag{2.60}$$

and the symmetry constrains the components so that $g_i(k) = g_i(-k)$. Plugging into the term for interactions within the right branch we get

$$\begin{aligned} \int \mathrm{d}x\,\mathrm{d}y\,g_4(x-y)\hat{J}_R(x)J_R(y) &= \frac{1}{L\sqrt{L}}\sum g_4(k)\hat{J}_R(p)\hat{J}_R(q)\int \mathrm{d}x\,e^{ix(k+p)}\int \mathrm{d}y\,e^{iyq-k} \\ &= \sqrt{L}\sum g_4(-p)\hat{J}_R(p)\hat{J}_R(-p). \end{aligned} \tag{2.61}$$

This procedure is repeated for the remaining terms, yielding

$$\hat{V} = \sqrt{L}\sum g_4(p)\Big(\hat{J}_R(p)\hat{J}_R(-p) + \hat{J}_L(p)\hat{J}_L(-p)\Big) + 2g_2(p)\hat{J}_L(p)\hat{J}_R(p). \tag{2.62}$$

In the first term of Eq. 2.62 we recognize the form of the free Hamiltonian from Eq. 2.37. For the other one, we can apply the inverse relations from Eq. 2.33 and obtain

$$\hat{H} = \sum\left(v_F + \frac{\sqrt{L}}{\pi}g_4(p)\right)|p|\hat{b}^\dagger(p)\hat{b}(p) + \frac{\sqrt{L}}{2\pi}g_2(p)|p|\Big(\hat{b}^\dagger(p)\hat{b}^\dagger(-p) + \hat{b}(-p)\hat{b}(p)\Big). \tag{2.63}$$

Notice that g_4 processes only affect the propagation velocity of the fluctuations, directly rescaling the Fermi velocity. This physical insight has been revealed due to our use of bosonization, and our focus on collective fluctuations, and their behavior when interactions are present. Furthermore, this implies a constrain on the actual coupling: $\pi v_F + g_4(p)\sqrt{L} > 0$, which prevents unstable excitations of negative energy.

In this quadratic form, the Hamiltonian is prime for a Bogoliubov transformation [54], in which we apply a unitary transformation,

$$\hat{b}(p) = \cosh\varphi_p \hat{\hat{b}}(p) + \sinh\varphi_p \hat{\hat{b}}^\dagger(-p), \tag{2.64}$$

for some set of angles φ_p. Notice that this transformation preserves the bosonic commutation we worked so hard to retrieve. Also, for simplicity, let us call

$$\alpha_p = \left(v_F + \frac{\sqrt{L}}{\pi} g_4(p)\right)|p| \quad \text{and} \quad \beta_p = \frac{\sqrt{L}}{2\pi} g_2(p)|p|. \tag{2.65}$$

Tranforming Eq. 2.63, we obtain

$$\begin{aligned} \hat{H} &= \sum \hat{\hat{b}}^\dagger(p)\hat{\hat{b}}(p)\left[\alpha_p\cosh^2\varphi_p + \alpha_p\sinh^2\varphi_{-p} + 4\beta_p\cosh\varphi_p\sinh\varphi_{-p}\right] \\ &+ \hat{\hat{b}}^\dagger(p)\hat{b}^\dagger(-p)\left[\alpha_p\cosh\varphi_p\sinh\phi_p + \beta_p\cosh\varphi_p\cosh\varphi_{-p} + \beta_p\sinh\varphi_p\sinh\varphi_{-p}\right] \\ &+ \hat{\hat{b}}(-p)\hat{b}(p)\underbrace{\left[\alpha_p\cosh\varphi_p\sinh\phi_p + \beta_p\cosh\varphi_p\cosh\varphi_{-p} + \beta_p\sinh\varphi_p\sinh\varphi_{-p}\right]}_{(\star)}. \end{aligned} \tag{2.66}$$

Assuming $\varphi_p = \varphi_{-p}$, we can diagonalize the transformed Hamiltonian by picking angles that make the quantity marked as $(\star)$ vanish. In this case,

$$\tanh(2\varphi_p) = -\frac{\sqrt{L}}{\pi v_F + g_4(p)\sqrt{L}} g_2(p), \tag{2.67}$$

yields

$$\hat{H} = \sum v_F|p|\left((1+\bar{g}_4)^2 - \bar{g}_2^2\right)^{\frac{1}{2}} \hat{\hat{b}}_p^\dagger \hat{\hat{b}}_p, \tag{2.68}$$

in accordance with the literature [35, 37], where $\bar{g}_i = \sqrt{L}g_i/\pi v_F$ and where we used the hyperbolic identities

$$\sinh x = \frac{\tanh x}{\sqrt{1-\tanh^2 x}} \quad \text{and} \quad \cosh x = \frac{1}{\sqrt{1-\tan^2 x}}, \tag{2.69}$$

to simplify the resulting expressions.

Bosonization has led us to a remarkable result. Not only have we diagonalized the Hamiltonian, but we have found that the interacting systems has eigenstates that represent collective particle-hole excitations of the fermions; excitations that are created by the $\hat{\hat{b}}^\dagger(p)$. As has been discussed previoulsy, this is caused by the dimensionality of the system, since particles in one-dimension have no choice but to bump into each other, and the influence of an interaction propagates across the chain. In a three-dimensional system, for instance, the fermions could miss each other entirely, and even if a collision were to happen, there is no guarantee that further interactions would happen fast enough for a global effect. Contrariwise, in our one-dimensional gas all of the particles fluctuate as a collective whole as shown by these results.

Additionally, we find that the role of the forward-scattering processes is to rescale the propagation velocity of the excitations, as well as change their exact nature. This is physically reasonable, since stronger interactions can lead to fluctuations that prevail for longer in the one-dimensional chain. However, remeber that our bosonized Hamiltonian is a perturbative treatment of the original system, since we are neglecting certain processes that can become relevant if the energy scale is increased. If we needed to, we could always go back and keep more terms, which would then yield more precise results up to the point where the basic assumptions of bosonization break. However, it is often the case that the low energy properties are accurately captured by the behavior of long-wavelength oscillations [31].

3 Applying bosonization

Now that we have developed a theoretical framework and understand the fundamentals of bosonization, let us apply the formalism to some simple systems. This will serve as a way to not only sharpen our skill with the technique, but to also prepare us for similar calculations that could be encountered down the road. The systems that we will study in this chapter have been selected for their similarity with that of the main objective of this work, which is a bosonic spinor gas. First, we will solve a spin-$\frac{1}{2}$ chain with a small anisotropy, and then we will explore the particularities of applying bosonization to bosons. The chapter will close with the calculation of correlations for a toy model of hard core bosons.

3.1 Heisenberg XXZ model

Let us consider a chain of spin-$\frac{1}{2}$ particles, interacting up to first neighbors according the so-called Heisenberg XXZ model

$$\hat{H} = -J \sum_n (\hat{S}_n^x \hat{S}_{n+1}^x + \hat{S}_n^y \hat{S}_{n+1}^y + \Delta \hat{S}_n^z \hat{S}_{n+1}^z), \tag{3.1}$$

where the transverse coupling constant is $J_z = \Delta J$. This example is instructive, because we will take it further than the last one by calculating the correlations of the system. To begin, it is necessary to map the anisotropic Heisenberg Hamiltonian of Eq. 3.1 into a system that can be treated through bosonization. Then, we treat separately the parts corresponding to the planar (xy plane) and transverse terms (z axis), before joining everything back together into the final results.

3.1.1 Fermionic Hamiltonian

Using the Jordan-Wigner transfomation [55] defined in Eq. C.3 between spins-$\frac{1}{2}$ and fermions, we use the inverse equations

$$\hat{S}_n^+ = e^{i\pi t_n} \hat{c}_n^\dagger \quad \text{and} \quad \hat{S}_n^- = e^{i\pi t_n} \hat{c}_n, \tag{3.2}$$

to transform the planar terms of Eq. 3.1, meaning

$$\begin{aligned}\hat{S}_n^+\hat{S}_{n+1}^- &= \hat{c}_n^\dagger\left(1-2\hat{c}_n^\dagger\hat{c}_n\right)\hat{c}_{n+1} = \hat{c}_n^\dagger\hat{c}_{n+1} \\ \hat{S}_n^-\hat{S}_{n+1}^+ &= \hat{c}_n\left(1-2\hat{c}_n^\dagger\hat{c}_n\right)\hat{c}_{n+1}^\dagger = -\hat{c}_n\hat{c}_{n+1}^\dagger.\end{aligned} \tag{3.3}$$

Since spin operator identities determine that

$$\hat{S}_n^x\hat{S}_{n+1}^x + \hat{S}_n^y\hat{S}_{n+1}^y = \frac{1}{2}\Big(\hat{S}_n^+\hat{S}_{n+1}^- + \hat{S}_n^-\hat{S}_{n+1}^+\Big), \tag{3.4}$$

for the planar part of the Hamiltonian we get

$$\begin{aligned}\hat{H}^0 &= -J\sum_n\left(\hat{S}_n^x\hat{S}_{n+1}^x + \hat{S}_n^y\hat{S}_{n+1}^y\right) \\ &= -t\sum_n\left(\hat{c}_n^\dagger\hat{c}_{n+1} + \hat{c}_{n+1}^\dagger\hat{c}_n\right),\end{aligned} \tag{3.5}$$

with $t = J/2$. Hence, the Jordan-Wigner transformation maps the planar part of the Heisenberg Hamiltonian into a system of free lattice fermions; now we are ready to proceed with bosonization, since it is well known [45] that the dispersion relation is $\epsilon(k) = -2t\cos(ka)$, where a is the lattice constant inherited from the original chain. The periodic boundary conditions discretize the momentum as $k = 2\pi n/L$, where L is the length of the system and there are $N_0 = L/a$ sites. We can now define the filling factor $\nu = N/N_0$, where N is the number of particles. If the Fermi surface is k_F, then $N = Lk_F/\pi$. Therefore,

$$\nu = \frac{ak_F}{\pi}. \tag{3.6}$$

If we work with a half-filled system, then $\nu = 1/2$, $ak_F = \pi/2$, and we can linearize around $\epsilon_F = 0$.

Recalling Eq. 2.7, we can express the terms of Eq. 3.5 as functions of the chiral fermions,

$$\hat{c}_{n+1}^\dagger\hat{c}_n = \Big(e^{-ik_F(x+a)}\hat{\psi}_R^\dagger(x+a) + e^{ik_F(x+a)}\hat{\psi}_L^\dagger(x+a)\Big)\Big(e^{ik_Fx}\hat{\psi}_R(x) + e^{-ik_Fx}\hat{\psi}_L(x)\Big), \tag{3.7}$$

where $x = an$, according to the lattice. It might be tempting to do a Taylor expansion to simplify the expression; however, it is crucial to remember that all fermions are only defined on the lattice. Failure to enforce this will lead to an incorrect point-split. As opposed to the scheme used in Sec. 2.3, the lattice already determines a minimum length so that the UV divergences are avoided; as such, we need to tread carefully. By applying the bosonization identity, we get

$$\begin{aligned}\hat{c}_{n+1}^\dagger\hat{c}_n + \text{h. c.} &= -i\Big(\hat{\psi}_R^\dagger(x+a)\hat{\psi}_R(x) - \hat{\psi}_L^\dagger(x+a)\hat{\psi}_L(x) - \text{h. c.}\Big) + (\text{fast oscillations}), \quad (3.8) \\ &= \frac{-i}{2\pi a}\Big(e^{-i2\sqrt{\pi}\hat{\phi}_R(x+a)}e^{i2\sqrt{\pi}\hat{\phi}_R(x)} - e^{i2\sqrt{\pi}\hat{\phi}_L(x+a)}e^{-i2\sqrt{\pi}\hat{\phi}_L(x)} - \text{h. c.}\Big) \\ &= \frac{1}{2\pi a}\Big(e^{-i2\sqrt{\pi}(\hat{\phi}_R(x+a)-\hat{\phi}_R(x))} - e^{i2\sqrt{\pi}(\hat{\phi}_L(x+a)-\hat{\phi}_L(x))} + \text{h. c.}\Big).\end{aligned}$$

Notice that the exponent is proportional to the lattice definition of the derivative. Neglecting the fast oscillations proportional to $(-1)^n$, we can then expand the power series

$$\begin{aligned}\hat{c}^\dagger_{n+1}\hat{c}_n + \text{h. c.} &= \frac{-1}{2\pi a}\Big(ia2\sqrt{\pi}\partial_x\hat{\phi}_R + 2a^2\pi(\partial_x\phi_R)^2 - ia2\sqrt{\pi}\partial_x\hat{\phi}_L + 2a^2\pi(\partial_x\phi_L)^2 + \text{h. c.}\Big),\\ &= -2a\big((\partial_x\phi_R)^2 + (\partial_x\phi_L)^2\big),\end{aligned} \tag{3.9}$$

where the bosonic fields vary slowly so it is fine to truncate at second order in a. Recall from Eq. 2.46 that $\hat{\Phi} = \hat{\phi}_R + \hat{\phi}_L$ and $\hat{\Pi} = \partial_x\hat{\phi}_R - \partial_x\hat{\phi}_L$. Thus, the Hamiltonian becomes

$$\hat{H}_0 = \frac{v_F}{2}\int \mathrm{d}x\,\Big((\partial_x\Phi)^2 + \hat{\Pi}^2\Big), \tag{3.10}$$

where $v_F = 2ta = Ja$, and in the continuum limit $\sum_n \to (1/a)\int \mathrm{d}x$. We have retrieved the same free bosonic field Hamiltonian as in Eq. 2.42 with a considerably less effort than in the previous sections; that is the power of the fundamental bosonization identity of Eq. 2.53.

Before moving on, let us discuss a nuance of reformulating a discrete system in terms of continuous fields: units. Notice that if we examine the Jordan-Wigner transformation of Eq. C.3, which we use to connect the localized spins with fermions, we can see that when taking the continuum limit, *i.e.* applying the bosonization identity, $\hat{S}^\pm(x) \propto (2\pi a)^{-1/2}$ and $\hat{S}^z(x) \propto (2\pi a)^{-1}$. However, the original spin operators are dimensionless since we are taking $\hbar = 1$; thus, we should scale the operators as

$$\hat{S}^\pm_n \to \sqrt{a}\hat{S}^\pm(x) \quad \text{and} \quad \hat{S}^z_n \to a\hat{S}^z(x). \tag{3.11}$$

In practice, this translates to retaining a factor in the final bosonized terms depending on the original discrete operator it came from. For instance, the Hamiltonian of Eq. 3.10 came from bilinears like $\hat{S}^+_{n+1}\hat{S}^-_n$, so there should be an additional factor of a, which cancels with the a^{-1} that accompanies the integral. Moreover, this means that the coupling constant J is rescaled in the continuum limit as Ja. Alternatively, one can set $a = 1$ and recover all factors at the end using dimensional analysis.

3.1.2 Transverse term

The final step is transforming the transverse term in the Heisenberg Hamiltonian

$$\hat{H}_I = -J_z\sum_n \hat{S}^z_n\hat{S}^z_{n+1}. \tag{3.12}$$

Since it is quadratic in $\hat{S}^z$, it becomes quartic in fermions after applying the Jordan-Wigner transformation and maps to a two-body interaction. In order to get there, we first transform the spin operator using the familiar map in Eq. 2.7,

$$\begin{aligned}
\hat{S}^x_n &= \hat{c}^\dagger_n(x)c_n(x) - \frac{1}{2} \\
&= \Big((-i)^n\hat{\psi}^\dagger_R(x) + i^n\hat{\psi}^\dagger_L(x)\Big)\Big((i)^n\hat{\psi}_R(x) + (-i)^n\hat{\psi}_L(x)\Big) - \frac{1}{2} \\
&= \hat{\psi}^\dagger_R(x)\hat{\psi}_R(x) + \hat{\psi}^\dagger_L(x)\hat{\psi}_L(x) + (-1)^n\Big(\hat{\psi}^\dagger_R(x)\hat{\psi}_L(x) + \hat{\psi}^\dagger_L(x)\hat{\psi}_R(x)\Big) - \frac{1}{2} \\
&= \frac{1}{\sqrt{\pi}}\partial_x\hat{\Phi} + (-1)^n\hat{M}(x) - \frac{1}{2}. \qquad (3.13)
\end{aligned}$$

As we can see, the transverse magnetic spin becomes the smooth fermionic density plus an oscillating magnetization field $\hat{M} = \hat{\psi}^\dagger_R\hat{\psi}_L + \hat{\psi}^\dagger_L\hat{\psi}_R$. This term can be shown to be equal to

$$\begin{aligned}
\hat{M} &= \frac{1}{2\pi a}\Big(e^{-i2\sqrt{\pi}\hat{\phi}_R}e^{-i2\sqrt{\pi}\hat{\phi}_L} + e^{i2\sqrt{\pi}\hat{\phi}_R}e^{i2\sqrt{\pi}\hat{\phi}_L}\Big) \qquad (3.14)\\
&= \frac{1}{\pi a}\cos\Big(2\sqrt{\pi}\hat{\Phi}\Big), \qquad (3.15)
\end{aligned}$$

emphasizing its density wave nature.

We are now ready to calculate the product

$$\begin{aligned}
\hat{S}^z_n\hat{S}^z_{n+1} &= \left(\frac{1}{\sqrt{\pi}}\partial_x\hat{\Phi}(x) + (-1)^n\hat{M}(x) - \frac{1}{2}\right)\left(\frac{1}{\sqrt{\pi}}\partial_x\hat{\Phi}(x+a) - (-1)^n\hat{M}(x+a) - \frac{1}{2}\right) \\
&= \frac{1}{\pi}(\partial_x\hat{\Phi})^2 - \hat{M}(x)\hat{M}(x+a) + (\text{fast oscillations}) + (\text{vacuum}), \qquad (3.16)
\end{aligned}$$

where the field $\hat{\Phi}$ varies slowly, so in the continuum $\partial_x\hat{\Phi}(x+a) \to \partial_x\hat{\Phi}(x)$; fast oscillations are neglected and constant terms are swept into the vacuum. The first term can be traced back to terms like $\hat{\psi}^\dagger_R\hat{\psi}_R\hat{\psi}^\dagger_R\hat{\psi}_R$, so we associate it with g_4 processes. Next, as mentioned in the previous section, we must be careful when calculating $\hat{M}(x)\hat{M}(x+a)$. Taking into account that the operators commute,

$$\begin{aligned}
\hat{M}(x)\hat{M}(x+a) &= \frac{1}{(\pi a)^2}\cos\Big(2\sqrt{\pi}\hat{\Phi}(x)\Big)\cos\Big(2\sqrt{\pi}\hat{\Phi}(x+a)\Big) \\
&= \frac{1}{2(\pi a)^2}\Big(\cos\Big(2\sqrt{\pi}(\hat{\Phi}(x) - \hat{\Phi}(x+a))\Big) + \cos\Big(2\sqrt{\pi}(\hat{\Phi}(x) + \hat{\Phi}(x+a))\Big)\Big), \\
&= -\frac{1}{\pi}(\partial_x\hat{\Phi})^2 + \frac{2}{(2\pi a)^2}\cos\Big(4\sqrt{\pi}\hat{\Phi}(x)\Big). \qquad (3.17)
\end{aligned}$$

The first term adds to the density-density interaction; it comes from terms like $\hat{\psi}^\dagger_R\hat{\psi}_L\hat{\psi}^\dagger_L\hat{\psi}_R$ after a proper point-split, so we associate it with g_2 processes. Finally, the cosine term corresponds to g_3 umklapp terms. It is appears due to our half-filled lattice; had we started with a different filling it would be fast-oscillating. Physically, this is so because a reciprocal lattice vector can take a fermion to the Fermi surface of the next Brillouin zone only if the system is half filled. However, we will neglect it in our present analysis as it is not very relevant [35].

Remebering to take care of the units, we can now put everything together to retrieve the Hamiltonian

$$\hat{H} = \hat{H}_0 + \hat{H}_I = \frac{v_F}{2}\int \mathrm{d}x \left(\left(\partial_x \hat{\Phi}\right)^2 + \hat{\Pi}^2\right) - \frac{2aJ_z}{\pi}\int \mathrm{d}x \left(\partial_x \hat{\Phi}\right)^2 \tag{3.18}$$

$$= \frac{Ja}{2}\int \mathrm{d}x \left(\left(1 - \frac{4\Delta}{\pi}\right)\left(\partial_x \hat{\Phi}\right)^2 + \hat{\Pi}^2\right), \tag{3.19}$$

where we used the fact that $\Delta = J_z/J$. Let us call $K = (1 - 4\Delta/\pi)^{\frac{1}{2}}$ and rescale the fields such that

$$\hat{\tilde{\Phi}} = \frac{1}{\sqrt{K}}\hat{\Phi} \quad \text{and} \quad \hat{\tilde{\Pi}} = \sqrt{K}\hat{\Pi}, \tag{3.20}$$

and the coupling as $\tilde{J} = aJ\sqrt{K}$. Using these rescaled fields, the Hamiltonian becomes

$$\hat{H} = \frac{\tilde{J}}{2}\int \mathrm{d}x \left(\left(\partial_x \hat{\tilde{\Phi}}\right)^2 + \hat{\tilde{\Pi}}^2\right), \tag{3.21}$$

which has the same form as the free Hamiltonian of Eq. 2.42, meaning it is diagonal. Let us stop right here; everything happened so fast that it might come as a stunning blow. When did we diagonalize the Hamiltonian? Where is the algebraically involved Bogoliubov transform of Sec. 2.7? What do these new fields mean? What comes next?

3.1.3 Discussion

We will address each of those questions in order. First, we diagonalized the Hamiltonian by rescaling the fields; keep in mind that the factor K, also called a Luttinger parameter [36], summarizes the information of the interaction. This simple operation was enough to get to a diagonal form. But where is the involved procedure of the Bogoliubov transform? It is there, hiding within the ways that the fields are rescaled. Obviously, $\hat{\Phi}/\sqrt{K}$ is rescaled different than $\sqrt{K}\hat{\Pi}$, but what about the other ones? In particular, consider $\hat{\theta}$ and $\hat{\phi}_\alpha$, which complete the set of operators on which we built our theory. The former is simple, because it is defined to have a derivative equal to $\hat{\Pi}$, but the latter, which we use extensively, are not at all trivial, since their definition is a combination of the fields, as seen in Eq. 2.46. For reference, here is how all the fields transform:

$$\hat{\tilde{\Phi}} = \frac{1}{\sqrt{K}}\hat{\Phi}, \qquad \hat{\tilde{\Pi}} = \sqrt{K}\hat{\Pi}, \tag{3.22}$$

$$\hat{\tilde{\theta}} = \sqrt{K}\hat{\theta}, \qquad \hat{\tilde{\phi}}_\alpha = \frac{1}{2}\left(\frac{1}{\sqrt{K}}\hat{\Phi} - \alpha\sqrt{K}\hat{\theta}\right).$$

That last transformation is not trivial, and serves as a warning to be careful when using the rescaled fields: although it was easy to do the Bogoliubov transform, it is still part of a powerful and coherent mathematical framework. In fact, if we define the angle φ such that $e^{\varphi} = K^{-\frac{1}{2}}$, then we can make a doublet out of the chiral fields that transforms as

$$\begin{pmatrix} \hat{\hat{\phi}}_R \\ \hat{\hat{\phi}}_L \end{pmatrix} = \begin{pmatrix} \cosh\varphi & \sinh\varphi \\ \sinh\varphi & \cosh\varphi \end{pmatrix} \begin{pmatrix} \hat{\phi}_R \\ \hat{\phi}_L \end{pmatrix}, \tag{3.23}$$

as pointed out in Ref. [56]. This highlights the true Bogoliubov nature that is behind the bold rescaling procedure. For all further calculations, it is crucial to remember how each field transforms. For a pedagogical treatment that clearly shows the Bogoliubov transformation hidden behind the rescaling, Ref. [37] is suggested.

The power of bosonization is showcased by the process of working through the XXZ chain: by working with the fundamental identity and the bosonic fields, not only did we efficiently reformulate the problem, but we swiftly diagonalized and solved it without many involved calculations. By working with the fields, the Bogoliubov transform reduces to a simple multiplication by a scalar. Everything we achieved at the end of Sec. 2.7 is here: the Fermi velocity is rescaled, and the collective excitations are represented by the new fields. We even had the different terms that correspond to the g-ology processes. The only thing remaining is to calculate the physical properties of the XXZ spin chain, such as the often difficult to obtain correlation functions.

3.1.4 Correlations

To calculate the correlations in the vacuum (ground) state we use the rescaled operators, which encode the information of the new spectrum. However, since the change brought by the Luttinger parameter involves only the excitations, the vacuum state remains unchanged. Let us begin with the transverse correlation $\left\langle \hat{S}_z^n \hat{S}_z^m \right\rangle$. Using Eq. 3.13, we get

$$\begin{aligned}
\hat{S}_n^z \hat{S}_m^z &= \left(\frac{1}{\sqrt{\pi}}\partial_x \hat{\hat{\Phi}}(x) + (-1)^n \hat{\hat{M}}(x) - \frac{1}{2}\right)\left(\frac{1}{\sqrt{\pi}}\partial_y \hat{\hat{\Phi}}(y) + (-1)^m \hat{\hat{M}}(y) - \frac{1}{2}\right) \\
&= \frac{1}{\pi}\partial_x \hat{\hat{\Phi}} \partial_y \hat{\hat{\Phi}} + (-1)^{m-n} \hat{\hat{M}}(x)\hat{\hat{M}}(y) \\
&+ \frac{(-1)^n}{\sqrt{\pi}} \hat{\hat{M}}(x)\partial_y \hat{\hat{\Phi}} + \frac{(-1)^m}{\sqrt{\pi}} \partial_x \hat{\hat{\Phi}} \hat{\hat{M}}(y) - \frac{1}{2\sqrt{\pi}}\left(\partial_x \hat{\hat{\Phi}} + \partial_y \hat{\hat{\Phi}}\right) \\
&- \frac{(-1)^n}{2}\hat{\hat{M}}(x) - \frac{(-1)^m}{2}\hat{\hat{M}}(y) + \frac{1}{4}.
\end{aligned} \tag{3.24}$$

Most of these terms vanish: the second line is composed of exclusively odd powers of $\hat{\Phi}$, leading to the expected value of odd numbers of bosonic operators which is zero. On the other hand, the third line is composed of a constant that is irrelevant to the information we pursue, and two terms linear on the magnetization field. These two terms can be traced back to processes such as $\hat{\psi}_R^\dagger \hat{\psi}_L$ that do not conserve the number of particles per branch. Neglecting those processes, we are left with two terms, whose expected values are calculated in appendix A. The first is called *universal* and, to first order in δ, it is

$$\frac{1}{\pi}\left\langle \partial_x \hat{\tilde{\Phi}} \partial_y \hat{\tilde{\Phi}} \right\rangle = \frac{-1}{2\pi^2 K (x-y)^2}, \tag{3.25}$$

using the result of Eq. A.9. The second term is the *staggered* term of the correlation and, to first order, is equal to

$$\hat{\tilde{M}}(x)\hat{\tilde{M}}(y) = \frac{1}{2\pi^2 (x-y)^{2/K}}, \tag{3.26}$$

in accordance to Eq. A.12.

Finally, by taking the anisotropy of the Heisenberg Hamiltonian to be small, $\Delta << 1$, we approximate $K^{-1} \approx (1 + 2\Delta/\pi)$. Therefore, the complete transverse correlation is

$$\left\langle \hat{S}_n^z \hat{S}_m^z \right\rangle = \frac{-1}{2\pi^2 K (x-y)^2} + (-1)^{(m-n)} \frac{1}{2\pi^2 (x-y)^{2/K}}. \tag{3.27}$$

Depending on the sign of Δ, different behaviors are observed:

- $\Delta > 0$: $K^{-1} < 1$ and the universal term dominates. This leads to a ferromagnetic (FM) bias, where all spins tend to be aligned. This corresponds to the fact that a positive J_z means that minimal energy is achieved through aligning.
- $\Delta < 0$: $K^{-1} < 1$ and the staggered term dominates. This leads to an antiferromagnetic (AF) bias in the chain, where adjacent spins tend to anti-align. Again, this is to be expected, since a negative J_z implies that opposite alignments minimize the energy.

At $\Delta = 0$, there is no transverse coupling and the model becomes the isotropic planar spin chain. Notice that these results, graphed in Fig. 3.1(a,b), are only valid for $\Delta << 1$; for stronger anisotropies we would need to keep more terms at each step of the process, and the functional form of $K(\Delta)$ changes correspondingly. Also notice that within the range of validity of our results, the correlations quickly decay away, meaning that the chain remains in a critical state, not fully FM or AF. This system can be solved exactly using the Bethe ansatz, as in Ref. [31], where they find the full phase diagram, showing the mentioned criticality, as well as the transitions and symmetric points.

However, although our perturbative treatment is limited, it is worth noting one important aspect regarding the increase of Δ. At $\Delta > \pi/4$, the Luttinger parameter as formulated becomes imaginary. Clearly, this is not physical and is evaded by a careful analysis with other methods [31, 57, 58], showing that in the large-anisotropy regime, the chain exhibits FM ordering, which is also confirmed by the literature. Thus, as pointed out by Schulz in Ref. [59], an imaginary Luttinger parameter in the context of spin chains corresponds to a FM phase, allowing us to further describe the phase diagram of the system with our bosonization approach.

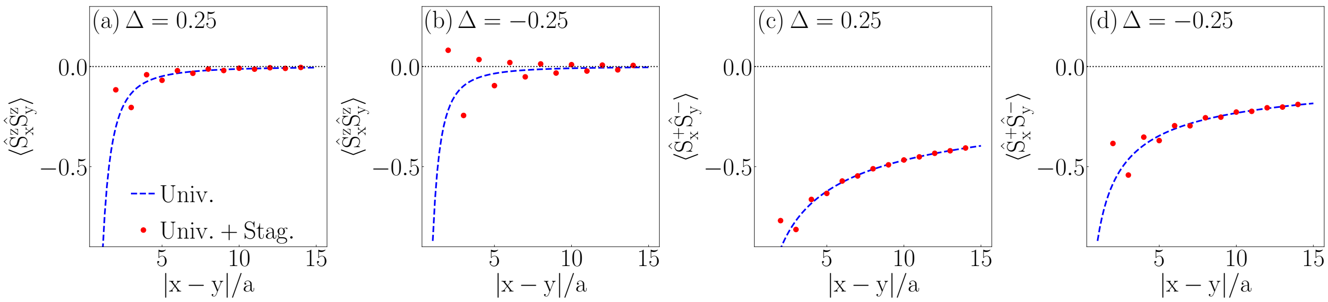

Figure 3.1: (a,b) Transverse and (c,d) planar correlations. Two Luttinger parameters are plotted for each one, showing the quickly decaying transverse correlation, and the quasi-long-range planar correlations, with oscillating perturbations.

It is of utmost importance to mention here that in one dimension, any ordering must come from an explicit asymmetry in the Hamiltonian. As opposed to higher dimensions, where a spontaneous break of a symmetry leads to long-range order, the strong collective fluctuations of one-dimensional systems disrupt this ordering. This is reflected in the Hohenberg-Mermin-Wagner theorem [60]. Therefore, it is necessary to keep this in mind when we discuss phases of chains, since often times, an ordering is at most quasi-long range, that is, a slow algebraic decay of correlations. Alternatively, a quasi-long range order implies that a small external coupling, say to other chains, induces an inmediate ordering; in other words, when we speak of an ordered chain we are referring to the most favorable ordering that it would adopt if it were not for its one-dimensional nature [35].

To round off our study of the XXZ Heisenberg Hamiltonian, we can calculate the planar correlation $\langle \hat{S}^+_n \hat{S}^-_m \rangle$ in a very similar way. The first step is to transform the spin ladder operators using the Jordan-Wigner transform and the fundamental bosonization identity. Although, the string operator, which counts the number of fermions before a site, might look apprehensively difficult, we can express it in terms of the fields by

$$\begin{aligned} \sum_0^{n-1} \hat{\psi}_k^\dagger \hat{\psi}_k &= \sum_0^{n-1} \left(:\hat{\psi}_k^\dagger \hat{\psi}_k: + \frac{n-1}{2} \right) \\ &= \frac{n}{2} + \frac{1}{\sqrt{\pi}} \int_0^{na} \mathrm{d}x\, \hat{\Phi}, \end{aligned} \tag{3.28}$$

where, in the first line, we used the fact that we are working at half-filling to find the expected value of the vacuum, and in the second line we can make the approximation $n-1 \approx n$, which becomes exact in the continuous limit. If we set $\hat{\Phi}(0) = 0$, the string operator becomes

$$e^{\sum_0^{n-1} \hat{\psi}_k^\dagger \hat{\psi}_k} = e^{i\sqrt{\pi}\hat{\Phi}} e^{i\pi n/2}. \tag{3.29}$$

Even if we had set $\hat{\Phi}(0)$ to some other value, it would only change the previous equation by a constant phase. Notice that this identity is completely in agreement with the interpretation of the fields we presented in Sec. 2.5: the number of charges between two points is the height of the counting (position) field, divided by the height of each kink. Furthermore, the vacuum expected value makes the expression exact.

We now use the bosonization identity to reach a full expression for $\hat{S}_n^+\hat{S}_m^-$ in terms of the bosonic fields, remembering to avoid the chiral fields for their non-trivial transformations, shown in Eq. 3.23. What we obtain is

$$\begin{aligned} \hat{S}_+^n\hat{S}_-^m &= \frac{1}{2\pi a}\Big(e^{i\sqrt{\pi}(\hat{\theta}(x)-\hat{\theta}(y))} + (-1)^{m-n}e^{i\sqrt{\pi}(2(\hat{\Phi}(x)-\hat{\Phi}(y))+\hat{\theta}(x)-\hat{\theta}(y))} \\ &- (-1)^m e^{-i\sqrt{\pi}(2\hat{\Phi}(y)+\hat{\theta}(y)-\hat{\theta}(x))} - (-1)^n e^{i\sqrt{\pi}(2\hat{\Phi}(x)+\hat{\theta}(x)-\hat{\theta}(y))}\Big), \end{aligned} \tag{3.30}$$

where the terms in the second line come from short wavelength processes that do not conserve the chiral particles and can thus be disregarded. Additional rigourous reasons for neglecting these terms can be found in chapter 6 of Ref. [35]. Next, we rescale all the fields according to Eq. 3.22 and apply the now familiar exponential identity of Eq. B.9 to calculate the correlation function. The quadratic correlations that need to be determined are

$$\begin{aligned} \left\langle \hat{\tilde{\theta}}(x)\hat{\tilde{\theta}}(y) \right\rangle &= \sum_{p,q} \frac{\operatorname{sgn}(pq)}{2L\sqrt{|pq|}} e^{ipx}e^{-iqy}\left\langle \hat{b}_p\hat{b}_q^\dagger \right\rangle \\ &= \frac{1}{4\pi}\int \mathrm{d}p\, \frac{1}{|p|}e^{ip(x-y)}e^{-\delta|p|}, \end{aligned} \tag{3.31}$$

which is the same as the integral in Eq. A.13. The other correlation required is

$$\begin{aligned} \left\langle \hat{\tilde{\Phi}}(x)\hat{\tilde{\theta}}(y) \right\rangle &= \sum_{p,q} \frac{\operatorname{sgn} p}{2L\sqrt{|pq|}} e^{ipx}e^{-iqy}\left\langle \hat{b}_p\hat{b}_q^\dagger \right\rangle \\ &= \frac{1}{4\pi}\int \mathrm{d}p\, \frac{1}{p}e^{ip(x-y)}. \end{aligned} \tag{3.32}$$

Both integrals can be solved using the results of appendix A, yielding

$$\begin{aligned} \left\langle \hat{\tilde{\theta}}(x)\hat{\tilde{\theta}}(y) \right\rangle &= \frac{-K}{4\pi}\ln\big((x-y)^2+\delta^2\big) \\ \left\langle \hat{\tilde{\Phi}}(x)\hat{\tilde{\theta}}(y) \right\rangle &= \frac{-i}{4}\operatorname{sgn}(x-y). \end{aligned} \tag{3.33}$$

Putting everything together, the planar correlation is

$$\left\langle \hat{S}_n^+\hat{S}_m^- \right\rangle \propto \frac{1}{(x-y)^{K/2}} + (-1)^{m-n}\frac{1}{(x-y)^{2(1/K+K/4)}}, \tag{3.34}$$

in accordance with the results in the literature [37, 56]. What can be seen is a FM quasi-long-range ordering in the plane, whose fluctuations are intesified for $\Delta < 0$, as shown in Fig. 3.1(c,d).

Although we are using one-dimensional spin-$\frac{1}{2}$ systems as a training ground for our main goal of spin-1, it is worth emphasizing that there is a vast sea of excellent research in this topic, studying from the ground state properties as we did, to the dynamical and transport properties of the systems. These studies are of great value to contemporary fundamental many-body physics, and to technological innovations. In order to exemplify the importance and interest of spin-$\frac{1}{2}$ physics, we present appendix G, where we investigate the transport properties of spin-$\frac{1}{2}$ electrons on a classical spin lattice. We are delighted to discuss there the paralels between that system and the main themes of our central work.

3.2 Bosonization of bosons

Bosonization seems to imply the reformulation of fermions in terms of bosons, and the framework developed to introduce the technique in the previous chapter is in accordance with that understanding. However, the name comes from the fact that it was introduced both in condensed matter and high-energy physics for this purpose [40, 41, 43], whereas in actuality, it has a wider range of applicability. The nature of the technique is tightly linked with dimensionality: in one spatial dimension interacting particles, irrespective of statistics, are forced to bump into each other. Just as was shown in Sec. 2.7, the eigenstates of interacting fermions in one dimension are collective excitations of the system caused by the inevitability of collision and propagation of fluctuations in a wire. Even free fermions exhibit this property, having a spectrum composed of particle-hole excitations equivalent to phonons at low energy; this is due to the Pauli exclusion principle acting as a repulsive interaction.

Interacting bosons in one dimension are subject to this same collectivity and for the same reason. As such, it is possible to formulate an effective theory for their low-energy behavior that stays within the field-theoretic framework developed thus far. Although free bosons require special treatment, due to Bose-Einstein condensation at low temperatures, we know from bosonic hydrodynamic approaches [61–64] that the appropriate variables are the density $\hat{\rho}(x)$ and the phase $\hat{\theta}(x)$. In the low-energy regime, the density can be expressed in terms of the fluctuations around the average density, meaning that $\hat{\rho}(x) = \bar{\rho} + \partial_x \hat{\Phi}/\sqrt{K}$, which is constructed to look analogous to Eq. 2.43. With this in mind, the bosonic field operators can be formulated as

$$\hat{a}^\dagger(x) = \sqrt{\rho_0 + \frac{1}{\sqrt{K}}\partial_x \hat{\Phi}}\; e^{i\sqrt{K}\hat{\theta}}, \tag{3.35}$$

where in order to get the appropriate units we must keep track of a factor of $\sqrt{a}$. In order to satisfy the commutation relations imposed by the statistics of the particles, $\left[\hat{a}(x), \hat{a}^\dagger(y)\right] = \delta(x-y)$, the following must hold:

$$e^{-i\sqrt{K}\hat{\theta}(x)}\sqrt{\hat{\rho}(x)}\sqrt{\hat{\rho}(y)}e^{-i\sqrt{K}\hat{\theta}(y)} - \sqrt{\hat{\rho}(y)}e^{-i\sqrt{K}\hat{\theta}(y)}e^{-i\sqrt{K}\hat{\theta}(x)}\sqrt{\hat{\rho}(x)} = \delta(x-y). \tag{3.36}$$

A sufficient condition to fulfill this commutation is [35]

$$e^{-i\sqrt{K}\hat{\theta}(y)}\hat{\rho}(x)e^{i\sqrt{K}\hat{\theta}(y)} - \hat{\rho}(x) = \delta(x-y), \tag{3.37}$$

which is equivalent to $\left[\hat{\rho}(x), e^{i\sqrt{K}\hat{\theta}(y)}\right] = e^{i\sqrt{K}\hat{\theta}(x)}\delta(x-y)$. Using the identity of Eq. B.5, we obtain that

$$\begin{aligned} i\sqrt{K}\left[\hat{\rho}(x), \hat{\theta}(y)\right]e^{i\sqrt{K}\hat{\theta}(x)} &= e^{i\sqrt{K}\hat{\theta}(x)}\delta(x-y) \\ \left[\partial_x\hat{\Phi}, \hat{\theta}(y)\right] &= -i\delta(x-y) \\ \left[\hat{\Phi}, \partial_y\hat{\theta}\right] &= i\delta(x-y), \end{aligned} \tag{3.38}$$

where after integrating and differentiating the second line, we retrieve the same canonical commutation relations as the fields defined in Eq. 2.38, recalling that $\hat{\Pi} = \partial_x\hat{\theta}$. The similarities between the low-energy effective field theories for fermions and bosons are not just formal correspondences of notation; the same bosonic fields that were found to describe fermions in Ch. 2, work just as well for bosons [36].

Although the derivation of what is essentially the fundamental bosonization identity for bosons might seem heuristic in the way presented here, the arguments hold under more rigorous scrutiny, and can be reviewed in Refs. [35, 36], where further discussions regarding short and long-wavelength fluctuations present in the low energy regime can also be found. In this work, we use the formulation expressed in Eq. 3.35, which describes long-wavelength fluctuations around the average density of the system.

3.2.1 Bosons on a lattice

Consider the Hamiltonian for free bosons on a lattice

$$\hat{H}_0 = -t\sum\left(\hat{a}_i^\dagger\hat{a}_{i+1} + \text{h. c.}\right). \tag{3.39}$$

Using Eq. 3.35, we can calculate

$$\begin{aligned} \hat{a}_i^\dagger\hat{a}_{i+1} &= \sqrt{\bar{\rho} + \frac{1}{\sqrt{K}}\partial_x\hat{\Phi}}e^{i\sqrt{K}\hat{\theta}(x)}e^{-i\sqrt{K}\hat{\theta}(x+a)}\sqrt{\bar{\rho} + \frac{1}{\sqrt{K}}\partial_x\hat{\Phi}(x+a)} \\ &= \bar{\rho}\left(1 + \frac{1}{2\bar{\rho}\sqrt{K}}\partial_x\hat{\Phi}\right)\exp\left(-i\sqrt{K}a\partial_x\hat{\theta}\right)\left(1 + \frac{1}{2\bar{\rho}\sqrt{K}}\partial_x\hat{\Phi}\right), \end{aligned} \tag{3.40}$$

where we keep in mind our point-splitting scheme for lattices. At unit filling, we can express $\rho_0 = a^{-1}$; with this in mind we can keep terms up to first order in a, such that

$$\hat{a}_i^\dagger\hat{a}_{i+1} = \hat{\rho}(x) - \frac{aK}{2}\Pi^2 + \frac{a}{4K}\left(\partial_x\hat{\Phi}\right)^2 + (\text{imaginary part}). \tag{3.41}$$

Adding the hermitian conjugate, the bosonized free Hamiltonian is

$$\hat{H}_0 = \frac{at}{\sqrt{2}} \int \mathrm{d}x \, \hat{\Pi}^2 - \left(\partial_x \hat{\Phi}\right)^2, \tag{3.42}$$

where the $K = 1/\sqrt{2}$, so that the fields are scaled appropriately, and the velocity is rescaled as at. Notice that there is a key difference between the Hamiltonian of Eq. 3.42 and that of Eq. 2.42: the minus sign is of crucial importance. To see why, let us express the Hamiltonian in terms of its modes. First,

$$\begin{aligned} \int \mathrm{d}x \, \hat{\Pi}^2 &= -\int \mathrm{d}x \sum_{p,q} \frac{\sqrt{|pq|}}{2L} \left(e^{ix(p+q)} \hat{b}_p \hat{b}_q + e^{-ix(p+q)} \hat{b}_p^\dagger \hat{b}_q^\dagger - e^{ix(p-q)} \hat{b}_p \hat{b}_q^\dagger - e^{-ix(p-q)} \hat{b}_p^\dagger \hat{b}_q \right) \\ &= -\sum_p \frac{|p|}{2} \left(\hat{b}_p \hat{b}_{-p} + \hat{b}_p^\dagger \hat{b}_{-p}^\dagger - \hat{b}_p \hat{b}_p^\dagger - \hat{b}_p^\dagger \hat{b}_p \right). \end{aligned} \tag{3.43}$$

Similarily,

$$\begin{aligned} \int \mathrm{d}x \left(\partial_x \hat{\Phi}\right)^2 &= -\int \mathrm{d}x \sum_{p,q} \frac{\sqrt{|pq|}}{2L} \operatorname{sgn}(pq) \left(e^{ix(p+q)} \hat{b}_p \hat{b}_q + e^{-ix(p+q)} \hat{b}_p^\dagger \hat{b}_q^\dagger \right. \\ &\quad \left. - e^{ix(p-q)} \hat{b}_p \hat{b}_q^\dagger - e^{-ix(p-q)} \hat{b}_p^\dagger \hat{b}_q \right) \\ &= \sum_p \frac{|p|}{2} \left(\hat{b}_p \hat{b}_{-p} + \hat{b}_p^\dagger \hat{b}_{-p}^\dagger + \hat{b}_p \hat{b}_p^\dagger + \hat{b}_p^\dagger \hat{b}_p \right). \end{aligned} \tag{3.44}$$

In the case of free fermions, by adding the two equations we retrieve the diagonal Hamiltonian of Eq. 2.37. For bosons, however, substracting means that

$$\hat{H}_0 = \frac{-at}{\sqrt{2}} \sum_{p \neq 0} |p| \left(\hat{b}_p \hat{b}_{-p} + \hat{b}_p^\dagger \hat{b}_{-p}^\dagger \right). \tag{3.45}$$

Although it might seem that a Bogoliubov transformation can be applied as in Sec. 2.7, since this is essentially a complex rotation in Hilbert space, and there is no diagonal term in the Hamiltonian for us to rotate into, it is to be expected that this method should not work. Incidentally, performing a Bogoliubov transformation on this Hamiltonian would be exactly as in Sec. 2.7, except that $\alpha_p = 0$; as such, the equation that defines the complex angles φ_p becomes $\beta_p \cosh(2\phi_p)$ which has no solution.

We have shown what was briefly mentioned at the beginning of the chapter: the low energy dynamics of free bosons cannot be described by individual modes, since there is nothing preventing them from collapsing into a Bose-Einstein condensate. This can be clearly seen in the bosonized Hamiltonian, since the term $-(\partial_x \hat{\Phi})^2$ represents an *attractive force* as expected. Alternatively, as mentioned in Sec. 3.1, this is equivalent to an imaginary Luttinger parameter, which signifies a break of the continuum limit [59]. What is required is a repulsive interaction so that the bosons do not collapse, and on the contrary, inevitably bump into each other to create the collective excitations that bosonization describes so well.

For the purposes of this work, we will consider bosons interacting through a repulsive contact potential. This type of interaction is very common in atomic physics, as it is the limitting case of s-wave scattering [65], and is a very useful simplification to describe low-energy collisions between particles. In this approximation, two particles interact when they are in the same point in space; on a lattice, interaction happen when a site is occupied by multiple bosons. With this in mind, the two-body potential term that is added to the Hamiltonian is

$$\hat{V} = \frac{g}{2}\sum_i \hat{a}_i^\dagger \hat{a}_i \hat{a}_i^\dagger \hat{a}_i, \tag{3.46}$$

where the interaction strength g is proportional to the scattering length of the system. Since this is density-density interaction, it is straightforward to express it in terms of the bosonized fields as

$$\hat{V} = \frac{ag}{\sqrt{2}} \int \mathrm{d}x \left(\partial_x \hat{\Phi}\right)^2, \tag{3.47}$$

leading to the complete, bosonized Hamiltonian

$$\hat{H} = \frac{u}{\sqrt{2}} \int \mathrm{d}x \, \frac{1}{K}\hat{\Pi}^2 + K\left(\partial_x \hat{\Phi}\right)^2, \tag{3.48}$$

where $u = a\sqrt{t(g-t)}$ is the phase-velocity of the excitations and $K = \sqrt{g/t - 1}$ is the Luttinger parameter [36]. As long as both of these values are real, bosonization works.

It is important to remember at this point that this is an effective field theory, characterized by phenomenological parameters. Even the interaction strength g is an empirical description of the detailed microscopic processes. As such, the values of all these variables are renormalized as the relevant scales of the system change. Often, for a specific model it is difficult to determine the exact functional relationship of the parameters and the microscopic variables. When possible, this can be found with other methods of one-dimensional systems, such as the Bethe-ansatz [31]. Other times, however, bosonization only allows for an accurate description of a system in the neighborhood of a known point in parameter space unless more advanced methods like renormalization group are employed. Thus, the precise values that phenomenologically characterize a bosonized systems are closely dependent on the energy scales of the detailed microscopic model, and each regime requires special treatment.

3.2.2 Hard-core bosons

To exemplify how the parameters of the system can change depending on the specific microscopic description, consider interacting bosons in a lattice with $g \to \infty$. Contrary to what could be expected from the functional form of u and K that were found at the end of the previous section, the momentum term in the Hamiltonian does not vanish. Instead, we need to analyze how the system behaves in this regime: since the energy cost for multiple occupancy is so high, it will be impossible for particles to share a site. This is reminiscent of fermionic Pauli exclusion, which led to Girardeau's 1960 proof of the direct map between infinitely repulsive bosons and free fermions [66]. It was shown that the many-body wavefunctions that describe both systems are identical, except for a space-dependent phase that ensures appropriate symmetry. This translates easily to a second-quantized formalism, where the relationship between bosons and fermions is given by the Jordan-Wigner transformation (see appendix C), yielding

$$\hat{a}_j = e^{-i\pi t_j}\hat{c}_j, \tag{3.49}$$

where we are following our convention of bosons as $\hat{a}$ and fermions as $\hat{c}$, and $t_j = \sum_{K=0}^{j-1}\hat{n}_k$ is the string operator that ensures the right phase for correct commutation. Incidentally, this also means that hard-core bosons can be mapped directly into a lattice of spins-$\frac{1}{2}$, so we can use a lot of the work done in Sec. 3.1.1 to reformulate the system. For instance, from Eq. 3.5, we know instantly that the Hamiltonian maps into

$$\hat{H} = -t\sum\left(\hat{c}_i^\dagger\hat{c}_{i+1} + \mathrm{h.\,c.}\right) + \frac{g}{2}\sum\hat{c}_i^\dagger\hat{c}_i\hat{c}_i^\dagger\hat{c}_i, \tag{3.50}$$

where $\hat{c}_i$ are fermionic operators. However, since double occupancy is forbidden, the second term is exactly zero, which means

$$\hat{H} = -t\sum\left(\hat{c}_i^\dagger\hat{c}_{i+1} + \mathrm{h.\,c.}\right) \tag{3.51}$$

showing that our original claim is indeed true, and hard-core bosons are equivalent to free fermions.

This is now easily bosonized, since all the work was again done in the previous chapter. In particular, from Eq. 3.10 we know that the Hamiltonian describing low-energy, long-wavelength excitations is

$$\hat{H} = \frac{at}{2}\int \mathrm{d}x\,\hat{\Pi}^2 + \left(\partial_x\hat{\Phi}\right)^2, \tag{3.52}$$

showing that the Luttinger parameter for hard-core bosons is $K = 1$. This breaks from the functional form found in Eq. 3.48, where if $K = \sqrt{g/t - 1}$ for all energy scales, we would expect that in the infinitely repulsive limit K would diverge. Clearly, this is not the case as increasing the interaction strength leads to a renormalization of the phenomenological parameters in non-trivial ways. For instance, it was shown in Ref. [67] that the interaction potential energy per boson only increases with g in a limited range; as g grows there comes a point for which the repulsion is so strong that the interaction energy per particle starts to decrease as particles avoid each other. This change towards a more kinetically dominated system is the reason why in the limit, hard-core bosons become equivalent to free fermions. As such, it is to be expected that K should also have a non-trivial behavior as the interaction strength is increased drastically.

Having bosonized the one-dimensional hard-core bosons, we can calculate the density-density correlation, and the single particle density matrix of the system. Once more borrowing from work done in the previous chapter, we get for the former

$$\langle \hat{\rho}(x)\hat{\rho}(y)\rangle \propto \frac{-1}{(x-y)^2} + (-1)^{(m-n)}\frac{1}{(x-y)^2}, \tag{3.53}$$

in accordance with Eq. 3.27, and for the latter

$$\left\langle \hat{a}^\dagger(x)\hat{a}(y)\right\rangle \propto \frac{1}{(x-y)^{1/2}} + (-1)^{m-n}\frac{1}{(x-y)^{5/2}}, \tag{3.54}$$

in accordance with Eq. 3.34. These results agree with those found in Ref. [36] in the Girardeau limit up to the first oscillating term.

Having studied the applications of bosonization to lattice spin systems and bosonic systems, we are ready to tackle our desired spin-1 in the next chapter. Using our bosonization for bosons approach, it will be possible to formulate an effective field theory for a general spin-1 gas in a lattice, whereas the lessons learned from localized spin-$\frac{1}{2}$ particles will guide us in further treatment of chains of $S = 1$.

4
Spin-1 physics

After constructing the theoretical framework of bosonization, and having toyed with some relatively simple models found in the literature, let us turn our look towards the main goal of this work, which is the application of bosonization to a one-dimensional gas of spin-1 bosons. In accordance with this, the next step is the formulation of the relevant Hamiltonian; however, we will first investigate the physics of spin-1 particles, as the inclusion of this degree of freedom entails more than a simple addition of a sub-index. For a brief description of spin, its place in non-relativistic quantum mechanics, algebraic properties, and explicit forms for spin-1 operators, we present appendix D as reference.

4.1 Spin-1 Hamiltonian

To understand the physics of a spin-1 system, we must begin with the appropriate Hamiltonian. The easiest part to write down is the kinetic term. On a deep, one-dimensional lattice, particles are bound to the lowest energy level of every site, and movement is achieved through tunneling into adjacent sites. Thus, the free term in the lattice Hamiltonian [22] is

$$\hat{H}_0 = -t \sum_{i,\sigma} \left(\hat{a}^\dagger_{i+1,\sigma} \hat{a}_{i,\sigma} + \hat{a}^\dagger_{i,\sigma} \hat{a}_{i+1,\sigma} \right), \tag{4.1}$$

where $\hat{a}_{i,\sigma}$ is the annihilation operator for a boson in site i and spin projection $\sigma = \pm 1, 0$, and t is the hopping parameter.

In order to formulate the interaction potential energy, we must consider a binary interaction between two spin-1 bosons [68, 69]. The spin degree of freedom of the two particles can be described by the coupled basis obtained from the addition of angular momentum (see appendix D), so that the Hilbert space of two colliding bosons is spanned by the states of Eq. D.24. However, since bosons are symmetric under permutations, only the states of total $S = 2$ and $S = 0$ are physical. These allowed subspaces are called interaction channels, since the collision process can only happen through a superposition of the following states, which respect the symmetry of the particles and where the subscript c specifies the coupled basis:

$$
\begin{aligned}
&|2,\quad 2\rangle_c = |1,1\rangle && |2,\quad 1\rangle_c = \frac{1}{\sqrt{2}}(|1,0\rangle + |0,1\rangle) \\
&|2,\quad 0\rangle_c = \frac{1}{\sqrt{6}}(|1,-1\rangle + 2\,|0,0\rangle + |-1,1\rangle) && |2,-1\rangle_c = \frac{1}{\sqrt{2}}(|-1,0\rangle + |0,-1\rangle) \\
&|2,-2\rangle_c = |-1,-1\rangle && |0,\quad 0\rangle_c = \frac{1}{\sqrt{3}}(|1,-1\rangle - |0,0\rangle + |-1,1\rangle).
\end{aligned}
\tag{4.2}
$$

The coupled states are $|S,m\rangle_c$ with quantum numbers S and m, total spin and total magnetic projection, respectively; and the uncoupled states are $|m_1,m_2\rangle$ with quantum numbers m_1 and m_2 the corresponding magnetic projections of each spin.

For low energies, we restrict our attention to s-wave scattering [70], which can be approximated by a contact pseudopotential of interaction [65], in which particles scatter off each other when occupying the same position. Since the interaction channels are linearly independent, the potential energy for two spin-1 bosons can be written as

$$\hat{v} = \sum_S g_S \hat{P}_S \delta(r_2 - r_1), \tag{4.3}$$

where $g_S = 4\pi\hbar^2 a_S/\mathrm{m}$, a_S and $\hat{P}_S$ are the scattering lengths and projectors for each channel S, and m is the mass of the boson. This expression can be further determined by first considering the identity

$$\hat{\mathbf{S}}_1 \cdot \hat{\mathbf{S}}_2 = \frac{1}{2}\Big(\hat{\mathbf{S}}_2 - \hat{\mathbf{S}}_1^2 - \hat{\mathbf{S}}_2^2\Big). \tag{4.4}$$

Our notation is as follows: the total spin operator is $\hat{\mathbf{S}} = \hat{\mathbf{S}}_1 + \hat{\mathbf{S}}_2$, where the subscript indicates the particle to which the operator corresponds. Because of the linear independence, we can use the interaction channels as a base for the space of linear operators acting on the two particles, yielding the decomposition

$$\hat{\mathbf{S}}_1 \cdot \hat{\mathbf{S}}_2 = \lambda_0 \hat{P}_0 + \lambda_2 \hat{P}_2. \tag{4.5}$$

Applying $\hat{\mathbf{S}}_1 \cdot \hat{\mathbf{S}}_2$ to the elements of the coupled basis according to the identity of Eq. 4.4, we obtain

$$\hat{\mathbf{S}}_1 \cdot \hat{\mathbf{S}}_2 \,|S,M\rangle_c = \frac{1}{2}(S(S+1) - 4)\,|S,M\rangle_c\,, \tag{4.6}$$

which implies $\lambda_0 = -2$ and $\lambda_2 = 1$. Additionally, the identity operator of the bosonic Hilbert space can be expanded as

$$\hat{I} = \hat{P}_0 + \hat{P}_2, \tag{4.7}$$

allowing us to use Eq. 4.5 to solve for the projectors

$$\hat{P}_0 = \frac{\hat{I} - \hat{\mathbf{S}}_1 \cdot \hat{\mathbf{S}}_2}{3}, \qquad \hat{P}_2 = \frac{2\hat{I} + \hat{\mathbf{S}}_1 \cdot \hat{\mathbf{S}}_2}{3}. \tag{4.8}$$

Having the explicit functional form of the projectors, we can express the interaction operator [71] as

$$\hat{v} = \left(\frac{g_0 + 2g_2}{3} + \frac{g_2 - g_0}{3}\hat{\mathbf{S}}_1 \cdot \hat{\mathbf{S}}_2\right)\delta(r_2 - r_1). \tag{4.9}$$

In this form, the operator gives insight into the process: one term is independent of spin, and is responsible for what is often called *charge* scattering; the other, proportional to $\hat{\mathbf{S}}_1 \cdot \hat{\mathbf{S}}_2$, is responsible for *spin* scattering.

The last term that we take into account in our spin-1 Hamitonian is the coupling to an external magnetic field. The elements that are most often used for the realization of these ultracold spinor gases are alkaline metals, which have a single valence electron and a nuclear spin of 3/2 in their most common and stable isotopes. Examples of Bose-Einstein condensates involving ^{7}Li [72], ^{23}Na [5, 73], ^{39}K [74, 75], and ^{87}Rb [76, 77] are readily available in the literature, and have the aforementioned nuclear spin 3/2 [78]. Therefore, let us define the Hamiltonian [79] for one of these atoms in a magnetic field $B\mathbf{z}$ as

$$\hat{H} = C_{hyp}\hat{\mathbf{s}} \cdot \hat{\mathbf{i}} + g_e \mu_B B \hat{s}^z. \tag{4.10}$$

In the above, C_{hyp} is the hyperfine constant coupling the spin of the valence electron $\hat{\mathbf{s}}$ and the nuclear spin $\hat{\mathbf{i}}$, $g_e \approx 2$ is the electron g-factor, and μ_B is the Bohr magneton. The coupling of the field to the nucleus is neglected as its contribution is negligible compared to the magnetic moment of the electron [79].

This Hamiltonian can be diagonalized analytically, which we do in appendix E. In the absence of field, consider the total spin $\hat{f}^2 = \hat{s}^2 + \hat{i}^2 + 2\hat{\mathbf{s}} \cdot \hat{\mathbf{i}}$, which rearranges to $\hat{H}(B=0) = C_{hyp}(\hat{f}^2/2 - 9/4)$, meaning that the eigenstates of $\hat{f}^2$ diagonalize the system. These are the coupled basis states obtained from the addition of a spin 1/2 and a spin 3/2 particle, calculated in appendix D and shown here:

$$\begin{aligned}
|2,\ \ 2\rangle_c &= \left|\frac{3}{2}, \frac{1}{2}\right\rangle & |2,\ \ 1\rangle_c &= \frac{\sqrt{3}}{2}\left|\frac{1}{2}, \frac{1}{2}\right\rangle + \frac{1}{2}\left|\frac{3}{2}, -\frac{1}{2}\right\rangle \\
|2,\ \ 0\rangle_c &= \frac{1}{\sqrt{2}}\left(\left|-\frac{1}{2}, \frac{1}{2}\right\rangle + \left|\frac{1}{2}, -\frac{1}{2}\right\rangle\right) & |2,-1\rangle_c &= \frac{\sqrt{3}}{2}\left|-\frac{1}{2}, -\frac{1}{2}\right\rangle + \frac{1}{2}\left|-\frac{3}{2}, \frac{1}{2}\right\rangle \\
|2,-2\rangle_c &= \left|-\frac{3}{2}, -\frac{1}{2}\right\rangle & |1,\ \ 1\rangle_c &= \frac{1}{2}\left|\frac{1}{2}, \frac{1}{2}\right\rangle - \frac{\sqrt{3}}{2}\left|\frac{3}{2}, -\frac{1}{2}\right\rangle \\
|1,\ \ 0\rangle_c &= \frac{1}{\sqrt{2}}\left(\left|-\frac{1}{2}, \frac{1}{2}\right\rangle - \left|\frac{1}{2}, -\frac{1}{2}\right\rangle\right) & |1,-1\rangle_c &= \frac{1}{2}\left|-\frac{1}{2}, -\frac{1}{2}\right\rangle - \frac{\sqrt{3}}{2}\left|-\frac{3}{2}, \frac{1}{2}\right\rangle,
\end{aligned} \tag{4.11}$$

where the coupled basis' quantum numbers in $|f, m\rangle_c$ are the total spin f and the total magnetic projection m, and the uncoupled quantum numbers in $|m_i, m_s\rangle$ are the nuclear magnetic projection m_i and the electronic magnetic projection m_s. With the coupled basis, we find a hyperfine shift in the energy $E^{f,m}$ determined by f as $E^{2m} = 3C_{hyp}/4$ and $E^{1,m} = -5C_{hyp}/4$. This shows that it

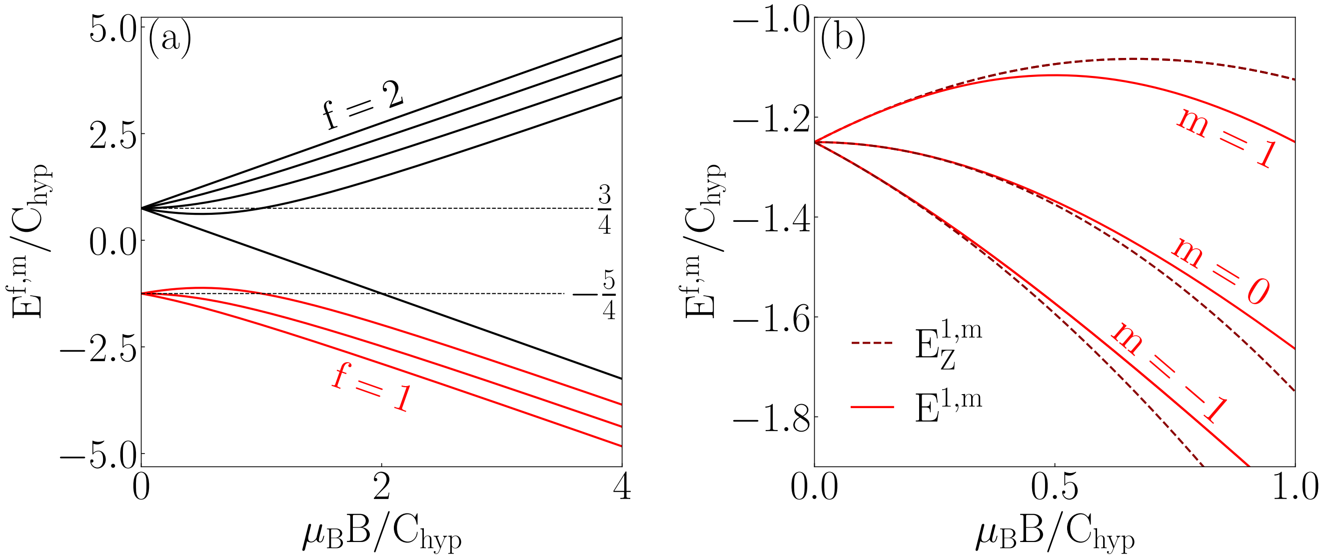

Figure 4.1: Panel (a) shows the exact spectrum as a function of B. Notice at $B = 0$ the hyperfine shifts we obtained analytically. Panel (b) shows the Zeeman splitting for a weak magnetic field in the $f = 1$ subspace, compared to our second order approximation.

is energetically favorable for the atoms to be in an $f = 1$ state, hence why these elements are used in experimental realizations of spin-1 systems.

Now, if we consider $B \neq 0$ it becomes necessary to include $\hat{s}^z$. By inspection, we can see that $|2,2\rangle_c$ and $|2,-2\rangle_c$ are still eigestates of $\hat{s}^z$; although the rest of the states get mixed, the matrix elements ${}_c\langle f,m|\,\hat{s}^z\,|f',m'\rangle_c \propto \delta_{mm'}$ signify a block diagonal reprepresentation where each block corresponds to a particular $m = 0, \pm 1$. By diagonalizing each block separately we obtain the spectrum of the Hamiltonian with Zeeman splitting. This is done in appendix E, yielding for weak field in the $f = 1$ subspace

$$E^Z_{1m} = -\frac{5C_{hyp}}{4} - \frac{\mu_B B}{2}m - \frac{\mu_B^2 B^2}{2C_{hyp}}\left(1 - \frac{m^2}{4}\right), \tag{4.12}$$

where $E^{1,m}_Z$ is a second order expansion of the exact spectrum $E^{1,m}$. By solving numerically, we can show the hyperfine shift and Zeeman splitting of the spectrum and compare it to our result for weak field; this is shown in Fig. 4.1.

Changing back to our usual notation for spin-1 operators, the Zeeman energy is equivalent to an external potential energy

$$\hat{v}_Z = -\sum_{i=1}^{2}\frac{\mu_B B}{2}\hat{S}^z_i - \sum_{i=1}^{2}\frac{\mu_B^2 B^2}{2C_{hyp}}\left(1 - \frac{(\hat{S}^z_i)^2}{4}\right), \tag{4.13}$$

where we considered two particles to make $\hat{v}_Z$ compatible with the interaction potential energy of Eq. 4.9, and neglected constant terms. The first term, the linear Zeeman field, dominates over the second one, the quadratic Zeeman field. However, notice that $\sum_i \hat{S}_i^z$ commutes with the interaction $\hat{v}$; this means that the linear Zeeman field has no effect in the population dynamics induced by the collisions, and thus is superfluous to our analysis. Therefore, we neglect it, as it is often done whenever a balanced population is condsidered in the literature, and keep only the quadratic Zeeman field [79–81].

Finally, in order to generalize our two-particle Hamiltonian to a many-body system, we must express all operators in second quantization [82]. Single-body operators like the quadratic Zeeman field are written as

$$\hat{V}_Z = \sum_{i,j} \langle ij| \, \hat{v}_Z \, |ij\rangle \, \hat{a}_i^\dagger \hat{a}_j, \tag{4.14}$$

whereas two-body operators such as the interaction are written as

$$\hat{V} = \frac{1}{2} \sum_{i,j,k,l} \langle ijkl| \, \hat{v} \, |ijkl\rangle \, \hat{a}_i^\dagger \hat{a}_j^\dagger \hat{a}_l \hat{a}_k, \tag{4.15}$$

where i, j, k, l represent any set of quantum numbers, and the prefactor prevents redundancy in the interaction energies. To calculate the matrix components of the interaction we use the explicit projectors, *i.e.* $\hat{P}_0 = |0,0\rangle_c \langle 0,0|_c$, and find that one obtains

$$\begin{aligned} \hat{H} \;=\; & -t \sum_{i,\sigma} \left(\hat{a}_{i+1,\sigma}^\dagger \hat{a}_{i,\sigma} + \hat{a}_{i,\sigma}^\dagger \hat{a}_{i+1,\sigma} \right) - \mu \sum_{i,\sigma} \hat{n}_{i,\sigma} + Q \sum_{i,\sigma} \sigma^2 \hat{n}_{i,\sigma} \\ & + \sum_i \Bigg(\frac{g_2}{2} \left(\hat{a}_1^\dagger \hat{a}_1^\dagger \hat{a}_1 \hat{a}_1 + \hat{a}_{-1}^\dagger \hat{a}_{-1}^\dagger \hat{a}_{-1} \hat{a}_{-1} + 2 \hat{a}_1^\dagger \hat{a}_0^\dagger \hat{a}_1 \hat{a}_0 + 2 \hat{a}_{-1}^\dagger \hat{a}_0^\dagger \hat{a}_{-1} \hat{a}_0 \right) \\ & + \frac{2g_2 + g_0}{6} \hat{a}_0^\dagger \hat{a}_0^\dagger \hat{a}_0 \hat{a}_0 + \frac{g_2 + 2g_0}{3} \hat{a}_1^\dagger \hat{a}_{-1}^\dagger \hat{a}_{-1} \hat{a}_1 + \frac{g_2 - g_0}{3} \left(\hat{a}_0^\dagger \hat{a}_0^\dagger \hat{a}_1 \hat{a}_{-1} + \hat{a}_1^\dagger \hat{a}_{-1}^\dagger \hat{a}_0 \hat{a}_0 \right) \Bigg)_i , \end{aligned} \tag{4.16}$$

the so called $S = 1$ Bose-Hubbard (BH) Hamiltonian, where the omission or inclusion of the chemical potential μ determines if we are working within the canonical or grand-canonical ensemble, and Q is the coupling to the quadratic Zeeman field. By using special effects like the ac Zeeman effect, whereby tuned microwaves are shone on the spinor gas, this coupling can be precisely varied [83–85].

Notice that although all interactions terms preserve the total spin, there are two distinct types of processes: those that preserve the individual spin projections of the particles ($\hat{a}_1^\dagger \hat{a}_0^\dagger \hat{a}_1 \hat{a}_0$), and those that do not ($\hat{a}_0^\dagger \hat{a}_0^\dagger \hat{a}_1 \hat{a}_{-1}$). This dichotomy is analogous to the abovementioned difference between charge and spin scattering. In fact, if we set $g_0 = g_2$, we get rid of the spin-changing interactions, or equivalently, the spin scattering term in Eq. 4.9, making this a special point that will be discussed further in Sec. 4.3.

4.2 Effective field theory

With the exception of the spin-changing term, the $S = 1$ Bose-Hubbard Hamiltonian is ready for bosonization, since it is formulated as a series of density-density interactions. We will leave out the quadratic Zeeman field for now, and define a pair of canonical fields for each magnetic projection, so that

$$\hat{\rho}_\sigma = \bar{\rho} + \frac{1}{\sqrt{K}} \partial_x \hat{\Phi}_\sigma, \tag{4.17}$$

where $\sigma = 1, 0, -1$. We assume that the ground state is non-magnetized, with equal initial populations of each species. Therefore, the three densities fluctuate around the same average $\bar{\rho}$. Next, recalling the form of the kinetic term in Eq. 3.42, the bosonized spin-preserving terms are

$$\hat{H} = \hat{H}_0^{(1)} + \hat{H}_0^{(0)} + \hat{H}_0^{(-1)} + \frac{\sqrt{2}}{a} \int \mathrm{d}x \begin{pmatrix} \hat{\rho}_1 & \hat{\rho}_0 & \hat{\rho}_{-1} \end{pmatrix} \begin{pmatrix} \frac{g_2}{2} & \frac{g_2}{2} & \frac{g_2+2g_0}{6} \\ \frac{g_2}{2} & \frac{2g_2+g_0}{6} & \frac{g_2}{2} \\ \frac{g_2+2g_0}{6} & \frac{g_2}{2} & \frac{g_2}{2} \end{pmatrix} \begin{pmatrix} \hat{\rho}_1 \\ \hat{\rho}_0 \\ \hat{\rho}_{-1} \end{pmatrix}, \tag{4.18}$$

where a is the lattice constant. Although the Hamiltonian couples all the fields, this can be undone by diagonalizing the interaction matrix [86]; the normalized eigenvectors indicate new fields, defined in terms of superpositions of the magnetic projections, which decouple the Hamiltonian. These are:

$$\begin{aligned} \hat{\Phi}_s &= \frac{1}{\sqrt{2}} \left(\hat{\Phi}_1 - \hat{\Phi}_{-1} \right) \\ \hat{\Phi}_q &= A \left(\hat{\Phi}_1 + \hat{\Phi}_{-1} - \frac{g_0 + 2g_2 + \lambda}{6g_2} \hat{\Phi}_0 \right) \\ \hat{\Phi}_c &= B \left(\hat{\Phi}_1 + \hat{\Phi}_{-1} + \frac{g_0 + 2g_2 - \lambda}{6g_2} \hat{\Phi}_0 \right), \end{aligned} \tag{4.19}$$

where $\lambda = \sqrt{g_0^2 + 4g_0 g_2 + 76 g_2^2}$, and A and B are normalization constants that depend on the two interaction strengths. Let us focus initially on the critical point $g_0 = g_2 = g$, where only spin preserving interactions are non-zero. If we were to move away from the critical point, the new fields would remain unchanged up to first order, so it is convenient to take the critical fields

$$\begin{aligned} \hat{\Phi}_s &= \frac{1}{\sqrt{2}} \left(\hat{\Phi}_1 - \hat{\Phi}_{-1} \right) \\ \hat{\Phi}_q &= \frac{1}{\sqrt{6}} \left(\hat{\Phi}_1 + \hat{\Phi}_{-1} - 2\hat{\Phi}_0 \right) \\ \hat{\Phi}_c &= \frac{1}{\sqrt{3}} \left(\hat{\Phi}_1 + \hat{\Phi}_{-1} + \hat{\Phi}_0 \right), \end{aligned} \tag{4.20}$$

as an adequate formulation. Notice that by decoupling the Hamiltonian, we already begin to extract useful information from the system: the field $\hat{\Phi}_s$ encodes the fluctuations of the spin density, whereas $\hat{\Phi}_c$ does so for the spinless charge. We have retrieved the spin-charge separation that was already briefly discussed, and is so prevalent in spinor gases [71]. Additionally, the field $\hat{\Phi}_q$, which differentiates between $\sigma = 0$ but treats $\sigma = 1, -1$ the same, has to do with the quadrupolar degrees of freedom of the system, a feature that will be explained further in Sec. 4.3. Thus, spin-1 systems in one dimension exhibit spin-charge-quadrupole separation.

Finally, the bosonized uncoupled critical Hamiltonian is

$$\hat{H} = \hat{H}_0^{(s)} + \hat{H}_0^{(q)} + \hat{H}_0^{(c)} + \frac{3ga}{\sqrt{2}} \int \mathrm{d}x \left(\partial_x \hat{\Phi}_c\right)^2, \tag{4.21}$$

where by working with a canonical ensemble, we ignore the chemical potential. As we can see, at the critical point the system only interacts through its charge, leaving the magnetic dependent s and q fields free. On one hand, this shows the veracity of our bosonization procedure, since it is capable of retrieving a property of the system which is well known in the literature [35, 71]. It also allows us to immediately diagonalize the c subspace by renormalizing the fields accordingly, as was done in Sec. 3.1.2. Note that as long as $t \leq 3g$, the net interaction will be a repulsive one, leading to a real Luttinger parameter and a diagonal Hamiltonian. On the other hand, this is not the case for the other two subspaces, s and q, which present the same issues regarding free bosons discussed previously. However, they indicate the existence of two massive free bosonic quasiparticles that are present at low energies. These can be denominated *spinon* and *quadruplon*, and lead us to an effective Hamiltonian

$$\hat{H} = -2t \sum_{k_s} \cos(k_s a) \hat{a}_{k_s}^{(s)\dagger} \hat{a}_{k_s}^{(s)} - 2t \sum_{k_q} \cos(k_q a) \hat{a}_{k_q}^{(q)\dagger} \hat{a}_{k_q}^{(q)} + u \sum_p |p| \hat{b}_p^{(c)\dagger} \hat{b}_p^{(c)}, \tag{4.22}$$

where $u = a\sqrt{t(3g - t)}$. The first two terms are the well-known momentum Hamiltonian for a free tight-binding system, whereas the third one is the contribution from the discrete phonons that becomes manifest due to bosonization, as obtained in Sec. 2.4. This Hamiltonian is diagonal and has a spectrum shown in Fig. 4.2.

As shown by theory [87–91], computation [92–95], and experiment [14, 24], Bose-Hubbard-type Hamiltonians have two distinct phases: the superfluid and the Mott insulator. The superfluid is a charge gapless phase characterized by a macroscopic wavefunction in which particles are delocalized so as to minimize the kinetic energy. It also exhibits long-range phase coherence [14]. On the other hand, the Mott insulator is a gapped phase charaterized by a constant fixed occupation per site, minimizing the interaction potential energy. The phase transition between these two states can be identified by the opening of a gap in the excitation spectrum, which can be seen in our results of Fig. 4.2 when $17t < 3g$. Although this result is not quantitatively decisive due to the nature of the dependence of the Luttinger parameter with the microscopic interactions, it is a qualitative demonstration of the phase transition, since the gap closes for weak interactions, and opens in the opposite limit.

Consider the Mott insulator limit in which $t/g \to 0$; the bands flatten as shown in Fig. 4.2(c), leading to a highly degenerate ground state in the spinon and quadruplon sectors, on top of which

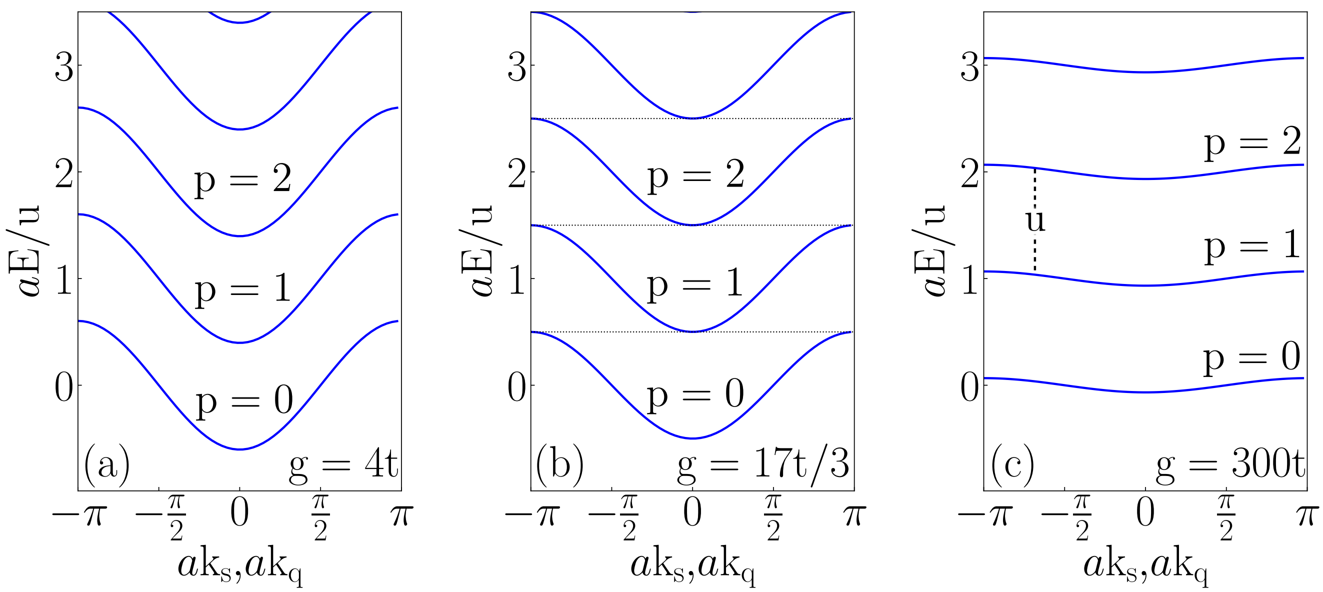

Figure 4.2: Spectrum of the 1D spin-1 gas with $g = g_0 = g_2$. Notice that as the interaction strength is increased from panel (a) to panel (c), a gap opens up, indicative of the superfluid to Mott insulator phase transition. As the energy between excited phonons increases, the spatial degree of freedom is eliminated, characterisc of a Mott insulator.

there are phononic (charge) excitations. Because of the degeneracy, small magnetic interactions are likely to cause the unfolding of novel phases and orderings. Let us now include the magnetic field once again and focus on this case so we may better understand the rich physics of spin-1 magnetism.

In the Mott insulator phase, $t << g$, which means the kinetic contribution to the energy can be treated perturbatively. Since t is the hopping amplitude which determines the tunneling of the wavefunction through each periodic well, a small t is equivalent to an overlap with close neighbors exclusively. Therefore, first order terms represent a localized particle tunneling and interacting with its first neighbor; however, recall that interactions in the $S = 1$ Bose-Hubbard Hamiltonian of Eq. 4.16 are constrained to onsite collisions. This means that in order to be influenced by its first neighbors, a particle must be able to tunnel to an adjacent site and back to the original position around which it is localized. This means that the first non-zero correction due to the kinetic energy is of second order. Furthermore, this reasoning also implies that every odd-order contribution vanishes.

The effective Hamiltonian that takes into account the second order kinetic perturbation in order to focus on the Mott insulator phase can be obtained by means of quasi-degenerate pertubation theory (QDPT) [96], and is calculated explicitely in appendix F. The result obtained in the presence of a quadratic Zeeman field is

$$\hat{H} = -J\sum_i \left(\cos(\Theta)\hat{\mathbf{S}}_i \cdot \hat{\mathbf{S}}_{i+1} + \sin(\Theta)\left(\hat{\mathbf{S}}_i \cdot \hat{\mathbf{S}}_{i+1}\right)^2 + D(\hat{S}_i^z)^2\right), \tag{4.23}$$

known as the bilinear-biquadratic Heisenberg model (BBH), where

$$J = 2t^2\frac{\sqrt{10g_0^2 + 4g_0g_2 + 4g_2^2}}{3g_0g_2} \quad \text{and} \quad \tan\Theta = \frac{g_0 + 2g_2}{3g_0}, \tag{4.24}$$

and Θ takes values in the third quadrant; the intensity of the Zeeman field is $Q = JD$. Notice that under this parametrization, the critical point $g_0 = g_2$ that has been explored so far corresponds to $\Theta = -3\pi/4$ and $D = 0$. Also notice that the Mott insulator regime bounds the parametrization angle such that $[\tan^{-1}(1/3), -\pi/2)$.

4.3 Symmetries of spin-1 systems

In order to elucidate the physics of the spin-1 chain, it is important to first determine the symmetries and possible relevant quantities that a spin-1 system can have. The simplest symmetry is under a $U(1)$ phase shift. Another possible symmetry is under rotations, which are given in Hilbert space by representations of $SU(2)$, as mentioned in appendix D. Since $SU(2)$ is the simplest non-Abelian unitary symmetry, it is worth exploring the way a particle with spin transforms under one of its elements. It can be shown that if $\hat{G} \in SU(2)$ acts on a spin operator, then

$$\hat{G}^\dagger \hat{S}^\alpha \hat{G} = \sum_j R_{\alpha\beta}\hat{S}^\beta, \tag{4.25}$$

where $R_{\alpha\beta}$ are the matrix elements of a Euclidean $SO(3)$ rotation. Furthermore, if we decompose $\hat{R}$ using Euler angles, we find that

$$\text{if } \hat{R} = e^{-i\gamma L_z}e^{-i\varphi L_y}e^{-i\chi L_z} \text{ then } \hat{G} = e^{-i\gamma\hat{S}^z}e^{-i\varphi\hat{S}^y}e^{-i\chi\hat{S}^z}, \tag{4.26}$$

where L_α are the generators of $SO(3)$. This means that the spin vector indeed transforms as a real vector under a rotation in Hilbert space; the real rotation that it undergoes corresponds precisely to the underlying unitary transformation. In this sense, it is perfectly rigorous to refer to the three spin operators as a vector.

If a system is invariant under one of the abovementioned transformations, it will have a number of conserved quantities corresponding to the generators of the symmetry groups. In the case of a rotationally invariant system, these will be the components of the spin vector itself; in the case of the $U(1)$ symmetry, the relevant operator will be a scalar, *i.e.* proportional to the identity. This quantity can be identified with $s(s+1)$, where s is the spin of the particles. In fact, our two conserved quantities so far can be constructed from the spin vector itself, as $s(s+1) = \mathbf{S}\cdot\mathbf{S}$ and $\mathbf{S} = -i\mathbf{S}\times\mathbf{S}$. However, in a spin-1 system, a general unitary transformation is represented by a Hermitian 3×3 matrix that is an element of $SU(3)$, a group with eight generators. Since the identity is not an element of the Lie algebra, we are left with five remaining operators that could still be conserved under a general transformation. Having already constructed a scalar and a vector, these five operators must constitute an object that transforms irreducibly.

The object in question is known as a spherical tensor operator [97], which has components that satisfy

$$\begin{aligned}\left[\hat{S}^{\pm}, \hat{T}_k^q\right] &= \mp\sqrt{(k\mp q)(k\pm q+1)}\hat{T}_k^{q\pm 1} \\ \left[\hat{S}^{z}, \hat{T}_k^q\right] &= q\hat{T}_k^q,\end{aligned} \tag{4.27}$$

where k is the rank of the tensor, and q indexes its $2k+1$ elements. Spherical tensor operators have the property of transforming irreducibly under a rotations due to the similarity between their algebra and that of angular momentum. It can be shown straightforwardly that the conserved scalar and vector are spherical tensors of rank 0 and 1 respectively. Furthermore, the five remaining generators correspond to the five components of a spherical tensor of rank 2. These can be calculated with their defining properties to be

$$\begin{aligned}\hat{T}_2^0 &= \frac{1}{\sqrt{3}}\Big(3(\hat{S}^z)^2 - s(s+1)\Big), \\ \hat{T}_2^{\pm 1} &= \frac{1}{\sqrt{2}}\Big\{\hat{S}^{\pm}, \hat{S}^z\Big\}, \\ \hat{T}_2^{\pm 2} &= \frac{1}{\sqrt{2}}(\hat{S}^{\pm})^2.\end{aligned} \tag{4.28}$$

By studying the possible symmetries of a general spin-1 system, we have obtained the relevant operators with which we can adequately study a particular case. However, we are yet to relate them to the generators of the general $SU(3)$ transformation. Consider the following basis for the $\mathfrak{su}(3)$ Lie algebra:

$$\begin{aligned}
&\lambda^1 = \begin{pmatrix} 0 & 0 & i \\ 0 & 0 & 0 \\ -i & 0 & 0 \end{pmatrix} &&\lambda^2 = \begin{pmatrix} 1 & 0 & 0 \\ 0 & 0 & 0 \\ 0 & 0 & -1 \end{pmatrix} &&\lambda^3 = \begin{pmatrix} 0 & 0 & -1 \\ 0 & 0 & 0 \\ -1 & 0 & 0 \end{pmatrix} \\
&\lambda^4 = \frac{1}{\sqrt{2}}\begin{pmatrix} 0 & -1 & 0 \\ -1 & 0 & 1 \\ 0 & 1 & 0 \end{pmatrix} &&\lambda^5 = \frac{1}{\sqrt{2}}\begin{pmatrix} 0 & i & 0 \\ -i & 0 & i \\ 0 & -i & 0 \end{pmatrix} &&\lambda^6 = \frac{1}{\sqrt{2}}\begin{pmatrix} 0 & i & 0 \\ -i & 0 & -i \\ 0 & i & 0 \end{pmatrix} \\
&\lambda^7 = \frac{1}{\sqrt{2}}\begin{pmatrix} 0 & 1 & 0 \\ 1 & 0 & 1 \\ 0 & 1 & 0 \end{pmatrix} && &&\lambda^8 = \frac{1}{\sqrt{3}}\begin{pmatrix} 1 & 0 & 0 \\ 0 & -2 & 0 \\ 0 & 0 & 1 \end{pmatrix}.
\end{aligned} \tag{4.29}$$

These are related to the conventional generators of $SU(3)$, the Gell-Mann matrices, through a change of basis [98]. Using the λ^α generators, we can express the components of the spherical tensors as

$$\begin{aligned} &\hat{T}_1^0 = \lambda^2 && \hat{T}_1^{\pm 1} = \frac{1}{\sqrt{2}}\big(\lambda^7 \mp i\lambda^5\big) && \\ &\hat{T}_2^0 = \lambda^8 && \hat{T}_2^{\pm 1} = \frac{-1}{\sqrt{2}}\big(\lambda^4 \pm i\lambda^6\big) && \hat{T}_2^{\pm 2} = \frac{-1}{\sqrt{2}}\big(\lambda^3 \pm i\lambda^1\big). \end{aligned} \tag{4.30}$$

From Eqs. 4.29, we can identify the spin-1 matrices, so that $\hat{\mathbf{S}} = (\hat{\lambda}^7,\ -\lambda^5,\ \lambda^2)$ and the rank 1 tensor components correspond to the spin vector. Finally, the remaining generators must be related to physical quantities; this can be achieved by changing the spherical tensor components into their more well-known cartesian counterparts [99]. These will form the traceless symmetric quadrupole tensor [100], given by $\hat{Q}_{ij} = \hat{S}^i\hat{S}^j + \hat{S}^j\hat{S}^i - \frac{s(s+1)}{3}\delta_{ij}$, or in terms of the λ matrices

$$\hat{Q} = \begin{pmatrix} -\hat{\lambda}^3 - \frac{1}{\sqrt{3}}\hat{\lambda}^8 & -\hat{\lambda}^1 & -\hat{\lambda}^4 \\ -\hat{\lambda}^1 & \hat{\lambda}^3 - \frac{1}{\sqrt{3}}\hat{\lambda}^8 & -\hat{\lambda}^6 \\ -\hat{\lambda}^4 & \hat{\lambda}^6 & \frac{2}{\sqrt{3}}\hat{\lambda}^8 \end{pmatrix}. \tag{4.31}$$

These components are often summarized in the literature by means of the so-called quadrupole vector [98, 100, 101], a quintuplet given by $\hat{\mathbf{Q}} = -(\hat{\lambda}^1,\ \hat{\lambda}^3,\ \hat{\lambda}^4,\ \hat{\lambda}^6,\ -\hat{\lambda}^8)$. Even though it is called a vector, it is important to remember that the components of the quadrupole tensor transform as a tensor under rotations [97].

Let us apply what we have learned to the BBH model in which we are interested. The bilinear term is already in terms of adequate operators, leaving the biquadratic term to be reformulated. It can be shown [98] that $\hat{\mathbf{Q}}_n \cdot \hat{\mathbf{Q}}_{n+1} = \hat{\mathbf{S}}_n \cdot \hat{\mathbf{S}}_{n+1} + 2\Big(\hat{\mathbf{S}}_n \cdot \hat{\mathbf{S}}_{n+1}\Big)^2 - 2s(s+1)/3$. Using this identity, the Hamiltonian can be expressed as

$$\begin{aligned} \hat{H} &= -J\sum_i \left(\cos(\Theta)\hat{\mathbf{S}}_i \cdot \hat{\mathbf{S}}_{i+1} + \frac{1}{2}\sin(\Theta)\hat{\mathbf{Q}}_i \cdot \hat{\mathbf{Q}}_{i+1} + D(\hat{S}_i^z)^2\right) \\ &= -\sum_{\alpha,i} J_\alpha \hat{\lambda}_i^\alpha \hat{\lambda}_{i+1}^\alpha - JD\sum_i (\hat{S}_i^z)^2, \end{aligned} \tag{4.32}$$

where $J_\alpha = J(\cos(\Theta) - \sin(\Theta)/2)$ for $\alpha = 2, 5, 7$ and $J\sin(\Theta)/2$ for $\alpha = 1, 3, 4, 6, 8$. In its original form, the BBH model is manifestly rotation invariant, since it is made up of scalar products which are preserved by the transformation. However, in its form of Eq. 4.32 it becomes clear that it can have a greater symmetry: when all the J_α are equal, the Hamiltonian commutes with all the generators of $SU(3)$ transformations acting upon the entire system. These conditions correspond to $(\Theta = -3\pi/4, D = 0)$, the critical point that was explored in the previous section. Therefore, this can be identified with an enhanced symmetric point of phase space which is invariant under full $SU(3)$ rotations.

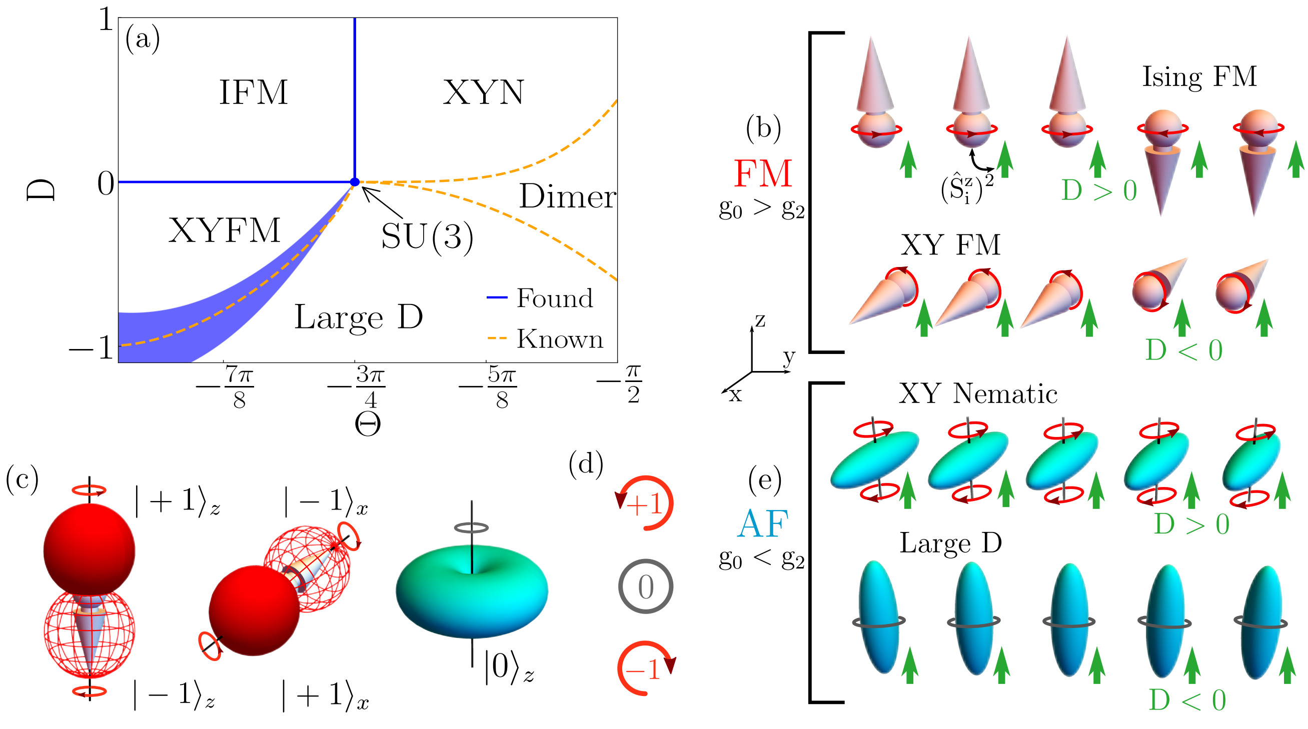

Figure 4.3: (a) shows the phase diagram of the system, where blue lines are phase transitions found with our bosonization approach, whereas orange dashed lines are phase transitions known from the literature, for instance Ref. [39]. In (c), spin-1 states are projected into the coherent spin states basis [102]. Clearly, the $|\pm 1\rangle$ states have a prefered direction, and so we represent them with arrows, as well as with a sense of rotation, shown in (d); $|0\rangle$ has no rotation associated. This convention allows us to produce diagrams for the FM phases, shown in (b). On the other hand, notice that $|0\rangle$ just has a preferred axis, called a director or nematic vector, which we represent as the major axis of an ellipsoid. Finally, (e) shows the diagrams for the AF phases.

4.4 Phases of the spin-1 chain

Spin-1 systems exhibit exotic phases not accessible to more common spin-$\frac{1}{2}$ set-ups. The phase space of the BBH model has been studied thoroughly using computational [39, 103] and theoretical approaches [98, 100]; thus, the physics of the chain is well understood and it's phase diagram [39] is shown in Fig. 4.3. The relevant parameters that determine the phase of the system are the angle Θ and the quadratic Zeeman field D. Let us consider first the influence of Θ: an angle that satisfies $\tan^{-1}(1/3) < \Theta < -\frac{3\pi}{4}$ is achieved for $g_0 > g_2$, leading to a predominance of interactions through the energetically favorable spin-2 channel. As such, this regime favors the spin quintuplet state which is magnetized and a ferromagnetic (FM) ground state. The orientation of the magnetization will be determined by the sign of the magnetic field; $D > 0$ leads to an Ising ferromagnetic (IFM) phase where the axial magnetization is the order parameter, whereas a weak $D < 0$ field induces an XY ferromagnetic (XYFM) phase, because, although it is energetically favorable to adopt a quintuplet ground state, the negative field prevents the system to realize the polarization in the transverse direction. If the field is decreased even more, the internal interactions are not enough to counteract the energetic favorability of the $m = 0$ state, and the systems enters a so-called large-D phase, dominated by high population of the non-magnetized 0 projection. Out of these three phases, the IFM and large-D exhibit *bona fide* long range order since the Hamiltonian is explicitely asymmetric. On the other hand, the XYFM cannot spontaneously break the planar symmetry due to being in one dimension, so it is a quasi-long range ordering.

On the other side of the critical point, $-\frac{3\pi}{4} < \Theta < -\frac{\pi}{2}$ and $g_2 > g_0$. In this case, the system tends towards a spin singlet ground state, which implies null magnetization and an antiferromagnetic ground state (AF). For strong $D < 0$ field, the same large-D phase is realized. Alternatively, a strong $D > 0$ field induces an XY nematic (XYN) phase. This is a novel phase of matter in which the $m = \pm 1$ projections are equally favored, leading the system to be in a superposition of these states. Therefore, the system has no preferred direction, but instead is defined by an axis, or director. This is better described using the so-called cartesian basis [98, 100] of a spin-1 system:

$$|x\rangle = -\frac{1}{\sqrt{2}}(|1\rangle - |-1\rangle), \qquad |y\rangle = \frac{i}{\sqrt{2}}(|1\rangle + |-1\rangle), \quad \text{and} \quad |z\rangle = |0\rangle \,. \tag{4.33}$$

The cartesian basis has a lot of nice properties; for one, it is the basis in which the quadrupolar operators λ^α take the form of the conventional Gell-Mann matrices. It is also a basis in which a rotation in Hilbert space has the same matrix representation as its corresponding real space rotation. Furthermore, it is time reversal invariant. However, the most relevant feature of this basis for the present discussion is the fact that the cartesian states have a null expected value of S^x, S^y, and S^z. Consequently, they enable an adequate description of the nematic phase. If we express these states as a superpositon of coherent spin states [102], so as to assign classical directions to spin-1 states, it becomes clear that there is a determined nematic director and a null magnetization as shown in Fig. 4.3(c). Additionaly, these nematic states are heavily associated with the quadrupolar degrees of freedom [104], and so we expect the relevant order parameters for the XYN phase to be among $\hat{\mathbf{Q}}$. In the XYN phase, the directors lie on the plane but because of the nature of one dimension, it can only be a quasi-long range ordering.

Between the large-D and the XYN phase, there is the dimer phase for small $|D|$. This phase is characterized by a strong coupling between nearest-neighboring spins due to the weak external magnetic field. The neighboring spins exhibit states from the coupled spin basis of Eq. 4.11; in particular, due to $g_2 > g_0$, the singlet state is energetically more favorable and the paired spins adopt the non-magnetized $|0, 0\rangle_c$ ground state. Due to the strong coupling between the particles, this phase is highly entangled and can be studied through the various formulations of entropy [105]. However, this is difficult to do in the bosonization formalism so we will not cover it in this work, and refer to Sec. 5.2 for additional discussion.

4.5 Effective Hamiltonians for the spin chain

Having reviewed the different phases of the system, we will attempt to find them using our bosonization formalism. A good first step would be the determination of appropriate order parameters for each phase. An order parameter is an operator whose expected value is finite within the respective phase, and vanishes elsewhere in parameter space. Thus, a good effective Hamiltonian should be made up of couplings that involve the relevant order parameters we wish to describe.

4.5.1 Ising FM and XY Nematic phases

Consider the IFM, perhaps the simplest phase in our diagram. The appropriate order parameter is clearly the local expected magnetization $\langle \hat{S}_i^z \rangle$. Notice that since we want to focus on a balanced mixture case, the total magnetization vanishes since positive and negative contributions would cancel out. Next we can inspect the XYN phase, an AF phase whose order parameters are $\langle (\hat{S}_i^{\pm})^2 \rangle$ due to the nematic superposition between $|1\rangle$ and $|-1\rangle$. If we focus solely on these two phases, the order parameters are good since they fulfill our definition. Furthermore, we can identify them with three $SU(3)$ generators in Eqs. 4.29 as so:

$$(\hat{S}_i^{\pm})^2 = -\frac{1}{2}\Big(\hat{\lambda}_i^3 \pm i\hat{\lambda}^1\Big), \quad \text{and} \quad \hat{S}_i^z = \hat{\lambda}_i^2. \tag{4.34}$$

Since the $m = 0$ proyection plays no role in these two phases, we can treat λ_1, λ_2, and λ_3 as the regular Pauli matrices σ^α. This suggests an effective Hamiltonian

$$\hat{H}_{IFM-XYN} = \sum J_p\big(\sigma_i^x\sigma_{i+1}^x + \sigma_i^y\sigma_{i+1}^y\big) + J_t\sigma_i^z\sigma_{i+1}^z. \tag{4.35}$$

This is just the XXZ Heisenberg model that was studied in Sec. 3.1, with $\Delta = J_t/J_p$, $J_p = J\sin(\Theta)/2$, and $J_t = J(\cos(\Theta) - \sin(\Theta)/2)$. The coefficients are taken to be the same ones that accompany each term in the full BBH model.

We know how to bosonize the XXZ model and study it at small values of Δ. In fact, the integrable point $\Delta = 0$, which corresponds to $\tan\Theta = 2$ and is satisfied in the region where $g_0 < g_2$, the Hamiltonian can be mapped into free fermions as done in Sec. 3.1.1 and bosonized straightforwardly. Setting the Luttinger parameter $K = 1$ in Eqs. 3.27 and 3.34, we obtain the correlations for these particular parameters:

$$\Big\langle \hat{S}_z^n \hat{S}_z^m \Big\rangle = \frac{-1}{2\pi^2(x-y)^2} + (-1)^{(m-n)}\frac{1}{2\pi^2(x-y)^2} \tag{4.36}$$

$$\Big\langle \hat{S}_+^n \hat{S}_-^m \Big\rangle \propto \frac{1}{(x-y)^{1/2}} + (-1)^{m-n}\frac{1}{(x-y)^{5/2}}. \tag{4.37}$$

While $\Big\langle \hat{S}_z^n \hat{S}_z^m \Big\rangle$ decays fast, $\Big\langle \hat{S}_+^n \hat{S}_-^m \Big\rangle$ is slowly decaying, which for the chain means planar ordering prevails. However, recalling the association of the plane with the nematic order parameters, this correlations shows that points around $\tan\Theta = 2$ are inside the XYN phase.

Now, if we consider an opposite situation in which $g_0 >> g_2$ and $\Delta >> 1$, the transverse term of the effective Hamiltonian dominates. This situation, which happens for $\Theta \to \tan^{-1}(1/3)$, also corresponds to an integrable point of the chain by neglecting the plane, and retrieving the quantum Ising model [58]

$$\hat{H} = J_t \sum \sigma_i^z \sigma_{i+1}^z, \tag{4.38}$$

which is known to be in a ferromagnetic phase in the absence of an external field and can be solved by first rotating in space so that $z \to x$ and then applying a Jordan-Wigner transformation (see App. C). This procedure yields

$$\hat{H} = \frac{J_t}{4} \sum_i \left(\hat{c}_i^\dagger \hat{c}_{i+1} + \hat{c}_{i+1}^\dagger \hat{c}_i + \hat{c}_i^\dagger \hat{c}_{i+1}^\dagger + \hat{c}_{i+1} \hat{c}_i \right), \tag{4.39}$$

or the equivalent expression in terms of the Fourier components

$$\hat{H} = \frac{J_t}{4} \sum_k \left(2\cos(ka) \hat{c}_k^\dagger \hat{c}_k + i \sin(ka) \left(\hat{c}_k^\dagger \hat{c}_{-k}^\dagger + \hat{c}_k \hat{c}_{-k} \right) \right). \tag{4.40}$$

This form is prime for a Bogoliubov transformation, which is a key aspect of bosonization, as discussed in Sec. 2.7. In this case, the fact that we are dealing with fermions, and the Hamiltonian is not strictly real means that the appropriate mapping is $\hat{c}_k = \cos\varphi_k \hat{d}_k + i \sin\varphi_k \hat{d}_{-k}^\dagger$. By choosing the angle to be $\varphi_k = -ka/2$, the Hamiltonian simplifies to the diagonal form

$$\hat{H} = 2J_t \sum \hat{d}_k^\dagger \hat{d}_k, \tag{4.41}$$

where the fermions $\hat{d}_k$ can be reconsidered as hard-core bosons, which, when expressed in terms of the original spin variables, create and annihilate domain walls [58], the quasiparticle excitations of the IFM phase.

Finally, we know the model is critical when $\Delta = 1$ [31, 35, 58], which is achieved for $\Theta = -3\pi/4$; thus we can infer a phase transition between the IFM and XYN at this value, represented as a straight blue line in Fig. 4.3(a), which terminates at the critical $SU(3)$ point, where all terms in the BBH model are equally relevant and our effective model is no longer valid.

4.5.2 Ferromagnetic side

Moving on, we can consider all the terms that are most relevant in the FM side; that is, those proportional to J_t. Therefore, we can formulate an effective Hamiltonian for that half of phase space as

$$\hat{H}_{FM} = -J_t \sum_n \left(\hat{S}_n^x \hat{S}_{n+1}^x + \hat{S}_n^y \hat{S}_{n+1}^y + \Delta \hat{S}_n^z \hat{S}_{n+1}^z + D \left(\hat{S}_n^z \right)^2 \right), \tag{4.42}$$

where we now take into account the effect of the Zeeman field, and the spin-1 operators $\hat{S}_n^x = \hat{\lambda}_n^5$, $\hat{S}_n^y = -\hat{\lambda}_n^7$, and $\hat{S}_n^z = \hat{\lambda}_n^2$. Although our couplings are such that $\Delta = 1$, this form is instructive as it has been studied before [59, 106–108] using bosonization, with new developements as recent as Ref. [109]. We begin by representing the spin-1 operators as two spin-$\frac{1}{2}$ particles, $\hat{\boldsymbol{\sigma}}_n$ and $\hat{\boldsymbol{\tau}}_n$. so that

$$\hat{\mathbf{S}}_n = \hat{\boldsymbol{\sigma}}_n + \hat{\boldsymbol{\tau}}_n, \tag{4.43}$$

and the $S = 1$ states are projected onto the triplet subspace. The singlet state represents a break in the chain, costing a large amount of energy of the order of J_t, so it can be neglected [35, 59, 108].

We follow the procedure used in Sec. 3.1 to study the spin-$\frac{1}{2}$ chain, by first calculatinng the planar terms of the Hamiltonian:

$$\begin{aligned} \hat{S}_n^+ \hat{S}_{n+1}^- + \hat{S}_n^- \hat{S}_{n+1}^+ &= \hat{\sigma}_n^+ \hat{\sigma}_{n+1}^- + \hat{\sigma}_n^- \hat{\sigma}_{n+1}^+ + \hat{\tau}_n^+ \hat{\tau}_{n+1}^- + \hat{\tau}_n^- \hat{\tau}_{n+1}^+ & (4.44)\\ &+ \hat{\tau}_n^+ \hat{\sigma}_{n+1}^- + \hat{\tau}_n^- \hat{\sigma}_{n+1}^+ + \hat{\sigma}_n^+ \hat{\tau}_{n+1}^- + \hat{\sigma}_n^- \hat{\tau}_{n+1}^+. & (4.45)\end{aligned}$$

We know from Sec. 3.1.1, that the same-species terms map to free tight-binding fermions after a Jordan-Wigner transformation, and further into a free bosonic field Hamiltonian. For the cross-terms, let us define the two species of fermions as $\hat{c}_n$ and $\hat{d}_n$, corresponding to the $\hat{\sigma}_n$ and $\hat{\tau}_n$ respectively. Thus, we get

$$\hat{\tau}_n^+ \hat{\sigma}_{n+1}^- + \hat{\tau}_n^- \hat{\sigma}_{n+1}^+ = \hat{T}_n \hat{d}_n^\dagger \hat{Z}_n \hat{c}_{n+1} + \hat{Z}_{n+1} \hat{c}_{n+1}^\dagger \hat{T}_n \hat{d}_n, \tag{4.46}$$

where $\hat{Z}_n$ and $\hat{T}_n$ are the Jordan-Wigner strings corresponding to $\hat{c}_n$ and $\hat{d}_n$. Using the continuum expression for the string operators given in Eq. 3.29, we get

$$\hat{T}_n \hat{d}_n^\dagger \hat{Z}_{n+1} \hat{c}_{n+1} = \frac{1}{2\pi a} \left(e^{i\sqrt{\pi}\hat{\theta}^d} + (-1)^n e^{i\sqrt{\pi}(2\hat{\Phi}^d + \hat{\theta}^d)} \right) \left(e^{-i\sqrt{\pi}\hat{\theta}^c} - (-1)^n e^{-i\sqrt{\pi}(2\hat{\Phi}^c + \hat{\theta}^d)} \right). \tag{4.47}$$

From the literature [35, 59], we know that the only relevant term out of that product is the one proportional to $\exp\Big(i\sqrt{\pi}(\hat{\theta}^a - \hat{\theta}^c)\Big)$. Thus, the full planar terms with appropriate units yield the Hamiltonian

$$\begin{aligned} \hat{H}_0 &= \frac{J_t a}{2} \int \mathrm{d}x \left(\left(\partial_x \hat{\Phi}^c\right)^2 + \left(\hat{\Pi}^c\right)^2 \right) + \frac{J_t a}{2} \int \mathrm{d}x \left(\left(\partial_x \hat{\Phi}^d\right)^2 + \left(\hat{\Pi}^d\right)^2 \right) & (4.48)\\ &- \frac{J_t a \pi}{(\pi a)^2} \int \mathrm{d}x \cos\Big(\sqrt{\pi}(\hat{\theta}^a - \hat{\theta}^c)\Big). \end{aligned}$$

On to the transverse components, which map to

$$\hat{S}_n^z \hat{S}_{n+1}^z = \hat{\sigma}_n^z \hat{\sigma}_{n+1}^z + \hat{\tau}_n^z \hat{\tau}_{n+1}^z + \hat{\sigma}_n^z \hat{\tau}_{n+1}^z + \hat{\tau}_n^z \hat{\sigma}_{n+1}^z, \tag{4.49}$$

and we know from Sec. 3.1.2 that single-species terms are

$$\hat{\sigma}_n^z \hat{\sigma}_{n+1}^z = \frac{2}{\pi} \left(\partial_x \hat{\Phi}^c\right)^2, \tag{4.50}$$

where all forward-scattering terms are taken into account, and umklapp collisions within the same species are neglected. The $\hat{\tau}_n$ particles contribute with an equivalent term. For the cross-terms, we have that

$$\hat{\sigma}^z_n \hat{\tau}^z_{n+1} = \frac{1}{\pi}\partial_x \hat{\Phi}^c \partial_x \hat{\Phi}^d - \hat{M}^c(x)\hat{M}^d(x+a). \tag{4.51}$$

Point-splitting is simpler due to the difference in species; straightforwardly we obtain

$$\begin{aligned} \hat{M}^c(x)\hat{M}^d(x+a) &= \frac{1}{(\pi a)^2}\cos\left(2\sqrt{\pi}\hat{\Phi}^c\right)\cos\left(2\sqrt{\pi}\hat{\Phi}^d\right) \\ &= \frac{2}{(2\pi a)^2}\left(\cos\left(2\sqrt{\pi}\left(\hat{\Phi}^c+\hat{\Phi}^d\right)\right)+\cos\left(2\sqrt{\pi}\left(\hat{\Phi}^c-\hat{\Phi}^d\right)\right)\right) \end{aligned} \tag{4.52}$$

The first term corresponds to umklapp processes between species, while the second to backscattering in the same context [59]. Notice that because these interactions are between species, we have no energetic argument to neglect them. Furthermore, the 2 inside the cosines is less than the coefficient found for same-species umklapp collisions, thus, in a way these are slower oscillations [35] that need to be taken into account. Moreover, these cross-terms are crucial to recover the original spin-1 behavior that we are after. Since the other cross-term contributes an equivalent term, we can express the complete transverse component as

$$\begin{aligned} \hat{S}^z_n \hat{S}^z_{n+1} &= \frac{2}{\pi}\left(\partial_x\hat{\Phi}^c\right)^2 + \frac{2}{\pi}\left(\partial_x\hat{\Phi}^d\right)^2 + \frac{2}{\pi}\partial_x\hat{\Phi}^c\partial_x\hat{\Phi}^d \\ &- \frac{1}{\pi^2 a^2}\cos\left(2\sqrt{\pi}\left(\hat{\Phi}^c+\hat{\Phi}^d\right)\right) - \frac{1}{\pi^2 a^2}\cos\left(2\sqrt{\pi}\left(\hat{\Phi}^c-\hat{\Phi}^d\right)\right). \end{aligned} \tag{4.53}$$

Moving on to the Zeeman field term, it is almost the same as the previous result; however, due to being a product of operators from the same site, the same-species terms will yield something like $\hat{c}^\dagger_n\hat{c}_n\hat{c}^\dagger_n\hat{c}_n = \hat{c}^\dagger_n\hat{c}_n - \hat{c}^\dagger_n\hat{c}^\dagger_n\hat{c}_n\hat{c}_n$. The first is proportional to the total number of particles so it can be vacuumed away and the second vanishes due to Pauli exclusion. Thus, the magnetic field only contributes with cross-terms. Additionally, because the megnetic field term is evaluated in the same site, there will be a sign difference in the cosines due to the absence of a $(-1)^{n+1}$ factor. Taking this into account, we obtain an interaction Hamiltonian

$$\begin{aligned} \hat{H}_I &= -J_t a\frac{2\Delta}{\pi}\int \mathrm{d}x\left(\left(\partial_x\hat{\Phi}^c\right)^2+\left(\partial_x\hat{\Phi}^d\right)^2\right) - J_t a\frac{2(\Delta+D)}{\pi}\int \mathrm{d}x\,\partial_x\hat{\Phi}^c\partial_x\hat{\Phi}^d \\ &+ J_t a\frac{(\Delta-D)}{(\pi a)^2}\int \mathrm{d}x\left(\cos\left(2\sqrt{\pi}\left(\hat{\Phi}^c+\hat{\Phi}^d\right)\right)+\cos\left(2\sqrt{\pi}\left(\hat{\Phi}^c-\hat{\Phi}^d\right)\right)\right). \end{aligned} \tag{4.54}$$

Notice that $\hat{H}_I$ can be decoupled like we did earlier for the $S=1$ BH Hamiltonian (see Sec. 4.2) by defining the doublet field $\hat{\Phi} = (\hat{\Phi}^c,\ \hat{\Phi}^d)^T$, with a symmetric interaction matrix such that

$$\hat{H}_I = -\frac{J_t a}{\pi}\int \mathrm{d}x\,(\partial_x\hat{\Phi})^T\begin{pmatrix} 2\Delta & \Delta+D \\ \Delta+D & 2\Delta\end{pmatrix}\partial_x\hat{\Phi} + (\text{cosines}). \tag{4.55}$$

Diagonalizing the interaction matrix yields the eigenvalues $3\Delta + D$ and $\Delta - D$, corresponding to the normalized eigenvector fields

$$\hat{\Phi}_1 = \frac{1}{\sqrt{2}}\Big(\hat{\Phi}^c + \hat{\Phi}^d\Big) \quad \text{and} \quad \hat{\Phi}_2 = \frac{1}{\sqrt{2}}\Big(\hat{\Phi}^c - \hat{\Phi}^d\Big). \tag{4.56}$$

The transformation to the new fields is unitary, so it does not affect the form of the free Hamiltonian terms. Thus, we obain a total Hamiltonian $\hat{H}_{FM} = \hat{H}_1 + \hat{H}_2$ in terms of two decoupled Hamiltonians:

$$\hat{H}_1 = \frac{J_t}{2}\int \mathrm{d}x \left(K_1^2\Big(\partial_x\hat{\Phi}_1\Big)^2 + \Big(\hat{\Pi}_1\Big)^2\right) + \frac{J_t\mu_1}{(\pi a)^2}\int \mathrm{d}x \cos\left(\sqrt{8\pi}\hat{\Phi}_1\right) \tag{4.57}$$

$$\hat{H}_2 = \frac{J_t}{2}\int \mathrm{d}x \left(K_2^2\Big(\partial_x\hat{\Phi}_2\Big)^2 + \Big(\hat{\Pi}_2\Big)^2\right) + \frac{J_t\mu_2}{(\pi a)^2}\int \mathrm{d}x \cos\left(\sqrt{8\pi}\hat{\Phi}_2\right) + \frac{J_t\mu_3}{(\pi a)^2}\int \mathrm{d}x \cos\Big(\sqrt{2\pi}\hat{\theta}_2\Big). \tag{4.58}$$

Above, $\mu_1 = \mu_2 = \Delta - D$, $\mu_3 = -\pi$, the coupling was rescaled as $J_t a$, and the Luttinger parameters are

$$K_1^2 = 1 - \frac{2}{\pi}(3\Delta + D) \quad \text{and} \quad K_2^2 = 1 - \frac{2}{\pi}(\Delta - D). \tag{4.59}$$

Our Hamiltonian matches exactly the reported expression in Ref. [59], except for a small difference in normalization which yields a different value for μ_3; chapter 6 of Ref. [35] matches our coefficient.

From the decoupled fields we can already infer properties of our system. On one hand, $\hat{\Phi}_1$ can be thought of as a FM order parameter, because its corresponding density is finite for the $m = \pm 1$ states. On the other hand, $\hat{\Phi}_2$ vanishes for the magnetized states and is only finite for $m = 0$. Thus we can assume that ordering of $\hat{\Phi}_1$ leads to an Ising FM phase, whereas ordering of $\hat{\Phi}_2$ corresponds to a Large-D phase. Moreover, K_1 is imaginary for $3\Delta + D > \pi/2$ which, as discussed in Sec. 3.1.4 and supported by Refs. [35, 57–59], breaks the continuum limit to establish an IFM phase. This joins nicely with our analysis of $\hat{H}_{IFM-XYN}$. Additionally, we know from the literature that $\hat{H}_{FM}$ is critical when $\Delta = 1$, which is the case that is compatible with our original BBH model of Eq. 4.32. This indicates a phase transition at $D = 0$, and an IFM phase for $D > 0$ as suggested by K_1.

Although further analysis of the phases of $\hat{H}_{FM}$ requires techniques outside of the scope of this work, Schulz (Ref. [59]) discusses this in more detail using renormalization group arguments, and finds a large-D phase for very negative values of D. Additionally, he finds a phase with planar quasi-long range order in between the IFM and large-D phases; this translates to our XYFM phase. Although the transition between XYFM and large-D is difficult to determine, due to the influence of quadrupolar terms in the latter (for instance $\hat{\lambda}_n^8$), we can reason that as the system approaches the critical $SU(3)$ point at $(\Theta = -3\pi/4, D = 0)$, where all spin and quadrupolar operators are equally relevant, the transition must get closer to $D = 0$ until it reaches the enhanced-symmetry point. Thus, we represent it schematically in Fig. 4.3(a) as a blue shaded area since we do not know where the transition is exactly, although numerical studies, such as that of Rodriguez *et al* (Ref. [39]), find the exact dashed orange curve.

After this analysis we have successfuly identified all but one of the phases of the spin-1 Mott insulator, as well as deduced the transitions between them. Through our effective Hamiltonian approach we managed to reduce phase space to different sectors that lent themselves to bosonization. This allowed us to obtain quantitative and qualitative results that aided us in the identification of the different regimes present.

5 Conclusions and perspectives

Having spent a considerable amount of time analyzing multiple topics, we finally arrive at the end of this work. To close, we wish to give some remarks on the different discussions that were made throughout the text. Thus, in this chapter we first present a concluding summary of the contents covered in the previous ones, highlighting the most important points that were discussed. Then we move on to perspectives and ways to build upon what we have shown. This part is split into two sections, the first of which concerns aspects of spin-1 systems that were not mentioned at all or thouroughly enough in this work. The second section is dedicated to the technique of bosonization itself. Here we discuss some advanced procedures and calculations that can be developed in order to gain further physical information from a bosonized system. Then we touch upon a generalization of bosonization that recruits some of the most elegant and exotic elements of mathematical physics.

5.1 Conclusions

In Ch. 2, we began by introducing and understanding the bosonization formalism in a pedagogical and clear way, taking care to logically and intuitively connect each step to the previous one. Unfortunately, although there exists a breadth of fine elegant literature reviewing this topic [35–38, 44, 46, 51, 52, 56], we found that most were difficult for a beginner to undertake. Therefore, in our derivation of the fundamental elements of bosonization, we made a deliberate choice to ground ourselves on a simple physical system, as are free fermions, and at the same time take the time to manipulate the Hamiltonian and the relevant operators in a transparent, methodical way, catering to the beginner researcher. The main results of this chapter were the retrieval of the bosonic excitations of a fermionic wire in the form of the operators $\hat{b}(p)$ and $\hat{b}(p)^\dagger$ in Eq. 2.32, both forms of the free fermion Hamiltonian in terms of the bosonic fields found in Eqs. 2.37 and 2.42, the fundamental bosonization identity of Eq. 2.53, and the analysis of interacting fermions summarized best in the Hamiltonian of Eq. 2.68.

Next, Ch. 3 covered two systems for which we applied bosonization following the literature, warming up and practicing our newly acquired skills. First, we solved the one-dimensional spin-$\frac{1}{2}$ chain with axial anisotropy: the so-called Heisenberg XXZ model. To do this, we introuduced the Jordan-Wigner transformation between localized spin-$\frac{1}{2}$ particles and tight-binding fermions. The transformation itself is relevant, since it is a common tool when approaching spin chains and ladders, not less so when the tool is bosonization [31, 35, 59, 106–108]. Bosonizing the fermions, we were able to calculate correlations between the spins, and from them showed and inferred some physical characteristics of the system. We also discussed some of the important nuances of mapping taking a discrete system into its continuum limit.

Later in this chapter, we applied bosonization to already bosonic systems, and formulated a bosonization identity for bosons by leaning on their hydrodynamic low-energy characteristics. After discussing the expected difficulties encountered when dealing with free particles, we went to the opposite limit and explored infinitely repulsive bosons, calculating some correlations that reproduced those found in the literature [36]. The main results of this chapter were the discussion of the point-splitting scheme used for taking the continuum limit of lattices, the bosonized Hamiltonan of the XXZ model in Eq. 3.21, the correlations for the XXZ model graphed in Fig. 3.1, and the bosonization identity for bosons of Eq. 3.35.

Finally, Ch. 4 was dedicated to the study of spin-1 bosons on a lattice. We began by retrieving all relevant terms in the spin-1 Hamiltonian, taking into account a general pseudopotential interaction between the spinors, and coupling to an external magnetic field. Then, using bosonization we retrieved the low-energy spectrum and showed that by increasing the interaction strength, the system entered the gapped Mott insulator phase in which particles localized on lattice sites. In this regime, the spacial degree of freedom is essentially excluded, so it became necessary to discuss the appropriate operators that describe the remaining sectors. With our symmetry-based approach, we showed that, in addition to the usual spin-1 operators, there are important observables in the form of the quadrupolar operators, supporting our earlier find of spin-quadrupole-charge separation. With this knowledge, we calculated a Hamiltonian using perturbation theory for the Mott insulator phase: the bilinear-biquadratic Heisenberg model. Thus, we focused on this spin-1 chain for the remainder of the chapter. By constructing effective Hamiltonians for different parts of the phase space, we were able to apply bosonization once again to retrieve most of the phases of the more general system.

This chapter had many important results, which together encompass the entire body of work, and make use of all the formalism that was built and applied. Among them, stand out the formulation of the $S = 1$ Bose-Hubbard Hamiltonian in Eq. 4.16 and its bosonized counterpart of Eq. 4.22, the latter of which shows the spin-quadrupole-charge separation; the low-energy spectrum of the $S = 1$ BH Hamiltonian shown in Fig. 4.2; the eight operators that can meaningfully describe a spin-1 system, represented in the magnetic projection basis in Eq. 4.29, with which we expressed the bilinear-biquadratic Heisenberg model in its manifestly symmetric form of Eq. 4.32; and Fig. 4.3, which neatly summarizes our discussions on the physics of each phase of the spin-1 chain, and its corresponding phase diagram, where the transitions that we retrieved using bosonization are emphasized.

5.2 Perspectives on spin-1 systems

We have explored properties of a spin-1 system on a lattice, and although our contact interaction potential represents a simple interaction, we retreived an array of novel and exotic physics alien to the more discussed spin-$\frac{1}{2}$ systems. For instance, the introduction of quadrupolar degrees of freedom which led to new phases of matter were a staple of our discussion. Unfortunately, the vastness of the topic and the difficulties involved forced us to leave out many interesting aspects that we will state in this section as perspectives of our work.

First, let us continue the discussion regarding the dimer phase and the inadequacy of bosonization to deal with it. We could attempt to proceed as we did for the rest of phase space and determine an effective Hamiltonian that is based on physical intuition; the quadrupolar terms $\hat{\lambda}^4_n\hat{\lambda}^4_{n+1}$, $\hat{\lambda}^6_n\hat{\lambda}^6_{n+1}$, and $\hat{\lambda}^8_n\hat{\lambda}^8_{n+1}$ have not been explored yet and we could reasonably believe that a dimer order parameter lies among them. However, closer inspection shows that this is not the case: while all these terms are non-zero for a dimerized ground state, they fail to vanish for the large-D phase rendering them unreliable to distinguish the transition. Furthermore, the only $\mathfrak{su}(2)$ subalgebra that includes both $\hat{\lambda}^4$ and $\hat{\lambda}^6$ is completed by $\hat{\lambda}^2 = \hat{S}^z$, which is not useful to describe any of the AF phases, which makes it unlikely that the dimer phase and its neighbors in phase space can be accurately captured together by a simpler spin-chain. This is further supported by research into spin-$\frac{1}{2}$ dimer phases, which are usually surrounded my magnetized pases [105].

The dimer phase is thus more adequately dealt with by using entropy based methods. However, entanglement entropy is notoriously difficult to calculate [110, 111]. Moreover, bosonization does not appear to be equipped to handle such a calculation in the form presented in our work. Although recent efforts have been made to change this [112–114], they are still lacking when general interactions are included. In short, the task remains difficult, as can be seen in the numerous papers that opt to complement bosonization with numerical techniques when faced with entanglement questions [109, 115]. Thus, while the dimer phase poses an interesting challenge and novel physics and mathematical techniques, it has not been covered in our work.

Another aspect of the spin-1 Hamiltonian that was formulated but not covered is the superfluid phase of the $S = 1$ Bose-Hubbard Hamiltonian. Although a bosonized Hamiltonian was formulated, it was not straightforward to analyze outside of the critical $SU(3)$ point because we would have had to deal with a cosine term. While this can be dealt with (see Sec. 5.3), an additional difficulty remains in the form of the weak interactions present in the superfluid. As we showed in Sec. 3.2.1 and 4.2, weakly interacting bosons edge closer to the unbosonizable free collapsing bosons, leading to less insightful analyses. Remarkably, due to the use of repulsive inteactions, we were able to demonstrate the existance of a phase transition between the gapless superfluid and the gapped Mott insulator with our bosonization approach, so there might still be hope for a bosonized treatment of sectors of the superfluid phase after all.

Finally, there are endless perturbations and modifications that can be applied to our general yet basic spin-1 system. Higher dimensions [116, 117], different lattices [101, 118], and long-range and exotic interactions [109, 115, 119] have all been explored in the literature and remain fertile ground for research. In order to highlight one of the directions that can be pursued, we wish to mention a specific example: spin superfluids.

A spin superfluid is a magnetic insulator, *i.e.* a lattice of localized spins, that due to intrinsic easy-plane anisotropy, equivalent to $D < 0$ in our bilinear-biquadratic model, exhibits long-range diffusiveless transport of spin currents. The typical approach to these systems is through classical and semi-classical models, and their transport properties have been studied in the works of Tserkovnyak *et al* [120–125], Sonin [126–128], and others [129, 130]. While their findings have been successful and sparked theoretical as well as experimental research [131–133], less has been done to investigate a fully quantum description. Furthermore, the current attempts have been limited to spin-$\frac{1}{2}$ [125], and although both Tserkovnyak and Sonin have presented some results for higher spin [122, 126], there is still room for active research and expansion of our spin-1 understanding.

5.3 Perspectives on bosonization

Bosonization is a powerful technique and it allowed us to understand a great deal of physics from interacting systems with and without spinorial degrees of freedom. However, there is still more to the technique that we were not able to cover in this work. For instance, during our bosonization of spin chains, both in Sec. 3.1 and 4.5.2, we obtained non-quadratic contributions to the Hamiltonian in the form of cosines of $\hat{\Phi}$. This was also an issue when bosonizing the $S = 1$ BH Hamiltonian in Sec. 4.2, where upon moving away from the critical $SU(3)$ point, a cosine term would emerge. As we were not equipped at the time to deal with these terms, we focused on cases in which these could be safely neglected or avoided. However, this meant leaving out interesting physical properties of the systems we discussed, that would have enriched our analysis and conclusions.

The Hamiltonians that include these cosine contributions, as well as sine, are known as sine-Gordon Hamiltonians, a fitting name allegedly introuduced by Kruskal [134, 135]. While the quadratic, Klein-Gordon part of the Hamiltonian defines fields with freely propagating wave excitations, the sine term provides a competing dynamic that tends to lock the field in one of its minimums allowing for massive phases. To determine the parameters that lead to a dominant cosine term, a scaling analysis supported by a renormalization group formalism is required. This is explained in Ref. [35], and we will limit ourselves to a brief overview.

By using a path-integral approach to calculate correlations, it becomes simpler to expand the expected value as a power series in terms of the cosine, or more riguorously, in terms of the coupling to the cosine term, let us call it g. After some calculations, an expression is retrieved where the correlation exhibits a power-law behavior determined by an effective Luttinger parameter $K_{\text{eff}} = K_{\text{eff}}(\alpha)$ which is a function of the cutoff. Since K_{eff} should be unaffected by small changes in α, differential equations for the renormalization of both the Luttinger parameter and the coupling to the cosine term can be obtained. These equations define a so-called renormalization flow, which informs us of the change of g in response to a change in K and viceversa. Consequently, for some values of K the coupling decreases rapidly, making the cosine irrelevant in a renormalization group sense and allowing us to neglect it. On the other hand, if the flow makes g grow, then the cosine is dominant, locking the fields and leading to massive phases.

By studying this advanced aspect of bosonization, the spin-1 system could be revisited at various stages, yielding more physical information, and a more complete picture of the system. Additionally, sine-Gordon Hamiltonians are common in systems exhibiting solitonic solutions [135], high-energy physics [40], and other low-energy condensed matter systems [136, 137], which would allow for a wider scope of application for bosonization and renormalization group techniques.

A particular application of bosonization within condensed matter, and a current research interest of the Theoretical Physics of the Solid State group, is the study of topological superconductors in one dimension, which can be realized experimentally by the use of spin-$\frac{1}{2}$ particles in an optical lattice, in a way similar to the spin-1 gases that were discussed in our work [138–140]. Through the appropriate tuning of couplings and interactions, these systems can exhibit zero-energy edge states when in the superconducting regime [141–143]. By applying bosonization [144, 145], global and local properties can be studied, elucidating the low-energy physics of novel and exciting topological phases [146–148].

After mastering bosonization, it is possible to go a step further and develop a more advanced theory that allows for integration of systems with complex symmetries. This is knows as non-Abelian bosonization, a technique introduced by Witten [149] and reviewed in Refs. [44, 150–152]. The main idea of non-Abelian bosonization is to exploit the continuous symmetries of a system in order to reformulate it in terms of conserved currents, just as we did in Ch. 2. In fact, our current $\hat{J}$ and density $\hat{\rho}$ correspond to the $U(1)$ symmetry of the fermionic Hamiltonian. However, more complex symmetries involve conserved currents that correspond to the generators of the group, and obey commutation relationships according to their Lie algebra plus an additional term known as the central extension of the algebra. This algebra suggests a mapping into a topological field theory in which each sector of symmetry decouples and is expressed as separate Hamiltonians of the so-called Wess-Zumino-Witten (WZW) model.

Although non-Abelian bosonization is a generalized version of what this work presents, it represents a large leap in understanding and difficulty. For instance, it is no longer possible, in general, to obtain closed expressions for the original operators, say the fermions, in terms of the bosonic fields. In other words, there is no generalized fundamental bosonization identity. Add to this the fact that the bosonic fields are no longer scalars, but are defined on curved manifolds and one can see that non-Abelian bosonization involves advanced and exotic topics of mathematical physics. This is not meant to be a discouraging: non-Abelian bosonization offers a compelling challenge, and an elegant and beautiful formalism. Moreover, it can be of great value for studying the same types of condensed matter systems that were presented in our work. In fact, our very own bilinear-biquadratic Heisenberg model can be exactly integrated at the $SU(3)$ point using non-Abelian bosonization [153], as can additional perturbations like spin-1 ladders [154]. Furthermore, non-Abelian bosonization has been used to treat some of the most relevant and exciting systems of contemporary condensed matter, such as twisted bilayer graphene [155, 156] and spin liquids [157–159].

Here we wish to give the briefest of introductions to the procedure itself, leaving the discussions to the specialized reviews. To do so, we will revisit the bilinear-biquadratic Heisenberg model, and extract the conserved currents of the system. This time, however, it will not suffice to map spins into fermions with the Jordan-Wigner transformation due to the artificial asymmetries that the method introduces. Thus, we shall use the slave particle approach [160, 161], by which the spin algebra is represented in groups of spinless particles. Depending on the desired statistics for the slave particles, one can map into so-called Schwinger bosons [162] or Abrikosov fermions [163]; considering the bosonization procedure ahead of us we will choose the latter one. Although there are several schemes which vary the number of fermion flavors required, we will use perhaps the most intuitive, in which each magnetic projection is mapped into a flavor of fermion.

Let us focus on the symmetric point, $\Theta = -3\pi/4$. Then, each generator of the symmetry group, $SU(3)$, corresponds to a conserved current whose operator is defined as

$$\hat{\Lambda}_n^\alpha = \sum_{a,b} \hat{c}_{an}^\dagger \lambda_{ab}^\alpha \hat{c}_{bn}, \tag{5.1}$$

where, as usual, the superscript α determines the generator with matrix representation λ_{ab}^α, and $\hat{c}_{an}$ annihilates a fermion of flavor a in site n. To focus on the low-energy properties, separate each flavor of fermion into left and right movers, and consider a half-filled vacuum for each. Thus, the fermionized generator becomes

$$\hat{\Lambda}_n^\alpha = \sum_\beta \sum_{a,b} \hat{\psi}_{a\beta}(x) \lambda_{ab}^\alpha \hat{\psi}_{b\beta}(x) + (-1)^n \sum_{a,b} \Big(\hat{\psi}_{aR}^\dagger(x) \lambda_{ab}^\alpha \hat{\psi}_{bL}(x) + \text{h. c.} \Big), \tag{5.2}$$

where $\hat{\psi}_{a\beta}$ is the β-moving fermion of flavor a, and is only defined on the lattice. This expression shows that the conserved currents can be separated as $\hat{\Lambda}_n^\alpha = \hat{J}_R^\alpha(x) + \hat{J}_L^\alpha(x) + (-1)^n \hat{M}(x)$.

Trivially, we know $\Big[\hat{J}_R^\alpha(x), \hat{J}_L^\beta(y)\Big] = 0$. If we consider same-branch commutators, we could naively think that $\Big[\hat{J}_R^\alpha(x), \hat{J}_R^\beta(y)\Big] = i f_{\alpha\beta\gamma} \hat{J}_R^\gamma(x) \delta(x-y)$, where $f_{\alpha\beta\gamma}$ are the structure constants of $\mathfrak{su}(3)$. However, due to the infinte Dirac sea, there is an additional term. Recall from Eq. A.20 that, for the $U(1)$ currents of Abelian bosonization

$$\Big[\hat{J}_R^{\text{Abel.}}(x), \hat{J}_R^{\text{Abel.}}(y)\Big] = \frac{1}{2\pi i} \partial_x \delta(x-y). \tag{5.3}$$

Thus, if we consider the diagonal generators, the commutation of the fermionized currents is

$$\begin{aligned} \Big[\hat{J}_R^\alpha(x), \hat{J}_R^\alpha(y)\Big] &= \Bigg[\sum_a \lambda_{aa}^\alpha \hat{\psi}_{aR}^\dagger(x) \hat{\psi}_{aR}(x), \sum_b \lambda_{bb}^\alpha \hat{\psi}_{bR}^\dagger(y) \hat{\psi}_{bR}(y)\Bigg] \\ &= \sum_a (\lambda_{aa}^\alpha)^2 \Big[\hat{J}_R^{\text{Abel.}}(x), \hat{J}_R^{\text{Abel.}}(y)\Big] \\ &= \frac{1}{2\pi i} \text{Tr}[\lambda^\alpha \lambda^\alpha] \partial_x \delta(x-y). \end{aligned} \tag{5.4}$$

where we used the fact that each flavor of fermion has been Abelian-bosonized. The commutator for the non-diagonal generators can be calculated in the same way by temproarily changing to a basis that diagonalizes them. Additionally, we can normalize the generators such that $\mathrm{Tr}[\lambda^\alpha\lambda^\beta] = \delta_{\alpha\beta}$. Since commutators are basis-independent, then

$$\left[\hat{J}^\alpha_\sigma(x), \hat{J}^\beta_\rho(y)\right] = if_{\alpha\beta\gamma}\hat{J}^\gamma_\sigma(x)\delta_{\sigma\rho}\delta(x-y) + \frac{\sigma k}{2\pi i}\delta^{\alpha\beta}\delta_{\sigma\rho}\partial_x\delta(x-y), \tag{5.5}$$

known as the Kac-Moody algebra with central extension k, an integral result in non-Abelian bosonization [149].

Next, the Hamiltonian is reformulated in terms of the conserved currents, yielding

$$\hat{H} = J\sum_{n,\alpha}\hat{\Lambda}^\alpha_n\hat{\Lambda}^\alpha_{n+1}. \tag{5.6}$$

Then, $\hat{H}$ is taken to the continuum limit, and using the Kac-Moody algebra between the chiral currents it can be mapped into a WZW type Hamiltonian. However, this is where we stop, for taking the continuum limit requires to perform an operator product expansion (OPE), which is already outside of the scope of this work, as are the implications of the Kac-Moody algebra and the WZW model.

On that remark, we conclude our work. Its results have allowed us insight into exotic physics and complex formalisms, while being pedagogical and easy to follow. We wish that the reader has found it useful and inspiring, looking forward to the many avenues for further research into more advanced and exciting topics

A

Correlations and commutators

In this appendix we will begin by calculating a very important integral that appears multiple times throughout this work. It arises from the correlations between the bosonized fields in terms of their Fourier modes. Most correlations can be formulated in relation to these integrals:

$$\begin{aligned}\mathcal{I}_\alpha &= \frac{1}{2\pi}\int \mathrm{d}p\, e^{-\delta|p|}e^{-ip(x-y)}\theta(\alpha p)\\ \mathcal{I} &= \frac{1}{2\pi}\int \mathrm{d}p\, e^{-\delta|p|}e^{-ip(x-y)}\\ &= \mathcal{I}_+ + \mathcal{I}_-.\end{aligned} \tag{A.1}$$

They can be solved using the integral representation of the step function [49]:

$$\theta(x) = \lim_{\varepsilon\to 0^+}\frac{1}{2\pi i}\int_{-\infty}^{\infty}\frac{1}{\tau - i\varepsilon}e^{ix\tau}\,\mathrm{d}\tau\,. \tag{A.2}$$

Therefore

$$\begin{aligned}\mathcal{I}_\alpha &= \frac{1}{2\pi}\int \mathrm{d}p\, e^{-\delta|p|}e^{-ip(x-y)}\theta(\alpha p)\\ &= \lim_{\varepsilon\to 0^+}\frac{1}{(2\pi)^2 i}\int \mathrm{d}p\,\mathrm{d}\tau\,\frac{1}{\tau - i\varepsilon}e^{i\alpha p\tau}e^{-\delta|p|}e^{-ip(x-y)}\\ &= \lim_{\varepsilon\to 0^+}\frac{1}{(2\pi)^2 i}\int \mathrm{d}p\,\mathrm{d}\tau\,\frac{1}{\tau - i\varepsilon}e^{\alpha ip(\tau-\omega_\alpha)},\end{aligned} \tag{A.3}$$

where $\omega_\alpha = \alpha(x-y) - i\delta$. Integrating over p yields a delta function, so

$$\begin{aligned}\mathcal{I}_\alpha &= \lim_{\varepsilon\to 0^+}\frac{1}{2\pi i}\int \mathrm{d}\tau\,\frac{1}{\tau - i\varepsilon}\delta(\tau-\omega_\alpha)\\ &= \frac{1}{2\pi i\omega_\alpha}\\ &= \frac{-i\alpha}{2\pi((x-y)-\alpha i\delta)}.\end{aligned} \tag{A.4}$$

Now it is simple to determine $\mathcal{I}$ as

$$\mathcal{I} = \frac{\delta}{\pi((x-y)^2+\delta^2)}. \tag{A.5}$$

A.1 Correlations

Having solved for $\mathcal{I}$, we can now use it to calculate some correlations between the bosonized fields. First, the correlation between fields of the same chirality is

$$\begin{aligned}\left\langle \hat{\phi}_R(x)\hat{\phi}_R(y)\right\rangle &= \sum_{p,q>0} \frac{1}{2L\sqrt{pq}} e^{ipx} e^{-iqy} \left\langle b_p b_q^\dagger \right\rangle \\ &= \sum_{p>0} \frac{1}{2Lp} e^{ip(x-y)} \\ &= \frac{1}{4\pi}\int_0^\infty \frac{1}{p} e^{ip(x-y)} e^{-\delta p}\, \mathrm{d}p\,. \\ &= \frac{i}{2}\int \mathrm{d}x\, \mathcal{I}_+,\end{aligned} \tag{A.6}$$

where in the last line we use the integral from Eq. A.1. Integrating with respect to x, we find that

$$\left\langle \hat{\phi}_R(x)\hat{\phi}_R(y)\right\rangle = \frac{-1}{4\pi}\ln((x-y)+i\delta). \tag{A.7}$$

Next, the density-density correlation is calculated by expressing it in terms of the counting field, as in Eq. 2.43, and recalling that

$$\partial_x \hat{\tilde{\Phi}} = \sum_{p\neq 0} i\sqrt{\frac{|p|}{2KL}}\,\mathrm{sgn}(p)\left(e^{ipx}\hat{b}_p - \mathrm{h.\,c.}\right), \tag{A.8}$$

the correlation can be expanded as

$$\begin{aligned}\frac{1}{\pi}\left\langle \partial_x\hat{\tilde{\Phi}}\partial_y\hat{\tilde{\Phi}}\right\rangle &= \frac{1}{\pi}\sum \frac{\mathrm{sgn}(p)\,\mathrm{sgn}(q)}{2KL}\sqrt{|pq|}e^{ipx}e^{-iqy}\left\langle \hat{b}_p\hat{b}_q^\dagger\right\rangle \\ &= \frac{1}{4\pi^2 K}\int \mathrm{d}p\,|p| e^{ip(x-y)}e^{-\delta|p|} \\ &= \frac{-1}{4\pi^2 k}\partial_\delta \mathcal{I},\end{aligned} \tag{A.9}$$

where $\mathcal{I}$ is the integral of Eq. A.1. This derivative becomes

$$\partial_\delta \mathcal{I} = \frac{2}{(x-y)^2+\delta^2} - \frac{4\delta^2}{\left((x-y)^2+\delta^2\right)^2}. \tag{A.10}$$

Another important result is the magnetization-magnetization correlation, which is proportional to

$$\begin{aligned}\hat{\tilde{M}}(x)\hat{\tilde{M}}(y) &= \frac{1}{a^2\pi^2}\left\langle\cos\Big(2\sqrt{\pi}\hat{\tilde{\Phi}}(x)\Big)\cos\Big(2\sqrt{\pi}\hat{\tilde{\Phi}}(y)\Big)\right\rangle \\ &= \frac{1}{2a^2\pi^2}\left\langle\cos\Big(2\sqrt{\pi}(\hat{\tilde{\Phi}}(x)+\hat{\tilde{\Phi}}(y))\Big)+\cos\Big(2\sqrt{\pi}(\hat{\tilde{\Phi}}(x)-\hat{\tilde{\Phi}}(y))\Big)\right\rangle,\end{aligned} \tag{A.11}$$

where the trigonometric identities can be applied so freely because the fields commute. The first term corresponds to short-wavelength excitations that do not conserve the chiral particles so we disregard it. The second term can be expanded as

$$\begin{aligned}\frac{1}{2a^2\pi^2}\left\langle\cos\Big(2\sqrt{\pi}(\hat{\tilde{\Phi}}(x)-\hat{\tilde{\Phi}}(x))\Big)\right\rangle &= \frac{1}{4a^2\pi^2}\left\langle e^{i2\sqrt{\pi}(\hat{\tilde{\Phi}}(x)-\hat{\tilde{\Phi}}(x))}+\text{h. c.}\right\rangle \\ &= \frac{1}{2a^2\pi^2}\exp\Big(-2\pi\left\langle\hat{\tilde{\Phi}}(x)^2+\hat{\tilde{\Phi}}(y)^2-2\hat{\tilde{\Phi}}(x)\hat{\tilde{\Phi}}(x)^2\right\rangle\Big),\end{aligned} \tag{A.12}$$

where we use the exponential identity from Eq. B.9. To finish the calculation, we need to determine the correlation $\left\langle\hat{\tilde{\Phi}}(x)\hat{\tilde{\Phi}}(y)\right\rangle$ in a similar fashion as we did in Eq. A.9. That is

$$\begin{aligned}\left\langle\hat{\tilde{\Phi}}(x)\hat{\tilde{\Phi}}(y)\right\rangle &= \sum\frac{1}{2LK\sqrt{|pq|}}e^{ipx}e^{-iqy}\left\langle\hat{b}_p\hat{b}_q^\dagger\right\rangle \\ &= \frac{1}{4\pi K}\int \mathrm{d}p\,\frac{1}{|p|}e^{ip(x-y)}e^{-\delta|p|} \\ &= \frac{-1}{4\pi K}\int \mathrm{d}\delta\,\mathcal{I},\end{aligned} \tag{A.13}$$

where we once again find the integral $\mathcal{I}$ from Eq. A.1, yielding

$$\left\langle\hat{\tilde{\Phi}}(x)\hat{\tilde{\Phi}}(y)\right\rangle = \frac{-1}{4\pi K}\ln\big((x-y)^2+\delta^2\big). \tag{A.14}$$

The calculation is complete by plugging in Eq. A.14 into Eq. A.12.

A.2 Commutators

Commutators are key to the definition of fields and operators. To wrap up this appendix, we calculate the ones that are used throughout our development of bosonization. We begin with the commutator between the chiral fields

$$\begin{aligned}
\left[\hat{\phi}_\alpha(x), \hat{\phi}_\alpha(y)\right] &= \frac{1}{2L}\sum_{\alpha p>0}\sqrt{\frac{1}{2L|p|}}\frac{e^{ip(x-y)}-e^{-ip(x-y)}}{|p|} \\
&= \frac{\alpha i}{2\pi}\int_0^\infty \mathrm{d}p\,\frac{\sin(p(x-y))}{p} \\
&= \alpha i\,\mathrm{Im}\left[\frac{1}{4\pi}\int_{-\infty}^{\infty}\mathrm{d}p\,\frac{e^{ip(x-y)}}{p}\right] \\
&= \frac{\alpha i}{4}\,\mathrm{sgn}(x-y),
\end{aligned} \tag{A.15}$$

where we use the Cauchy principal value of the integral in the third line. Notice that fields of opposite chirality commute since we exclude the $p = 0$ mode. Similarily, we can compute the commutator

$$\begin{aligned}
\left[\hat{\phi}_\alpha(x), \hat{\theta}(y)\right] &= -\sum_{p>0}\frac{1}{2Lp}\left(e^{ip(x-y)}-e^{-ip(x-y)}\right) \\
&= -\frac{i}{L}\sum_{p>0}\frac{1}{p}\sin(p(x-y)) \\
&= -\frac{i}{2\pi}\int_0^\infty \mathrm{d}p\,\frac{1}{p}\sin(p(x-y)) \\
&= -\frac{i}{4}\,\mathrm{sgn}(x-y),
\end{aligned} \tag{A.16}$$

where we used the integral from Eq. A.15 in the third line. In consequence, $[\hat{\Phi}(x), \hat{\theta}(y)] = -\frac{i}{2}\,\mathrm{sgn}(x-y)$. Furthermore, by integrating with respect to y, the previous result yields $[\hat{\phi}_\alpha(x), \hat{\Pi}(y)] = \frac{i}{2}\delta(x-y)$.

With all these results we can calculate the commutators that involve the chiral currents with the bosonic fields. First, consider

$$\begin{aligned}
\left[\hat{J}_\alpha(x), \hat{\phi}_\alpha(y)\right] &= \frac{1}{\sqrt{\pi}}\left[\partial_x\hat{\phi}_\alpha, \hat{\phi}_\alpha(y)\right] \\
&= \frac{1}{\sqrt{\pi}}\partial_x\left[\hat{\phi}_\alpha(x), \hat{\phi}_\alpha(y)\right] \\
&= \frac{\alpha i}{4\sqrt{\pi}}\partial_x\,\mathrm{sgn}(x-y) \\
&= \frac{\alpha i}{2\sqrt{\pi}}\delta(x-y),
\end{aligned} \tag{A.17}$$

where in the second line we use the linearity of the commutator and the derivative. Incidentally, this result also defines $[\hat{J}_\alpha(x), \hat{\Phi}(y)] = \frac{\alpha i}{2\sqrt{\pi}}\delta(x-y)$, since opposite chiralities commute. Related to this commutator, we can also determine

$$\begin{aligned}\left[\hat{J}_\alpha(x), \hat{J}_\alpha(y)\right] &= \frac{1}{\pi}\left[\partial_x\hat{\phi}_\alpha, \partial_y\hat{\phi}_\alpha(y)\right] \\ &= \frac{1}{\pi}\partial_x\partial_y\left[\hat{\phi}_\alpha(x), \hat{\phi}_\alpha(y)\right] \\ &= \frac{\alpha i}{4\sqrt{\pi}}\partial_x\partial_y \operatorname{sgn}(x-y) \\ &= \frac{\alpha}{2\pi i}\partial_x\delta(x-y), \end{aligned} \tag{A.18}$$

which is an important result that allows bosonization to be generalized and treat more complex systems (see Sec. 5.3). The remaining relevant commutator that involves the chiral currents is

$$\begin{aligned}\left[\hat{J}_\alpha(x), \hat{\Pi}(y)\right] &= \frac{1}{\sqrt{\pi}}\sum_{p>0}\frac{p}{2L}\left(-e^{ip(x-y)} + e^{ip(x-y)}\right) \\ &= -\frac{1}{2L\sqrt{\pi}}\sum_{p=-\infty}^{\infty} pe^{ip(x-y)} \\ &= \frac{i}{2\sqrt{\pi}}\partial_x\left(\frac{1}{2\pi}\int \mathrm{d}p\, e^{ip(x-y)}\right) \\ &= \frac{i}{2\sqrt{\pi}}\partial_x\delta(x-y), \end{aligned} \tag{A.19}$$

and from Eq. A.16, we obtain that $[\hat{J}_\alpha(x), \hat{\theta}(y)] = -\frac{i}{2\sqrt{\pi}}\delta(x-y)$. To close this appendix, we summarize all the commutators we calculated:

$$\begin{aligned}\left[\hat{\phi}_\alpha(x), \hat{\phi}_\alpha(y)\right] &= \frac{\alpha i}{4}\operatorname{sgn}(x-y) & \left[\hat{\phi}_\alpha(x), \hat{\theta}(y)\right] &= -\frac{i}{4}\operatorname{sgn}(x-y) \\ \left[\hat{\Phi}(x), \hat{\theta}(y)\right] &= -\frac{i}{2}\operatorname{sgn}(x-y) & \left[\hat{\phi}_\alpha(x), \hat{\Pi}(y)\right] &= \frac{i}{2}\delta(x-y) \\ \left[\hat{\Phi}(x), \hat{\Pi}(y)\right] &= i\delta(x-y) & \left[\hat{J}_\alpha(x), \hat{J}_\alpha(y)\right] &= \frac{\alpha}{2\pi i}\partial_x\delta(x-y) \\ \left[\hat{J}_\alpha(x), \hat{\phi}_\alpha(y)\right] &= \frac{\alpha i}{2\sqrt{\pi}}\delta(x-y) & \left[\hat{J}_\alpha(x), \hat{\Phi}(y)\right] &= \frac{\alpha i}{2\sqrt{\pi}}\delta(x-y) \\ \left[\hat{J}_\alpha(x), \hat{\Pi}(y)\right] &= \frac{i}{2\sqrt{\pi}}\partial_x\delta(x-y) & \left[\hat{J}_\alpha(x), \hat{\theta}(y)\right] &= -\frac{i}{2\sqrt{\pi}}\delta(x-y). \end{aligned} \tag{A.20}$$

B
Some useful identities

In this appendix, we will prove two important identities used in the main text. The first one concerns commutators, while the second one will allow us to calculate many correlations that emerge from bosonization.

The first identity we will prove is $\left[\hat{A}, e^{\hat{B}}\right] = \left[\hat{A}, \hat{B}\right] e^{\hat{B}}$. Consider a function and its derivative

$$f(\lambda) = e^{-\lambda \hat{B}} \left[\hat{A}, e^{\lambda \hat{B}}\right] \tag{B.1}$$

$$f'(\lambda) = e^{-\lambda \hat{B}} \left[\hat{A}, \hat{B}\right] e^{\lambda \hat{B}}, \tag{B.2}$$

where $\hat{A}$ and $\hat{B}$ are operators constant with respect to λ. Integrating Eq. B.2 we get

$$f(\lambda) = \int_0^\lambda \mathrm{d}s \, e^{-s\hat{B}} \left[\hat{A}, \hat{B}\right] e^{s\hat{B}}. \tag{B.3}$$

By plugging into Eq. B.1 and setting $\lambda = 1$ we obtain

$$\left[\hat{A}, e^{\hat{B}}\right] = \int_0^1 \mathrm{d}s \, e^{(1-s)\hat{B}} \left[\hat{A}, \hat{B}\right] e^{s\hat{B}}. \tag{B.4}$$

Finally, if we suppose that $\hat{A}$ and $\hat{B}$ are such that $[[\hat{A}, \hat{B}], \hat{B}] = 0$ we retrieve the identity we wanted to prove:

$$\left[\hat{A}, e^{\hat{B}}\right] = \left[\hat{A}, \hat{B}\right] e^{\hat{B}}. \tag{B.5}$$

The second identity we will prove is $\langle \exp\left(\hat{B}\right) \rangle = \exp\left(\frac{1}{2}\langle \hat{B}^2 \rangle\right)$. Consider the expected value $\langle \exp\left(\hat{B}\right) \rangle$, with $\hat{B} = \sum \beta_i \hat{b}_i + \gamma_i \hat{b}_i^\dagger$ linear on the Fourier components. If we expand the exponent function as a power series, odd terms vanish, since only correlations of an even number of bosonic operators can be non-zero. Therefore

$$\left\langle e^{\hat{B}} \right\rangle = \sum_n \frac{1}{(2n)!} \left\langle \hat{B}^{2n} \right\rangle. \tag{B.6}$$

Using Wick's theorem, each term can be split into normal ordered terms, whose expected value is zero, and constant terms in which all contractions are taken. That is

$$\left\langle \hat{B}^{2n} \right\rangle = \mathcal{N} \left\langle \hat{B}^2 \right\rangle^n, \tag{B.7}$$

where $\mathcal{N}$ is the number of ways that the string of operators can be paired. A combinatoric analysis yields that

$$\mathcal{N} = \frac{(2n)!}{2^n n!}. \tag{B.8}$$

Putting Eqs. B.6, B.7, and B.8 together, we retrieve the desired identity:

$$\begin{aligned} \left\langle e^{\hat{B}} \right\rangle &= \sum \frac{1}{(2n)!} \frac{(2n)!}{2^n n!} \left\langle \hat{B}^2 \right\rangle^n \\ &= \sum \frac{1}{n!} \left\langle \frac{\hat{B}^2}{2} \right\rangle^n \\ &= e^{\frac{1}{2}\left\langle \hat{B}^2 \right\rangle}. \end{aligned} \tag{B.9}$$

C

Jordan-Wigner transformations

In this appendix we explain and develop de transformation due to Jordan and Wigner [55] between localized spin-$\frac{1}{2}$ particles and fermions on a lattice. These results are useful for the treatment of the anisotropic Heisenberg model in Sec. 3.1, and for interacting bosons in the hard core limit, as shown in Sec. 3.2.2. To begin, we associate the two systems mentioned above as outlined in table C.1. where the label i refers to a specific place in the chain. It seems reasonable to take $\hat{c}_n^\dagger \hat{c}_n = \hat{S}_n^z + 1/2$, keeping in mind that in this case the equal sign denotes a correspondence between Hilbert spaces. If we now inspect how the fermionic operators act on their eigenstates, we get

$$\hat{c}_i \left|\mathbf{n}\right\rangle = e^{i\pi t_i} \left|\mathbf{n}'\right\rangle , \tag{C.1}$$

with $\left|\mathbf{n}'\right\rangle$ the state after annihilating a particle in the i-th state, and $t_i = \sum_0^{i-1} \hat{c}_k^\dagger \hat{c}_k$ is called a string operator and ensures the correct antisymmetric phase. If we are to associate the fermionic operators to some in $\hat{O} \in \mathcal{H}_S$ then it must act in the same way. Therefore, let us take $\hat{c}_i = e^{i\pi t_i} \hat{S}_i^-$. Furthermore, we can rewrite

$$e^{i\pi t_i} = \prod^{i-1} \left(1 - 2\hat{c}_k^\dagger \hat{c}_k\right) = \prod^{i-1} \left(-2\hat{S}_k^z\right), \tag{C.2}$$

	Fermions	Spins
Hilbert space	$\mathcal{H}_F$	$\mathcal{H}_S$
States	$\left|\mathbf{n}\right\rangle = \left|\ldots n_i \ldots\right\rangle$	$\left|\mathbf{m}\right\rangle = \left|\ldots m_i \ldots\right\rangle$
Operators	$\hat{c}_i^\dagger, \hat{c}_i$	$\hat{S}_i^+, \hat{S}_i^-$
	$\hat{c}_i^\dagger \hat{c}_i$	$\hat{S}_i^z$
Eigenvalues	$n_i = 0, 1$	$m_i = \pm\frac{1}{2},$

Table C.1: Correspondence between the Hilbert spaces of a spin-chain and fermions on a lattice.

which always yields the right phase. Altogether, we propose the Jordan-Wigner transformations

$$\begin{aligned}
\hat{c}_n^\dagger \hat{c}_n &= \hat{S}_n^z + 1/2 \\
\hat{c}_n &= \prod^{n-1} \left(-2\hat{S}_k^z\right) \hat{S}_n^- \\
\hat{c}_n^\dagger &= \prod^{n-1} \left(-2\hat{S}_k^z\right) \hat{S}_n^+ .
\end{aligned} \tag{C.3}$$

Before moving forward, it is important to show that the proposed transformation is actually valid. First, we check Eqs. C.3 for self consistency:

$$\begin{aligned}
\hat{c}_n^\dagger \hat{c}_n &= \prod^{n-1} \left(-2\hat{S}_k^z\right) \hat{S}_n^+ \prod^{n-1} \left(-2\hat{S}_k^z\right) \hat{S}_n^- \\
&= \hat{S}_n^+ \hat{S}_n^- \\
&= \hat{S}_n^2 - (\hat{S}_n^z)^2 + \hat{S}_n^z \\
&= \hat{S}_n^z + \frac{1}{2},
\end{aligned} \tag{C.4}$$

which is fulfilled as expected. Secondly, we check that the fermions satisfy the correct anticommutation relations. Using the fact that spins from different sites commute, and the commutator

$$\left[\prod^{j-1} \left(-2\hat{S}_k^z\right), \hat{S}_i^\pm\right] = \begin{cases} 0 & \text{if } j \le i \\ \prod^{j-1} \left(-2\hat{S}_k^z\right) \left(-2\hat{S}_i^z\right) \left(\mp 2\hat{S}_i^\pm\right) & \text{if } j > i, \end{cases} \tag{C.5}$$

we can apply $\{\hat{c}_i, \hat{c}_j^\dagger\}$ to $|\mathbf{m}\rangle$. If $m_j = 1/2$ or $m_i = -1/2$, then the result vanishes. Otherwise, if $j \neq i$ ($j < i$ without loss of generality) then

$$\begin{aligned}
\left\{\hat{c}_i, \hat{c}_j^\dagger\right\} |\mathbf{m}\rangle &= \prod^{i-1} \left(-2\hat{S}_k^z\right) \hat{S}_i^- \prod^{j-1} \left(-2\hat{S}_k^z\right) \hat{S}_j^+ |\mathbf{m}\rangle + \prod^{j-1} \left(-2\hat{S}_k^z\right) \hat{S}_j^+ \prod^{i-1} \left(-2\hat{S}_k^z\right) \hat{S}_i^- |\mathbf{m}\rangle \\
&= \prod_j^{i-1} \left(-2\hat{S}_k^z\right) \hat{S}_i^- \hat{S}_j^+ |\mathbf{m}\rangle \\
&+ \prod^{j-1} \left(-2\hat{S}_k^z\right) \left[\prod^{i-1} \left(-2\hat{S}_k^z\right) \left(-2\hat{S}_j^z\right) \left(2\hat{S}_j^+\right) + \prod^{i-1} \left(-2\hat{S}_j^z\right) \hat{S}_j^+\right] \hat{S}_i^- |\mathbf{m}\rangle \\
&= 2\prod_j^{i-1} \left(-2\hat{S}_k^z\right) \hat{S}_i^- \hat{S}_j^+ |\mathbf{m}\rangle - 2\prod_j^{i-1} \left(-2\hat{S}_k^z\right) \hat{S}_i^- \hat{S}_j^+ |\mathbf{m}\rangle = 0.
\end{aligned} \tag{C.6}$$

In the sole case that $i = j$ then

$$\begin{aligned}
\left\{\hat{c}_j, \hat{c}_j^\dagger\right\} |\mathbf{m}\rangle &= \hat{S}_j^- \hat{S}_j^+ |\mathbf{m}\rangle + \hat{S}_j^+ \hat{S}_j^- |\mathbf{m}\rangle \\
&= 2\left(\hat{S}_j^2 - (\hat{S}_j^z)^2\right) |\mathbf{m}\rangle = |\mathbf{m}\rangle.
\end{aligned} \tag{C.7}$$

The remaining relations are done analogously, yielding

$$\left\{\hat{c}_i, \hat{c}_j^\dagger\right\} = \delta_{ij} \tag{C.8}$$

$$\left\{\hat{c}_i, \hat{c}_j\right\} = \left\{\hat{c}_i^\dagger, \hat{c}_j^\dagger\right\} = 0, \tag{C.9}$$

as expected from fermions, meaning that the Jordan-Wigner transformation is well defined.

D
An introduction to spin

In many ways, the concept of spin encompasses the unintuitive nature of quantum mechanics. Not only is it a historical and pedagogical example of the quantization of physical quantities, as shown by the Stern-Gerlach experiment, but it is also the quintessential introduction to superpositions of states. It is even exploited in more advanced topics covered in undergraduate courses, such as entanglement and teleportation. For it's overwhelming ubiquity both in the lecture hall and in popular science, it is a difficult subject to satisfactorily explain at an introductory level. Without the intricacies of the relativistic formalism of quantum field theory, spin is a quirk, a whim of nature placed *ad hoc* on quantum mechanics textbooks. In this appendix, I will undertake the necessary, albeit incomplete labor of motivating, if not justifying, the existence of spin in the framework of non-relativistic quantum mechanics, as well as showing some relevant properties and facts about it that are useful and necessary for the main body of this work. The following is based mainly on Refs. [164] and [165], as well as the contents of my undergraduate quantum mechanics course, taught in 2019 by my advisor, Prof. Rodriguez.

A good place to start is the definition of spin as an intrinsic angular momentum that particles posess. This, in turn, is followed by the dissonant fact that nothing is actually spinning. Much as electric charge can be thought of as the property of matter that allows it to interact through the electromagnetic force, spin is a property of matter that allows it to interact in some magnetic way, and has the units and properties of angular momentum. As such, a theory of quantum angular momentum is needed, and it begins with the study of rotations.

D.1 Rotations and isometries

In quantum mechanics, the angular momentum operator is defined as the generator of rotations, a property generalized from it's classical counterpart. In $\mathbb{R}^3$, a rotation is a three-dimensional linear transformation that preserves the norm of the vectors it acts upon. By choosing a basis, we can calculate a matrix for the transformation R, which by definition implies

$$\begin{aligned} \mathbf{x}^T\mathbf{x} &= \mathbf{x}'^T\mathbf{x}' \\ &= (R\mathbf{x})^T R\mathbf{x} \\ &= \mathbf{x}^T R^T R\mathbf{x}, \end{aligned} \tag{D.1}$$

where the prime indicates the image of the vector after applying the rotation matrix R. Consequently, such transformations satisfy $R^T R = I$. This further implies that $\det R = \pm 1$; by ignoring R with negative determinant that invert parity, we retrieve the set of all proper rotations,

$$SO(3) = \left\{R \in \mathbb{T}_3 : R^T R = I \text{ and } \det R = 1\right\}, \tag{D.2}$$

which forms the special orthogonal group in three dimensions $SO(3)$. This is a non-abelian Lie group parametrized by three angles; although it is common to use the Euler angles, it is simpler to to specify the axis of rotation $\mathbf{n}$, and the subtended angle φ. Also of interest is the Lie algebra $\mathfrak{so}(3)$ formed by the generators of this group. A matrix L is a generator of the group if $e^{tL} \in SO(3)$. By considering the two defining properties of the group, and the identity $\det\left(e^X\right) = e^{\operatorname{Tr} X}$, we can find a similar condition for the algebra:

$$\begin{aligned} I &= e^{tL^T} e^{tL} I \\ &= e^{t(L^T+L)} \\ L^T &= -L. \end{aligned} \tag{D.3}$$

Therefore, the elements of the algebra are traceless and antisymmetric. Since Lie algebras are vector spaces, we can define a basis as

$$L^x = \begin{pmatrix} 0 & 0 & 0 \\ 0 & 0 & -1 \\ 0 & 1 & 0 \end{pmatrix} \qquad L^y = \begin{pmatrix} 0 & 0 & 1 \\ 0 & 0 & 0 \\ -1 & 0 & 0 \end{pmatrix} \qquad L^z = \begin{pmatrix} 0 & -1 & 0 \\ 1 & 0 & 0 \\ 0 & 0 & 0 \end{pmatrix}. \tag{D.4}$$

A Lie algebra is also defined by it's commutations relations. It is straightforward to show that

$$\left[L^\alpha, L^\beta\right] = \epsilon_{\alpha\beta\gamma} L^\gamma. \tag{D.5}$$

which suggest that any set that claims to generate rotations in some sense must obey the same commutations as $\mathfrak{so}(3)$.

Rotations are a particular example of an isometry. In a general normed vector space isometries are transformations that preserve the norm of the elements. Therefore, if we are interested in rotations in quantum mechanics, we must study the isometries of Hilbert space H. These must be unitary transformations generated by operators that obey the commutation relations of Eq. D.5. With this in mind, we define the angular momentum operators as hermitian operators obeying the algebra

$$\left[\hat{J}^\alpha, \hat{J}^\beta\right] = i\hbar\epsilon_{\alpha\beta\gamma}\hat{J}^\gamma, \tag{D.6}$$

so that rotations in Hilbert space can be expressed as

$$\hat{D}(\mathbf{n}, \varphi) = \exp\left(-\frac{i}{\hbar}\varphi\mathbf{n} \cdot \hat{\mathbf{J}}\right).$$

This is a silghtly different definition of generator than was used in the case of $\mathbb{R}^3$ but the mathematical framework is not affected.

These turn out to be the elements of the Lie algebra $\mathfrak{su}(2)$, which generates the special unitary group $SU(2)$ and has an intimate relationship with $SO(3)$ that falls outside the scope of this text [166]. However, a practical question regarding the dimensionality of $\mathcal{H}$ remains. There must clearly be a difference between rotating an infinite dimensional Hilbert space and a finite one, which in turn means that the basis chosen for the algebra must also be dependent on this. Without diving into the ocean of representation theory, it is true that infinite dimensional rotations are generated by orbital angular momentum $\hat{\mathbf{L}} = \hat{\mathbf{r}} \times \hat{\mathbf{p}}$, whereas systems described by states belonging to a finite dimensional Hilbert space posess a different kind of angular momentum generated by the finite-dimensional representations of $\mathfrak{su}(2)$: spin.

Before investigating spin further, allow me to list some important and fundamental properties of them. This is not intended to be a self-contained set of proofs, but merely to act as reference to build the present work upon. For a complete treatment of the subject, Ref. [164] is recommended.

From the commutation relations of Eq. D.6, it can be shown that $\left[\hat{J}^2, \hat{J}^\alpha\right] = 0$, where $\hat{J}^2 = \sum \hat{(}J^\alpha)^2$. Choosing z as the quantization axis, a complete set of observables is $(\hat{J}^2, \hat{J}^z)$; consequently, a suitable basis for the Hilbert space is $|j, m\rangle$, such that

$$\hat{J}^2 |j, m\rangle = \hbar^2 j(j+1) |j, m\rangle \quad \text{and} \quad \hat{J}^z |j, m\rangle = \hbar m |j, m\rangle . \tag{D.7}$$

The remaining operators are used to define the, so called, ladder operators $\hat{J}_\pm = \hat{J}_x \pm i\hat{J}_y$, which follow the commutation relations

$$\left[\hat{J}^+, \hat{J}^-\right] = 2\hbar\hat{J}^z \qquad \left[\hat{J}^z, \hat{J}^\pm\right] = \hbar\hat{J}^\pm. \tag{D.8}$$

and act upon the basis states as

$$\hat{J}_\pm |j, m\rangle = \hbar\sqrt{(j \mp m)(j \pm m + 1)}\, |j, m \pm 1\rangle . \tag{D.9}$$

This is enough to show that each semi-integer j has a $2j + 1$ degeneracy which is lifted by the quantum number m.

D.2 Spin operators

Let us focus on spin, which, as previously stated, emerge from rotations of finite dimensional Hilbert space. The spin operators $\hat{S}^\alpha$ follow the commutation relations of Eq. D.6, and as such have the same properties listed in the previous section. However, their concrete form depends on the dimensionality: for example, in a two-dimensional space we should expect $\hat{S}^\alpha$ to be projected onto 2×2 matrices. By studying the representations of $\mathfrak{su}(2)$, these precise forms can be calculated. A representation is a map from a Lie algebra to the space of operators that act on an n-dimensional vector space, preserving the commutation relations. Changing j for s, and taking into account the $2s+1$ degeneracies of angular momentum, the lowest nontrivial dimension for representing $\mathfrak{su}(2)$ is 2, corresponding to $s = 1/2$ and $m = \pm 1/2$. Working with the basis that diagonalizes $\hat{S}^z$, the matrix corresponding to $\hat{S}^z$ is trivially

$$S_z = \frac{\hbar}{2}\begin{pmatrix} 1 & 0 \\ 0 & -1 \end{pmatrix}. \tag{D.10}$$

Next, expressing $\hat{S}^x = \frac{1}{2}(\hat{S}^+ + \hat{S}^-)$ we find that

$$\begin{aligned} \hat{S}^x \left|\frac{1}{2}\right\rangle &= \frac{1}{2}(\hat{S}^+ + \hat{S}^-)\left|\frac{1}{2}\right\rangle \\ &= \frac{1}{2}\hat{S}^- \left|\frac{1}{2}\right\rangle \\ &= \frac{\hbar}{2}\left|-\frac{1}{2}\right\rangle . \end{aligned} \tag{D.11}$$

In a similar way we find that $\hat{S}^x \left|-\frac{1}{2}\right\rangle = \frac{\hbar}{2}\left|\frac{1}{2}\right\rangle$, which imply that the matrix components are

$$S^x = \frac{\hbar}{2}\begin{pmatrix} 0 & 1 \\ 1 & 0 \end{pmatrix}. \tag{D.12}$$

Now, the commutation relations determine the last spin operator, which is represented as

$$S^y = \frac{\hbar}{2}\begin{pmatrix} 0 & -i \\ i & 0 \end{pmatrix}. \tag{D.13}$$

As expected, the Pauli matrices emerge from the representation, and are the matrices corresponding to the spin-$\frac{1}{2}$ operators.

The next dimension up is 3, with $s = 1$ and $m = \pm 1, 0$. This will be the main focus of this work, so we explicitely calculate its representation by applying the same procedure. First, $\hat{S}^z$ corresponds to the diagonal matrix

$$S^z = \hbar\begin{pmatrix} 1 & 0 & 0 \\ 0 & 0 & 0 \\ 0 & 0 & -1 \end{pmatrix}. \tag{D.14}$$

Next, by going up and down in the eigenvalues we get

$$\begin{aligned}
\hat{S}^x |1\rangle &= \frac{\hbar\sqrt{2}}{2} |0\rangle \\
\hat{S}^x |0\rangle &= \frac{\hbar\sqrt{2}}{2} (|1\rangle + |-1\rangle) \\
\hat{S}^x |-1\rangle &= \frac{\hbar\sqrt{2}}{2} |0\rangle ,
\end{aligned} \tag{D.15}$$

which yield the matrix components for $\hat{S}^x$. Finally, through the commutation relations we get the last of the three matrices. All together, the spin-1 operators are represented by the matrices

$$S^x = \frac{\hbar\sqrt{2}}{2}\begin{pmatrix} 0 & 1 & 0 \\ 1 & 0 & 1 \\ 0 & 1 & 0 \end{pmatrix} \qquad S^y = \frac{\hbar\sqrt{2}}{2}\begin{pmatrix} 0 & -i & 0 \\ i & 0 & -i \\ 0 & i & 0 \end{pmatrix} \qquad S^z = \hbar\begin{pmatrix} 1 & 0 & 0 \\ 0 & 0 & 0 \\ 0 & 0 & -1 \end{pmatrix}. \tag{D.16}$$

Notice, that the common trick used for spin-$\frac{1}{2}$ of working directly with the Pauli matrices and ignoring the accompanying factors does not work as well for spin-1, since these factors are not the same for all three matrices.

D.3 Addition of angular momentum

To roud off our review of spin and total angular momentum in quantum mechanics, let us consider angular momentum operators belonging to separate Hilbert spaces $\hat{J}_1^\alpha$ and $\hat{J}_2^\alpha$. This could be, for instance, the subspaces of a larger $\mathcal{H}$ that describes two particles. Each set of operators internally obeys the commutations of Eq. D.6, but commutes with operators of the other space. We can define a total angular momentum operator as

$$\hat{\mathbf{J}} = \hat{\mathbf{J}}_1 + \hat{\mathbf{J}}_2 = \hat{\mathbf{J}}_1 \otimes \hat{I}_2 + \hat{I}_1 \otimes \hat{\mathbf{J}}_2. \tag{D.17}$$

so that $\left[\hat{J}^\alpha, \hat{J}^\beta\right] = i\hbar\epsilon_{\alpha\beta\gamma}\hat{J}^\gamma$, which means that the total $\hat{J}^\alpha$ generate rotations in $\mathcal{H}$ and are well defined angular momentum operators.

When choosing a basis for the larger Hilbert space we have two options: the independent basis, or the coupled basis. The former takes the set of compatible observables to be $(\hat{J}_1^2, \hat{J}_2^2, \hat{J}_1^z, \hat{J}_2^z)$, whereas the latter one takes $\left\{\hat{J}_1^2, \hat{J}_2^2, \hat{J}^2, \hat{J}^z\right\}$. Consequently, the two bases are

$$\begin{array}{l|lll}
\text{Independent basis} & |j_1, j_2, m_1, m_2\rangle & \text{short:} & |m_1, m_2\rangle \\
\text{Coupled basis} & |j_1, j_2, j, m\rangle_c & \text{short:} & |j, m\rangle_c ,
\end{array} \tag{D.18}$$

where the subscript c specifies the coupled basis. The two bases are related by

$$|j, m\rangle = \sum_{m_1, m_2} |m_1, m_2\rangle \langle m_1, m_2 | j, m\rangle \tag{D.19}$$

where $\langle m_1, m_2|j, m\rangle$ are the so-called Clebsch-Gordan coefficients. For a detailed treatment of the formal theory of angular momentum addition, Refs. [164, 167] are provided. From the literature we know that the spectrum of the coupled basis satisfies $|j_1 - j_2| \leq j \leq j_1 + j_2$, and $m = m_1 + m_2$. Using this and the method proposed in Ref. [167], we can calculate the Clebsch-Gordan coefficients for the addition of two spin-1 particles, something that will turn out to be very useful for our goals.

We begin by listing the highest weight states for each possible s (we changed notation for spin), which must be a normalized superposition of all states that satisfy the constraint for m:

$$|2,2\rangle_c = |1,1\rangle\,, \quad |1,1\rangle_c = a_1\,|1,0\rangle + a_2\,|0,1\rangle\,, \quad |0,0\rangle = a_3\,|1,-1\rangle + a_4\,|-1,1\rangle + a_5\,|0,0\rangle\,. \tag{D.20}$$

To determine the coefficients, we apply the total ladder operators $\hat{S}^{\pm} = \hat{S}_1^{\pm} + \hat{S}_2^{\pm}$ to each state. First, $\hat{S}^{+}$ makes the left hand side vanish, and yields from the right side

$$0 = (a_1 + a_2)\sqrt{2}\,|1,1\rangle \qquad 0 = (a_3 + a_5)\sqrt{2}\,|1,0\rangle + (a_4 + a_5)\sqrt{2}\,|0,1\rangle\,, \tag{D.21}$$

meaning that $a_1 = -a_2 = 1/\sqrt{2}$, and $a_3 = a_4 = -a_3 = 1/\sqrt{3}$. The next step is to apply $\hat{S}^{-}$ to the highest weight states, in order to obtain the rest of states for each s. This will be shown explicitely for $s = 2$, and is applied analogously for the other states. Consider then

$$\begin{aligned} \hat{S}^{-}\,|2,2\rangle_c &= 2\,|2,1\rangle_c \\ &= \sqrt{2}(|0,1\rangle + |1,0\rangle), \end{aligned} \tag{D.22}$$

meaning that $|2,1\rangle_c = (|0,1\rangle + |1,0\rangle)/\sqrt{2}$. Repeating this procedure, one obtains

$$\begin{aligned} \hat{S}^{-}\,|2,1\rangle_c &= \sqrt{6}\,|2,0\rangle_c \\ &= |-1,1\rangle + |1,-1\rangle + 2\,|0,0\rangle\,, \end{aligned} \tag{D.23}$$

meaning that $|2,0\rangle_c = (|-1,1\rangle + |1,-1\rangle + 2\,|0,0\rangle)/\sqrt{6}$. This is enough, since, for the states with $m < 0$, the coefficients are the same, and the only change that needs to be done is $m_i \to -m_i$.

The result is that the coupled basis for two spin-1 particles can be expressed in terms of the independent basis as

$$\begin{aligned} |2,\ \ 2\rangle_c &= |1,1\rangle & |1,\ \ 1\rangle_c &= \frac{1}{\sqrt{2}}(|1,0\rangle - |0,1\rangle) \\ |2,\ \ 1\rangle_c &= \frac{1}{\sqrt{2}}(|1,0\rangle + |0,1\rangle) & |1,\ \ 0\rangle_c &= \frac{1}{\sqrt{2}}(|1,-1\rangle - |-1,1\rangle) \\ |2,\ \ 0\rangle_c &= \frac{1}{\sqrt{6}}(|1,-1\rangle + 2\,|0,0\rangle + |-1,1\rangle) & |1,-1\rangle_c &= \frac{1}{\sqrt{2}}(|-1,0\rangle - |0,-1\rangle) \\ |2,-1\rangle_c &= \frac{1}{\sqrt{2}}(|-1,0\rangle + |0,-1\rangle) & |0,\ \ 0\rangle_c &= \frac{1}{\sqrt{3}}(|1,-1\rangle - |0,0\rangle + |-1,1\rangle) \\ |2,-2\rangle_c &= |-1,-1\rangle\,. \end{aligned} \tag{D.24}$$

As a second example that is used in the text, we calculate here the coupled basis states of a system composed of a spin 3/2 and a spin 1/2 particles. By the same method, the highest weigth states are

$$|2,2\rangle_c = \left|\frac{3}{2},\frac{1}{2}\right\rangle, \quad |1,1\rangle_c = a_1\left|\frac{1}{2},\frac{1}{2}\right\rangle + a_2\left|\frac{3}{2},-\frac{1}{2}\right\rangle, \tag{D.25}$$

and determine the coefficients of $|1,1\rangle_c$ by applying the $\hat{S}^+$, finding them to be $a_1 = 1/2$ and $a_2 = -\sqrt{3}/2$. Now, by repeatedly applying $\hat{S}^-$, the states with lower m can be constructed. This will be shown explicitely for $s = 1$:

$$\begin{aligned}\hat{S}^-|1,1\rangle_c &= \sqrt{2}\,|1,0\rangle_c \\ &= \left(\left|-\frac{1}{2},\frac{1}{2}\right\rangle - \left|\frac{1}{2},-\frac{1}{2}\right\rangle\right),\end{aligned} \tag{D.26}$$

meaning that $|1,0\rangle_c = (\left|-\frac{1}{2},\frac{1}{2}\right\rangle - \left|\frac{1}{2},-\frac{1}{2}\right\rangle)/\sqrt{2}$. The state $|1,-1\rangle_c$ has the same coefficients as $|1,1\rangle_c$, after changing $m_i \to -m_i$.

This procedure yields the coupled basis states for a spin 3/2 and a spin 1/2 particle

$$\begin{aligned}
|2,\ \ 2\rangle_c &= \left|\frac{3}{2},\frac{1}{2}\right\rangle & |2,\ \ 1\rangle_c &= \frac{\sqrt{3}}{2}\left|\frac{1}{2},\frac{1}{2}\right\rangle + \frac{1}{2}\left|\frac{3}{2},-\frac{1}{2}\right\rangle \\
|2,\ \ 0\rangle_c &= \frac{1}{\sqrt{2}}\left(\left|-\frac{1}{2},\frac{1}{2}\right\rangle + \left|\frac{1}{2},-\frac{1}{2}\right\rangle\right) & |2,-1\rangle_c &= \frac{\sqrt{3}}{2}\left|-\frac{1}{2},-\frac{1}{2}\right\rangle + \frac{1}{2}\left|-\frac{3}{2},\frac{1}{2}\right\rangle \\
|2,-2\rangle_c &= \left|-\frac{3}{2},-\frac{1}{2}\right\rangle & |1,\ \ 1\rangle_c &= \frac{1}{2}\left|\frac{1}{2},\frac{1}{2}\right\rangle - \frac{\sqrt{3}}{2}\left|\frac{3}{2},-\frac{1}{2}\right\rangle \\
|1,\ \ 0\rangle_c &= \frac{1}{\sqrt{2}}\left(\left|-\frac{1}{2},\frac{1}{2}\right\rangle - \left|\frac{1}{2},-\frac{1}{2}\right\rangle\right) & |1,-1\rangle_c &= \frac{1}{2}\left|-\frac{1}{2},-\frac{1}{2}\right\rangle - \frac{\sqrt{3}}{2}\left|-\frac{3}{2},\frac{1}{2}\right\rangle.
\end{aligned} \tag{D.27}$$

E

Diagonalization of the Zeeman Hamiltonian

In this appendix we calculate analytically the eigenstates of the Hamiltonian

$$\hat{H} = C_{hyp}\hat{\mathbf{s}} \cdot \hat{\mathbf{i}} + g_e \mu_B B \hat{s}^z, \tag{E.1}$$

where C_{hyp} is the hyperfine constant coupling the spin of the valence electron $\hat{\mathbf{s}}$ and the nuclear spin $\hat{\mathbf{i}}$ in a magnetic field $B\mathbf{z}$, $g_e \approx 2$ is the electron g-factor, and μ_B is the Bohr magneton.

As mentioned in the main text in Sec. 4.1, the first term can be expressed in terms of the total spin operator $\hat{\mathbf{f}}$, so that if $B = 0$, then $\hat{H} = C_{hyp}(\hat{f}^2 - 9/4)$. Thus, the coupled basis states of Eq. D.27 that diagonalize $\hat{f}^2$ are the eigenstates of the system in the absence of external magnetic field, and the energy E^{fm} is degenerate and dependent only on f: $E^{1m} = -5C_{hyp}/4$ and $E^{2m} = 3C_{hyp}/4$. This is the so-called hyperfine shift that shows an energetic preference for the $f = 1$ subspace.

When the magnetic field is turned on, the term linear in $\hat{s}^z$ must be diagonalized. By inspection, we find that $|2,2\rangle_c$ and $|2,-2\rangle_c$ are still eigestates of $\hat{s}^z$, whereas the matrix elements ${}_c\langle f, m| \hat{s}^z |f', m'\rangle_c \propto \delta_{mm'}$, which signifies a block diagonal reprepresentation,

$$H = \frac{1}{4}\begin{pmatrix} 3C_{hyp} & 0 & 0 & 0 & 0 & 0 & 0 & 0 \\ 0 & 3C_{hyp} + a & a\sqrt{3} & 0 & 0 & 0 & 0 & 0 \\ 0 & a\sqrt{3} & -5C_{hyp} - a & 0 & 0 & 0 & 0 & 0 \\ 0 & 0 & 0 & 3C_{hyp} & 2a & 0 & 0 & 0 \\ 0 & 0 & 0 & 2a & -5C_{hyp} & 0 & 0 & 0 \\ 0 & 0 & 0 & 0 & 0 & 3C_{hyp} - a & -a\sqrt{3} & 0 \\ 0 & 0 & 0 & 0 & 0 & -a\sqrt{3} & -5C_{hyp} + a & 0 \\ 0 & 0 & 0 & 0 & 0 & 0 & 0 & -5C_{hyp} \end{pmatrix},$$

where blocks correspond to descending m, *i.e.* the first block corresponds to $m = 2$, the second to $m = 1$, the third to $m = 0$, and so on. Addtitionally, the first column of each block corresponds to the $f = 2$ state, and $a = g_e \mu_B B$. Each block can be straightforwardly diagonalized, yielding the following energies:

$$
\begin{aligned}
E^{2,\ 1} &= -C_{hyp} + \sqrt{16C_{hyp}^2 + 8C_{hyp}a + 4a^2} \qquad & E^{1,\ 1} &= -C_{hyp} - \sqrt{16C_{hyp}^2 + 8C_{hyp}a + 4a^2} \\
E^{2,\ 0} &= -C_{hyp} + \sqrt{16C_{hyp}^2 + 4a^2} \qquad & E^{1,\ 0} &= -C_{hyp} - \sqrt{16C_{hyp}^2 + 4a^2} \\
E^{2,-1} &= -C_{hyp} + \sqrt{16C_{hyp}^2 - 8C_{hyp}a + 4a^2} \qquad & E^{1,-1} &= -C_{hyp} - \sqrt{16C_{hyp}^2 - 8C_{hyp}a + 4a^2}.
\end{aligned}
\tag{E.2}
$$

We are only interested in the $f = 1$ subspace in weak fields, so we expand the appropriate energies up to second order in a/C_{hyp}, yielding the approximate spectrum

$$E_Z^{1,m} = -\frac{5C_{hyp}}{4} - \frac{a}{4}m - \frac{a^2}{8C_{hyp}}\left(1 - \frac{m^2}{4}\right), \tag{E.3}$$

where the first term comes from the hyperfine shift, the second is the linear Zeeman splitting, and the third is the quadratic Zeeman splitting. Having included the functional dependence with m, it becomes clear that we can formulate an effective Hamiltonian for the $f = 1$ subspace in a weak magnetic field,

$$\hat{H}_Z = -\frac{5C_{hyp}}{4} - \frac{\mu_B B}{2}\hat{f}^z - \frac{\mu_B^2 B^2}{2C_{hyp}}\left(1 - \frac{1}{4}(\hat{f}^z)^2\right), \tag{E.4}$$

where we replaced $g_e \approx 2$. In this expression we can see the linear and quadratic Zeeman field contributions explicitely, of which only the latter is taken usually taken into account.

F

Perturbation theory of the $S = 1$ BHH Hamiltonian

In this appendix, we retrieve the effective Hamiltonian for the Mott insulator phase by taking the kinetic energy of the $S = 1$ Bose-Hubbard Hamiltonian of Eq. 4.16 as a small perturbation. To do this, we will apply quasi-degenerate perturbation theory (QDPT) [96], which restricts the Hilbert space to a subspace of relevant states upon which a perturbed Hamiltonian acts. To do this, we must first diagonalize the unperturbed Hamiltonian

$$\begin{aligned}\hat{H}_0 &= -\mu\sum_{i,\sigma}\hat{n}_{i,\sigma} + Q\sum_{i,\sigma}\sigma^2\hat{n}_{i,\sigma} \\ &+ \sum_i\Bigg(\frac{g_2}{2}\Big(\hat{a}_1^\dagger\hat{a}_1^\dagger\hat{a}_1\hat{a}_1 + \hat{a}_{-1}^\dagger\hat{a}_{-1}^\dagger\hat{a}_{-1}\hat{a}_{-1} + 2\hat{a}_1^\dagger\hat{a}_0^\dagger\hat{a}_1\hat{a}_0 + 2\hat{a}_{-1}^\dagger\hat{a}_0^\dagger\hat{a}_{-1}\hat{a}_0\Big) \\ &+ \frac{2g_2+g_0}{6}\hat{a}_0^\dagger\hat{a}_0^\dagger\hat{a}_0\hat{a}_0 + \frac{g_2+2g_0}{3}\hat{a}_1^\dagger\hat{a}_{-1}^\dagger\hat{a}_{-1}\hat{a}_1 + \frac{g_2-g_0}{3}\Big(\hat{a}_0^\dagger\hat{a}_0^\dagger\hat{a}_1\hat{a}_{-1} + \hat{a}_1^\dagger\hat{a}_{-1}^\dagger\hat{a}_0\hat{a}_0\Big)\Bigg),\end{aligned} \tag{F.1}$$

where the first term is the chemical potential, the second one is the quadratic Zeeman field, and the third is the interaction between spin 1 bosons. For simplicity, we will assume a two-celled lattice, since it is the smallest possible one where a hopping perturbation makes sense. Taking this into account, the basis states are

$$\begin{array}{lll} |1,0,0\rangle\,|1,0,0\rangle & |0,0,1\rangle\,|1,0,0\rangle & |2,0,0\rangle\,|0,0,0\rangle \\ |1,0,0\rangle\,|0,1,0\rangle & |0,0,1\rangle\,|0,1,0\rangle & |0,2,0\rangle\,|0,0,0\rangle \\ |1,0,0\rangle\,|0,0,1\rangle & |0,0,1\rangle\,|0,0,1\rangle & |0,0,2\rangle\,|0,0,0\rangle \\ |0,1,0\rangle\,|1,0,0\rangle & & |1,1,0\rangle\,|0,0,0\rangle \\ |0,1,0\rangle\,|0,1,0\rangle & & |1,0,1\rangle\,|0,0,0\rangle \\ |0,1,0\rangle\,|0,0,1\rangle & & |0,1,1\rangle\,|0,0,0\rangle \end{array}$$

where the first ket corresponds to the first site, and the quantum numbers are $|n_{-1}, n_0, n_1\rangle$. There is a fourth column with the same states as the third but with the sites flipped. These states however would be redundant since the system is symmetric under parity, so we exclude them for now.

Notice that the only states that are not already eigenstates of $\hat{H}_0$ are $|1,0,1\rangle\,|0,0,0\rangle$ and $|0,2,0\rangle\,|0,0,0\rangle$. Fortunately, in this basis the Hamiltonian is block diagonal, so we only have to worry about the subspace spanned by these two states. This block is given by

$$\begin{pmatrix} 2Q + \frac{2g_0+g_2}{3} & \frac{g_2-g_0}{3}\sqrt{2} \\ \frac{g_2-g_0}{3}\sqrt{2} & \frac{g_0+2g_2}{3} \end{pmatrix}, \tag{F.2}$$

where we disregard the already diagonal chemical potential. Diagonalizing, we obtain the eigenvalues

$$\lambda_{\pm} = Q + \frac{g_0 + g_2}{2} \pm \frac{1}{2}\sqrt{4Q^2 + (g_0 - g_2)^2 + \frac{4}{3}Q(g_0 - g_2)}. \tag{F.3}$$

It is now possible to obtain the eigenstates

$$|+\rangle = \cos\phi\,|1,0,1\rangle + \sin\phi\,|0,2,0\rangle \qquad |-\rangle = -\sin\phi\,|1,0,1\rangle + \cos\phi\,|0,2,0\rangle\,, \tag{F.4}$$

where

$$\tan\phi = \frac{3\lambda_+ - 6Q - 2g_0 + g_2}{\sqrt{2}(g_2 - g_0)}. \tag{F.5}$$

We now take the QDPT formula [96] to calculate the matrix elements of the effective Hamiltonian second order corrections:

$$H^{(2)}_{mm'} = \frac{1}{2}\sum_l \langle m\,|H_t|\,l\rangle\,\langle l\,|H_t|\,m'\rangle \left[\frac{1}{E_m - E_l} + \frac{1}{E_{m'} - E_l}\right], \tag{F.6}$$

where m and m' are the target states, and l are the virtual states. In the following table we show these states numbered and with their respective energies:

Target			Virtual		
m	State	E_m	l	State	E_l
1	$\|100\rangle\,\|100\rangle$	$-2\mu + 2Q$	1	$\|200\rangle\,\|000\rangle$	$-2\mu + 2Q + g_2$
2	$\|100\rangle\,\|010\rangle$	$-2\mu + Q$	2	$\|+\rangle\,\|000\rangle$	$-2\mu + \lambda_+$
3	$\|100\rangle\,\|001\rangle$	$-2\mu + 2Q$	3	$\|002\rangle\,\|000\rangle$	$-2\mu + 2Q + g_2$
4	$\|010\rangle\,\|100\rangle$	$-2\mu + Q$	4	$\|110\rangle\,\|000\rangle$	$-2\mu + Q + g_2$
5	$\|010\rangle\,\|010\rangle$	-2μ	5	$\|-\rangle\,\|000\rangle$	$-2\mu\lambda_-$
6	$\|010\rangle\,\|001\rangle$	$-2\mu + Q$	6	$\|011\rangle\,\|000\rangle$	$-2\mu + Q + g_2$
7	$\|001\rangle\,\|100\rangle$	$-2\mu + 2Q$			
8	$\|001\rangle\,\|010\rangle$	$-2\mu + Q$			
9	$\|001\rangle\,\|001\rangle$	$-2\mu + 2Q$			

Before calculating the whole set of 81 components, let us inspect the states more closely in order to find symmetries and relations that will simplify the affair. First, the Hamiltonian is hermitian, which means that we only need half of the matrix to determine it completely. Second, as mentioned earlier, there is an additional set of virtual states obtained by transposing the sites. This implies that calculations done with this reduced set will yield half of the actual result. Third, the target states presented already contain these transposed states, for example $|2\rangle$ and $|4\rangle$, meaning that these rows and columns are interchangable, *i.e.* $H^{(2)}_{2j} = H^{(2)}_{4j}$. Finally, there is also a simmetry under spin inversion that leaves the Hamiltonian invariant under a simultaneous change of $|1\rangle$ for $|9\rangle$, $|2\rangle$ for $|8\rangle$, $|3\rangle$ for $|7\rangle$, and so on. These four conditions imply that there are only five non-zero components that are needed to determine the whole matrix:

$$
\begin{aligned}
H_{11} &= -\frac{4t^2}{g_2} & H_{22} &= -\frac{2t^2}{g_2} & H_{33} &= 2t^2\Delta \\
H_{53} &= t^2\sqrt{2}\xi & H_{55} &= -4t^2\Omega,
\end{aligned}
$$

where

$$
\begin{aligned}
\Delta &= \frac{\cos^2\phi}{2Q-\lambda_+} + \frac{\sin^2\phi}{2Q-\lambda_-} \\
\Omega &= \frac{\sin^2\phi}{\lambda_+} + \frac{\cos^2\phi}{\lambda_-} \\
\xi &= \sin\phi\cos\phi\left(\frac{1}{2Q-\lambda_+} - \frac{1}{\lambda_+} - \frac{1}{2Q-\lambda_-} + \frac{1}{\lambda_-}\right).
\end{aligned}
$$

All other matrix elements are either zero or can be determined using the symmetry relations. Therefore, the complete matrix representation of the effective Hamiltonian is

$$
H^{(2)} = \begin{pmatrix}
-\frac{4t^2}{g_2} & 0 & 0 & 0 & 0 & 0 & 0 & 0 & 0 \\
0 & -\frac{2t^2}{g_2} & 0 & -\frac{2t^2}{g_2} & 0 & 0 & 0 & 0 & 0 \\
0 & 0 & 2t^2\Delta & 0 & t^2\sqrt{2}\xi & 0 & 2t^2\Delta & 0 & 0 \\
0 & -\frac{2t^2}{g_2} & 0 & -\frac{2t^2}{g_2} & 0 & 0 & 0 & 0 & 0 \\
0 & 0 & t^2\sqrt{2}\xi & 0 & -4t^2\Omega & 0 & t^2\sqrt{2}\xi & 0 & 0 \\
0 & 0 & 0 & 0 & 0 & -\frac{2t^2}{g_2} & 0 & -\frac{2t^2}{g_2} & 0 \\
0 & 0 & 2t^2\Delta & 0 & t^2\sqrt{2}\xi & 0 & 2t^2\Delta & 0 & 0 \\
0 & 0 & 0 & 0 & 0 & -\frac{2t^2}{g_2} & 0 & -\frac{2t^2}{g_2} & 0 \\
0 & 0 & 0 & 0 & 0 & 0 & 0 & 0 & -\frac{4t^2}{g_2}
\end{pmatrix}. \tag{F.7}
$$

Since a small hopping amplitude t effectively constrains interaction to close neighbors, it makes sense for the perturbed Hamiltonian up to lowest order to describe the nearest neighbor couplings. Thus, we can expect the matrix of Eq. F.7 to be decomposable into a sum of operators such as

$\hat{S}_1^\alpha \hat{S}_2^\beta$, where the superscripts are projection directions and the subscripts are the sites. We can use the following decomposition:

$$\hat{H} = Q \sum_i (S_i^z)^2 + a_1(\mathbf{S}_1 \cdot \mathbf{S}_2) + a_2(\mathbf{S}_1 \cdot \mathbf{S}_2)^2 + a_3(S_1^x S_2^y + S_1^y S_2^x)^2 + a_4(S_1^z S_2^z)^2. \tag{F.8}$$

Since Q is a weak magnetic field, we can neglect terms proportional to $Qt^2 \propto t^4$, which leaves us with

$$a_1 = -\frac{2t^2}{g_2} \qquad a_2 = -\frac{4t^2}{3g_0} - \frac{2t^2}{3g_2} \tag{F.9}$$

$$a_3 = 0 \qquad a_4 = 0. \tag{F.10}$$

The two non-zero constants can be parametrized as $a_1 = -J\cos\Theta$ and $a_2 = -J\sin\Theta$, where

$$J = 2t^2 \frac{\sqrt{10g_0^2 + 4g_0 g_2 + 4g_2^2}}{3g_0 g_2} \qquad \tan\Theta = \frac{g_0 + 2g_2}{3g_0} \tag{F.11}$$

and Θ takes values in the third quadrant. Thus, the effective Hamiltonian for the Mott insulator phase is given by the so-called Heisenberg bilinear biquadratic Hamiltonian,

$$\hat{H} = -J \sum_i \left(\cos(\Theta) \hat{\mathbf{S}}_i \cdot \hat{\mathbf{S}}_{i+1} + \sin(\Theta) \left(\hat{\mathbf{S}}_i \cdot \hat{\mathbf{S}}_{i+1} \right)^2 + D(\hat{\mathbf{S}}_i^z)^2 \right), \tag{F.12}$$

where $D = -Q/J$, and it is clear that particles are interacting with their nearest neighbor.

G

Topics in spin-$\frac{1}{2}$ transport.

Although the main objectives of our work focus on the ground state properties of a spin-1 system, it is undeniable that we can and do lean on the vast body of work that centers on spin-$\frac{1}{2}$ quantum mechanics. For instance, in Ch. 3, we solved the spin-$\frac{1}{2}$ Heisenberg XXZ chain in order to gain experience and insight into spinor systems. This knowledge was invaluable when we tackled the spin-1 chain in Ch. 4. Furthermore, in Ch. 5, we discussed how our spin-1 results can serve as a basis for exploring further topics in condensed matter like magnetic transport. Thus, in this appendix we will cover an example of a transport problem involving spin-$\frac{1}{2}$ particles in a magnetized one-dimensional wire. This work was developed in paralel with the main objectives, and represents the results of the author's research internship at the University of Delaware (UD). Accordingly, the author thanks Prof. Branislav Nikolic and the Quantum Transport Theory group (QTTG) at UD for funding, guidance, and direction during the stay and with the following content.

Spin transport studies the dynamics of electrons in materials that often exhibit specific magnetic textures. These textures can take many forms, from simple ferromagnetic samples to domain walls (DWs) [168–171], skyrmions [172], and vortex cores [173, 174]. When the dynamics of these non-colinear and non-coplanar textures is taken into account [175], the research becomes of great interest to fundamental non-equilibrium many body dynamics, as well to technological applications involving spintronics, like novel types of digital memories or computing methods [176–178]. In this appendix, we will investigate a particular topic of interest pertaining to nanomagnetic wires hosting ferromagnetic DWs: adiabaticity [179–182].

A DW occurs in between different ferromagnetic domains, *i.e.* regions of space within which the magnetization is aligned in a specific direction, where the direction of magnetization is inverted. The theoretical literature presents an intuitive picture of adiabaticity in DWs: a regime in which the traversing electron's spin tracks the magnetic texture, or equivalently, that the electron remains in its lowest energy state as it moves through space [169, 179]. In clean magnetic wires [169, 181, 183], this is achieved for strong *sd* coupling J_{sd} between the texture and the electrons, and a slow moving electron. Thus, adiabaticity is often assumed to be reached for

$$\frac{J_{\mathrm{sd}} w S}{\hbar v_F} \gg 1, \tag{G.1}$$

where w is the width of the domain wall, v_F the Fermi velocity of the electrons, and S the spin of the magnetic texture. This adiabaticity parameter compares the time it takes for the electron to align itself with the texture with the time it takes to cross the DW. The coupling J_{sd} is typically measured to be close to 0.1 eV [184], while v_F is set by the specific material, so adiabaticity becomes mostly a function of the width w. With this approach, it becomes possible to explain the vanishing electrical resistance reported for wide DWs [169].

However, any deviation from adiabaticity leads to novel effects. Of particular interest is the non-adiabatic spin-transfer torque (STT) [180, 182, 185], by which the flowing electrons transfer angular momentum to the localized spins that make up the underlying magnetic texture. While its counterpart, adiabatic STT is well understood and has been reproduced by a number of transport theories [186–188], the mechanisms behind non-adiabatic STT have proven to be controversial over the past 20 years. Proposed theories refer to spin-orbit coupling, magnetic impurities [189–191], momentum transfer [168, 192], genuine spin mistracking [183], and relativistic effects [188] as the source of the so-called β term [181, 186], which is used to characterize non-adiabatic STT. In fact, great effort has been dedicated to the calculation of this dimensionless β parameter, without questioning the explicit form and modelling of non-adiabatic STT itself [186, 189–191]. An exception is Ref. [182], where non-adiabatic STT is argued to have both in-plane as well as out-of-plane components, as opposed to the standard model used in much of the spintronics literature which only has the latter.

However, all attempts to model non-adiabatic STT so far indicate a quickly decaying contribution as w is increased. While this agrees with much of the current theoretical understanding, it fails drastically to match experimental measurements of β, which find non-vanishing non-adiabatic signatures even for wide DWs [170, 171, 173]. Therefore, it is reasonable to believe that the current state of theory does not capture all of the relevant effects behind the elusive non-adiabatic STT in non-colinear textures.

In order to investigate the nature of non-adiabatic STT further and add to the lively discussion, we employ a numerically exact, fully microscopic formalism to simulate an open quantum system consisting of a one-dimensional magnetized conducting nanowire hosting a ferromagnetic DW that is driven out of equilibrium by two normal metal (NM) leads that connect the wire to two electrochemical reservoirs assumed to be infinitely far away. This is represented schematically in the diagram of Fig. G.1. The wire is modeled as a 1D tight-binding (TB) chain with a localized magnetic moment (LMM), $\mathbf{M}_i(t)$, at each site i. The LMMs are unit vectors pointing along the direction of the local magnetization, and evolve classically according to the Landau-Lifshitz-Gilbert (LLG) equation [193],

$$\frac{\partial \mathbf{M}_i}{\partial t} = -g\mathbf{M}_i \times \mathbf{B}_i^{\mathrm{eff}} + \lambda \mathbf{M}_i \times \frac{\partial \mathbf{M}_i}{\partial t} + \frac{g}{\mu_M}\big(\mathbf{T}_i^{\mathrm{ad}} + \mathbf{T}_i^{nad}\big), \tag{G.2}$$

where g is the gyromagnetic ratio, and λ is the Gilbert damping parameter, here chosen to be $\lambda = 0.01$ as is the case for real nanowires [194]. Notice that the time-dependent coupling to the conduction electrons is given by the adiabatic and non-adiabatic torques, $\mathbf{T}_i^{\mathrm{ad}}$ and $\mathbf{T}_i^{\mathrm{nad}}$ respectively,

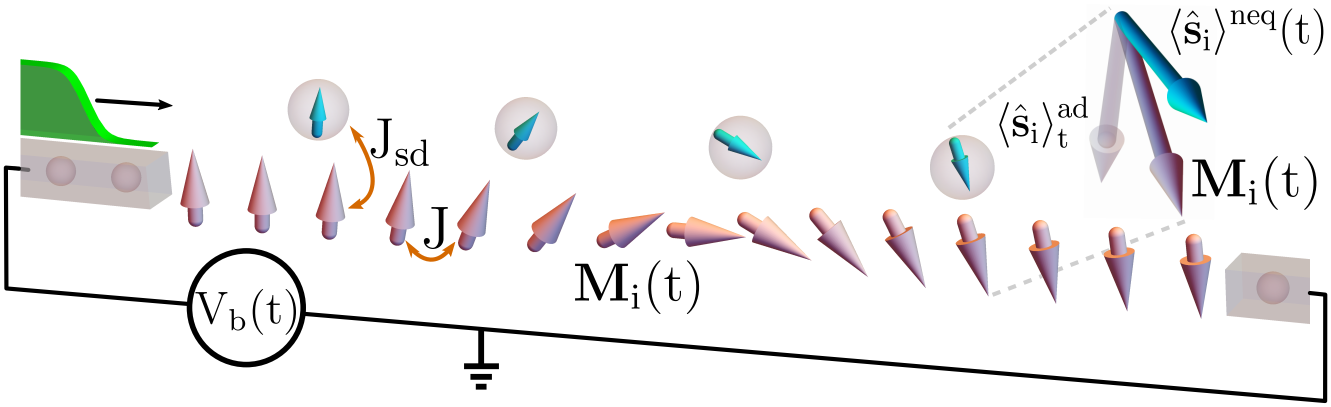

Figure G.1: Schematic diagram of the 1D wire hosting a Néel DW. In the active region between the NM leads, red arrows represent LMMs coupled to each other through a Heisenberg exchange, and subject to easy-axis anisotropy. Electrons flow on top, and acquire a non-zero expected value of spin (blue arrows) due to the local magnetization. In equilibrium, this local spin density aligns with an adiabatic direction, in general different than $\mathbf{M}_i$. In a non-equilibrium regime, like after injection of current, additional time-dependent deviations from $\langle\hat{\mathbf{s}}_i\rangle^{\mathrm{ad}}_t$ (grey arrow) are obtained.

which will be rigorously defined below. The effective magnetic field, $\mathbf{B}^{\mathrm{eff}}_i = -\frac{1}{\mu_M}\partial\mathcal{H}/\partial\mathbf{M}_i$, that acts upon each site is given in terms of the classical Hamiltonian

$$\mathcal{H} = -J\sum_i \mathbf{M}_i\cdot\mathbf{M}_{i+1} - K\sum_i (M_i^z)^2 + D\sum_i (M_i^y)^2, \tag{G.3}$$

where the LMMs are coupled to to their nearest neighbors through a $J = 0.1$ eV exchange, and are subject to an easy-axis anisotropy, $K > 0$, and a demagnetization field, $D = 0.03$ meV, which corresponds to approximately 1 T. Here we find a difference between the current treatment and that of the main body of work: the magnetic texture is treated classically, even though the real quantum behavior could potentially be captured by a spin lattice like our own BBH model in the IFM phase. This is especially clear when we recognize that the easy-axis anisotropy could be simulated with our quadratic Zeeman field. Although the classical approximation and the LLG evolution is widely and successfuly used in the literature, its actual range of validity is not perfectly understood and has recently been investigated in the QTTG [195].

The Hamiltonian $\mathcal{H}$ allows ground states that exhibit DWs, which smoothly separate two opposite ferromagnetic domains [169]. The width of the DW is determined by the ratio $w = \sqrt{J/K}$, and its profile can be determined to be

$$\begin{aligned} M_i^x &= \mathrm{sech}((X_{\mathrm{DW}} - i)/w), \\ M_i^y &= 0, \\ M_i^z &= \tanh((X_{\mathrm{DW}} - i)/w), \end{aligned} \tag{G.4}$$

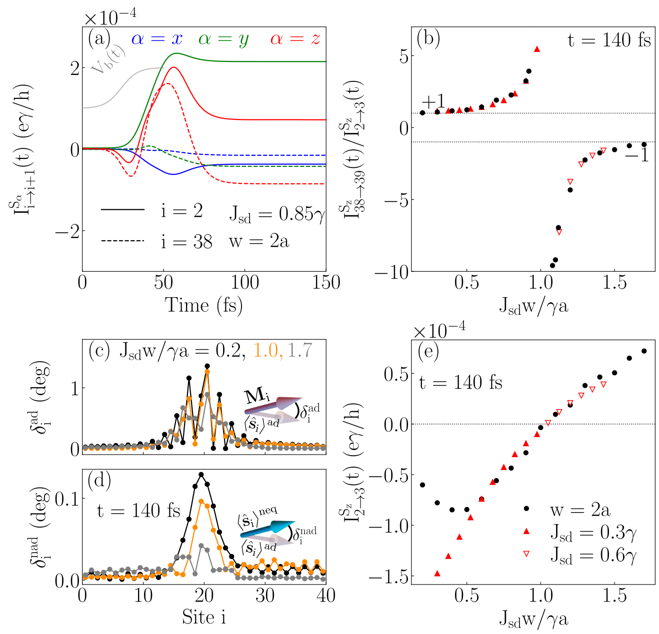

Figure G.2: A dc bias, $V_b = 0.05$ eV, is gradually turned on. Panel (a) shows the spin currents $I^{S_z}_{ch}$ measured to the L and R of the DW as they reach a steady state. The ratio of these currents defines a transmission coefficient for polarized current shown in (b): the adiabatic regime is reached for $J_{sd}w/\gamma a > 1.0$. Otherwise, polarization to the left of the DW decreases due to $e\uparrow$ being reflected. At $J_{sd}w \approx 0.5\gamma a$, the reflected current perfectly cancels the incoming polarization, as shown by (d), explaining the divergence in (b). Panel (c) shows the alignments of the relevant vectors as we move into the adiabatic regime.

corresponding to a Néel DW, where X_{DW} is the center of the DW. Furthermore, the inclusion of the demagnetization field allows the DW to be driven by current injected into the system.

In addition to the LMMs, the conduction electrons in the nanowire are described with the one-dimensional TB Hamiltonian

$$\hat{H} = -\gamma \sum_i \hat{c}_i^\dagger \hat{c}_{i+1} - J_{sd} \sum_i \hat{c}_i^\dagger \boldsymbol{\sigma} \cdot \mathbf{M}_i(t) \hat{c}_i, \tag{G.5}$$

where $\hat{c}_i = (\hat{c}^\dagger_{i\uparrow},\ \hat{c}^\dagger_{i\downarrow})$ is the row vector of creation operators for electrons with spin $\sigma =\uparrow, \downarrow$ on site i, $\boldsymbol{\sigma}$ is the vector of Pauli matrices, and $\gamma = 1$ eV is the hopping parameter to nearest neighbors. The electrons are time-dependent through the J_{sd} exchange with the LMMs. To the left (L) and right (R) of the nanowire, semi-infinite NM leads are attached, modeled by the first term of the Hamiltonian in Eq. G.5. To run current through the wire, a dc bias voltage is applied by changing the electrochemical potentials, $\mu_{L/R} = E_F \pm eV_b/2$, of the L and R reservoirs at the assumed ends of the leads. Thus, by allowing the bias voltage V_b to change in time, the desired potential difference can be achieved either instantly or gradually.

To study the STT of the system, it becomes necessary to rigorously define the adiabatic and non-adiabatic contributions to the time dependent local spin density, since the coupling between LMMs and conduction electrons rely on this quantity. In an open system, we can use the adiabatic density matrix [196–198]

$$\hat{\rho}_t^{\mathrm{ad}} = -\frac{1}{\pi}\int dE\, \mathrm{Im}\, \hat{G}_t^r f(E), \tag{G.6}$$

given in terms of the retarded Green function (GF) $\hat{G}_t^r = \left[E - \hat{H}\left[\mathbf{M}_i(t)\right] - \hat{\Sigma}_L - \hat{\Sigma}_R\right]^{-1}$, where $\hat{\sigma}_{L/R}$ are the self-energies due to the NM leads. It is important to note that $\hat{\rho}_t^{\mathrm{ad}}$ evolves parametrically with time by considering instantaneous configurations of $\mathbf{M}_i(t)$ and effectively assuming $\partial_t \mathbf{M}_i = 0$. Thus, $\hat{\rho}_t^{\mathrm{ad}}$ can be understood as the lowest order term in a power series expansion in $\partial_t \mathbf{M}_i$ of a non-equilibrium density matrix

$$\hat{\rho}^{\mathrm{nad}}(t) = -i\hbar \hat{G}^<(t,t), \tag{G.7}$$

computed using the time diagonal of the lesser Green function $\hat{G}^<(t,t')$ from time-dependent non-equilibrium Green function (TDNEGF) formalism [199]. The complete coupled evolution of the LMMs and the TB electrons is done using the algorithm of TDNEGF+LLG introduced in Ref. [200], which evolves both the quantum and classical system in time steps of 0.1 fs, and self-consistently feeds each system with the information of the other in every step.

The obtained density matrices allow us to calculate the expected value of the local non-equilibrium spin density of the conduction electrons as

$$\begin{aligned} \langle \hat{\mathbf{s}}_i \rangle^{\mathrm{neq}}(t) &= \mathrm{Tr}[\hat{\rho}^{\mathrm{neq}}(t)\, |i\rangle \langle i|\, \hat{\boldsymbol{\sigma}}] \\ &= \langle \hat{\mathbf{s}}_i \rangle_t^{\mathrm{ad}} + \delta \langle \hat{\mathbf{s}}_i \rangle (t), \end{aligned} \tag{G.8}$$

where the natural decompostion of the second line separates the adiabatic and non-adiabatic contributions to the spin density. The intuitive picture given by much of the theoretical literature is based on the assumption that $\langle \hat{\mathbf{s}}_i \rangle_t^{\mathrm{ad}}$ aligns with the LMMs. However, this has been shown to be false by spintronics [201], Berry phase [202, 203], and non-colinear DFT research [204]; the electron spin in the adiabatic regime does not align with $\mathbf{M}_i$, but with a different direction that points along an effective magnetization [182, 202]. This is reproduced by our calculations and shown in Fig. G.2(c) and (d). Consequently, it becomes necessary to emphasize that, while in some literature, $\delta\langle \hat{\mathbf{s}}_i \rangle$ is retrieved from semiclassical transport theory and denotes a deviation of the spin density from $\mathbf{M}_i$, here we rigourously define it with respect to the effective adiabatic direction, equivalent to $\langle \hat{\mathbf{s}}_i \rangle_t^{\mathrm{ad}}$. All the spin densities and their respective directions are illustrated in the inset of Fig. G.1.

With the spin density properly defined, it is natural to extend this definition to the torques exerted by the electron upon the DW. Therefore, let

$$\mathbf{T}_i^{\mathrm{ad}}(t) = J_{sd} \langle \hat{\mathbf{s}}_i \rangle_t^{\mathrm{ad}} \times \mathbf{M}_i(t) \quad \text{and} \quad \mathbf{T}_i^{\mathrm{nad}}(t) = J_{sd}\delta \langle \hat{\mathbf{s}}_i \rangle (t) \times \mathbf{M}_i(t), \tag{G.9}$$

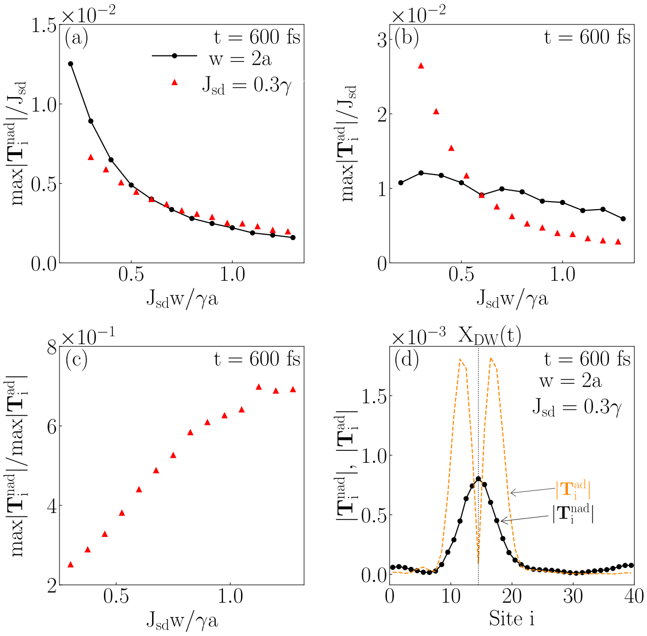

Figure G.3: Panel (d) shows the spatial profile of the torques exerted throughout the chain, peaking at and around X_{DW}. Maximum values for $|\mathbf{T}_i^{\text{nad,ad}}|$ are analyzed in (a)-(c) finding that $|\mathbf{T}_i^{\text{nad}}|$ saturates to a finite value and both torques are equally relevant in the adiabatic regime.

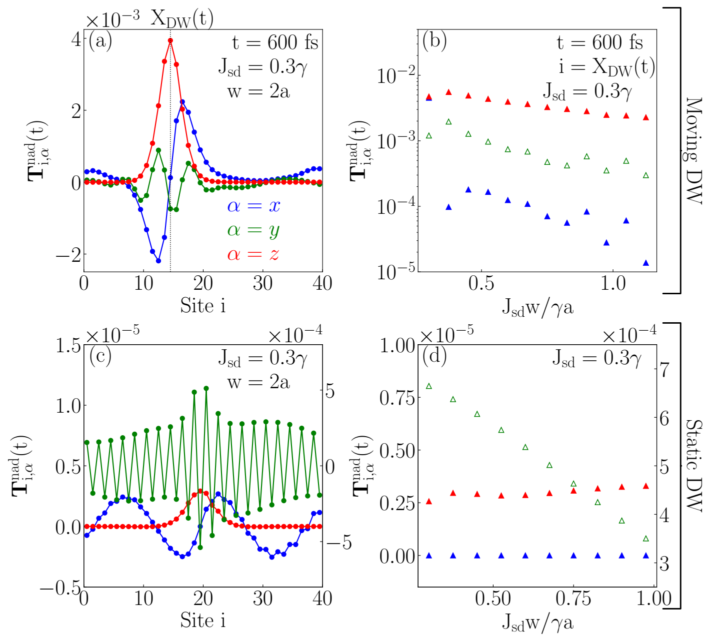

Figure G.4: The components of $\mathbf{T}_i^{\text{nad}}$ are plotted in (a) and (c) for a moving and static DW. Panels (b) and (d) show that some of the previously reported features of non-adiabatic STT, like fast decaying $\mathbf{T}_i^{\text{nad}}$, non-local oscillations, and only out-of-plane components are found to be as artifacts of an improper treatment of DW motion.

which is equivalent to introducing the usual mean field coupling $-J_{sd}\mathbf{M}_i(t)\cdot\langle\hat{\mathbf{s}}_i\rangle^{\text{neq}}(t)$ in the classical Hamiltonian of Eq. G.3 [200].

Before simulating the full coupled evolution of the DW and the conduction electrons, it is useful to reformulate the adiabatic parameter of Eq. G.1 in terms of our system as $J_{\text{sd}}w/\gamma a$ and establish the range in which adiabaticity is obtained in our lattice. Thus, we set the LMMs in an initial Néel DW configuration as given by Eq. G.4, and suppress LLG dynamics so that we can study the scattering of electrons exclusively. Then, a dc voltage was gradually established according to $V_b = V(\tanh((t-t_0)/\tau)+1)$, where $V = 0.05$ eV, $t_0 = 25$ fs, and $\tau = 10$ fs, establishing a charge current accross the wire. As shown in Fig. G.2(a), the current becomes polarized over a period of time of about 50 fs, longer than it takes for the constant voltage to be established; at around 100 fs, a steady state is obtained. We then measure the local current between site i and $i+1$, $I^{S^z}_{i\to i+1}(t)$ at time 140 fs for sites $i=2$ and $i=38$, so that we obtain the incident and transmitted polarized spin currents. In our convention, $I^{S^z}_{i\to i+1} > 0$ implies a spin-up current in the $+x$ direction. These currents allow us to define a transmission coefficient $I^{S^z}_{38\to 39}(t)/I^{S^z}_{2\to 3}(t)$, plotted in Fig. G.2(b) as a function of the adiabatic parameter $J_{\mathrm{sd}}w/\gamma a$. We find that fixing w and varying J_{sd} is equivalent to its opposite, cementing $J_{\mathrm{sd}}w/\gamma a$ as an adequate characterization of the scattering. Furthermore, our calculation yields negative $I^{S^z}_{2\to 3}(t)$ for small $J_{\mathrm{sd}}w/\gamma a$, meaning most spin-up electrons are reflected by the DW. The reflection gradually decreases, until at $J_{\mathrm{sd}}w/\gamma a \approx 1.0$ it is small enough that it is perfectly cancelled by the incident spin current and $I^{S^z}_{2\to 3}(t) = 0$ for a null polarization. Consequently, this is shown as a divergence in our transmission coefficient, and marks the beginning of the adiabatic regime. Further increasing the adiabatic parameter causes even more current to be transmitted, eventually converging to $I^{S^z}_{38\to 39}(t)/I^{S^z}_{2\to 3}(t) \to -1$ signifying a total transmission and inversion of polarization of the spin current due to the tracking of the electrons.

Having elucidated on the range of the adiabatic regime in our lattice system, we turn LLG dynamics back on, and allow for current driven motion of the DW itself. This allows us to calculate the torques along the wire, whose spacial profiles are plotted in Fig. G.3(d). In Fig. G.3(a-c), we analyze the maximum values of $|\mathbf{T}^{\mathrm{nad}}_i|$, reached at $X_{DW}(t)$, and of $|\mathbf{T}^{\mathrm{ad}}_i|$, reached at $X_{DW}(t) \pm 2$. The plot of Fig. G.3(d) demonstrates that non-adiabatic STT does not decay to zero in the adiabatic regime deciphered from our scattering analysis, but instead saturates for wide DWs. This result agrees with experiments that report a relative insensitivity of nonadiabatic STT to w. Furthermore, we find that, while the DW lies in the xz plane, $\mathbf{T}^{\mathrm{nad}}_i$ has a non-vanishing y component (see Fig. G.4(a) and (b)), which is often associated with non-adiabatic STT in the literature. In addition to this, our rigorously defined $\mathbf{T}^{nad}_i$ also has in-plane components, similar to those found by Ref. [182]. We note that when computed with a static DW, *i.e.* suppressing the self-consistent LLG evolution, the out-of-plane component is the dominant contribution to the non-adiabatic STT, and it does decay quickly as shown in Fig. G.4(d), suggesting that previous approaches have neglected the proper non-equilibrium evolution and therefore missed the source of the non-vanishing β term. Additionally, the large oscillations of the $\mathbf{T}^{\mathrm{nad}}_i$ outside of the static DW region shown in Fig. G.4(c) were reported by Ref. [182] and interpreted as signatures of non-locality. However, our results reframe it as an omission of the self-consistent non-equilibrium evolution of the system.

In conclusion, we showed that a proper treatment of the non-equilibrium dynamics and a rigorous definition of adiabaticity leads to proper calculation of non-adiabatic STT, matching the experimental reports of a non-vanishing β term, even for wide DWs. We achieved this through a fully microscopic and self consistent simulation of the coupled classical-quantum system. The discrepancies with the previous theoretical approaches are due to an inadequate treatment of DW motion, producing widely applied models for STT. We can also trace the incongruencies to the expectation that electronic dynamics can be "integrated out", leaving closed expressions for STT that only depend parametrically on macroscopic characteristics of the electrons, such as polarization and current. Notice that further research in this area could resemble our main focus of study, as a full quantum treatment of the magnetization dynamics would include a one-dimensional lattice of localized quantum spins, something that combines the main themes of the whole work: one dimension, and spin chains.

Bibliography

[1] F. Reyes Osorio and B. K. Nikolić, *Wide ferromagnetic domain walls can host both adiabatic reflectionless spin transport and finite nonadiabatic spin torque: a time-dependent quantum transport picture*, 2021, arXiv:2112.08356 [cond-mat.mes-hall].

[2] F. Reyes Osorio, J. M. Scarpetta Ramirez, and K. Rodriguez Ramirez, "Computational relaxation method for modeling electrostatic systems with non-trivial geometries," European Journal of Physics **41**, 025201 (2020).

[3] K. Lange, J. Peise, B. Lücke, I. Kruse, G. Vitagliano, I. Apellaniz, M. Kleinmann, G. Tóth, and C. Klempt, "Entanglement between two spatially separated atomic modes," Science **360**, 416–418 (2018).

[4] M. H. Anderson, J. R. Ensher, M. R. Matthews, C. E. Wieman, and E. A. Cornell, "Observation of bose-einstein condensation in a dilute atomic vapor," Science **269**, 198–201 (1995).

[5] K. B. Davis, M. O. Mewes, M. R. Andrews, N. J. van Druten, D. S. Durfee, D. M. Kurn, and W. Ketterle, "Bose-einstein condensation in a gas of sodium atoms," Phys. Rev. Lett. **75**, 3969–3973 (1995).

[6] S. N. Bose, "The beginning of quantum statistics: a translation of 'Planck's law and the light quantum hypothesis'," Am. J. Phys **44**, 1056–1057 (1976).

[7] A. Einstein, "Quantentheorie des einatomigen idealen gases. zweite abhandlung," in *Albert einstein: akademie-vorträge* (John Wiley & Sons, Ltd, 2005), pp. 245–257.

[8] M. Kardar, *Statistical physics of particles* (Cambridge University Press, 2007).

[9] P. D. Lett, R. N. Watts, C. I. Westbrook, W. D. Phillips, P. L. Gould, and H. J. Metcalf, "Observation of atoms laser cooled below the doppler limit," Phys. Rev. Lett. **61**, 169–172 (1988).

[10] J. Dalibard and C. Cohen-Tannoudji, "Laser cooling below the doppler limit by polarization gradients: simple theoretical models," J. Opt. Soc. Am. B **6**, 2023–2045 (1989).

[11] S. Chu, L. Hollberg, J. E. Bjorkholm, A. Cable, and A. Ashkin, "Three-dimensional viscous confinement and cooling of atoms by resonance radiation pressure," Phys. Rev. Lett. **55**, 48–51 (1985).

[12] R. Chang, A. L. Hoendervanger, Q. Bouton, Y. Fang, T. Klafka, K. Audo, A. Aspect, C. I. Westbrook, and D. Clément, "Three-dimensional laser cooling at the doppler limit," Phys. Rev. A **90**, 063407 (2014).

[13] P. Bouyer, V. Boyer, S. G. Murdoch, G. Delannoy, Y. L. Coq, A. Aspect, and M. Lecrivain, *Rf-induced evaporative cooling and bec in a high magnetic field*, 2000, arXiv:physics/0003050 [physics.atom-ph].

[14] M. Greiner, O. Mandel, T. Esslinger, T. W. Hänsch, and I. Bloch, "Quantum phase transition from a superfluid to a mott insulator in a gas of ultracold atoms," Nature **415**, 39–44 (2002).

[15] S. Adhikari, M. Casas, A. Puente, A. Rigo, M. Fortes, M. Solís, M. de Llano, A. Valladares, and O. Rojo, "Superconductivity as a bose-einstein condensation?" Physica C **341-348**, 233–236 (2000).

[16] L. V. Hau, S. E. Harris, Z. Dutton, and C. H. Behroozi, "Light speed reduction to 17 metres per second in an ultracold atomic gas," Nature **397**, 594–598 (1999).

[17] C. Liu, Z. Dutton, C. H. Behroozi, and L. V. Hau, "Observation of coherent optical information storage in an atomic medium using halted light pulses," Nature **409**, 490–493 (2001).

[18] M. Greiner and S. Fölling, "Optical lattices," Nature **453**, 736–738 (2008).

[19] I. Bloch, "Ultracold quantum gases in optical lattices," Nature Physics **1**, 23–30 (2005).

[20] M. Takamoto, F.-L. Hong, R. Higashi, and H. Katori, "An optical lattice clock," Nature **435**, 321–324 (2005).

[21] A. Maksymov, P. Sierant, and J. Zakrzewski, "Many-body localization in a one-dimensional optical lattice with speckle disorder," Phys. Rev. B **102**, 134205 (2020).

[22] M. Lewenstein, A. Sanpera, V. Ahufinger, B. Damski, A. Sen(De), and U. Sen, "Ultracold atomic gases in optical lattices: mimicking condensed matter physics and beyond," Advances in Physics **56**, 243–379 (2007), eprint: https://doi.org/10.1080/00018730701223200.

[23] R. Grimm, M. Weidemüller, and Y. B. Ovchinnikov, "Optical dipole traps for neutral atoms," in , Vol. 42, edited by B. Bederson and H. Walther, Advances In Atomic, Molecular, and Optical Physics (Academic Press, 2000), pp. 95–170.

[24] C. Gross and I. Bloch, "Quantum simulations with ultracold atoms in optical lattices," Science **357**, 995–1001 (2017).

[25] R. P. Feynman, "Simulating physics with computers," International Journal of Theoretical Physics **21**, 467–488 (1982).

[26] T. H. Johnson, S. R. Clark, and D. Jaksch, *What is a quantum simulator?* July 2014.

[27] J. J. García-Ripoll, M. A. Martin-Delgado, and J. I. Cirac, "Implementation of spin hamiltonians in optical lattices," Physical Review Letters **93**, 10.1103/physrevlett.93.250405 (2004).

[28]G.-B. Jo, J. Guzman, C. K. Thomas, P. Hosur, A. Vishwanath, and D. M. Stamper-Kurn, “Ultracold atoms in a tunable optical kagome lattice,” Phys. Rev. Lett. **108**, 045305 (2012).

[29]C. Wei and T. A. Sedrakyan, “Optical lattice platform for the sachdev-ye-kitaev model,” Phys. Rev. A **103**, 013323 (2021).

[30]T. Giamarchi, “One-dimensional physics in the 21st century,” Comptes Rendus Physique **17**, Physique de la matière condensée au XXIe siècle: l’héritage de Jacques Friedel, 322–331 (2016).

[31]F. Franchini, “An introduction to integrable techniques for one-dimensional quantum systems,” Lecture Notes in Physics, `10.1007/978-3-319-48487-7` (2017).

[32]B. Paredes, A. Widera, V. Murg, O. Mandel, S. Fölling, I. Cirac, G. V. Shlyapnikov, T. W. Hänsch, and I. Bloch, “Tonks–girardeau gas of ultracold atoms in an optical lattice,” Nature **429**, 277–281 (2004).

[33]A. Dehkharghani, A. Volosniev, J. Lindgren, J. Rotureau, C. Forssén, D. Fedorov, A. Jensen, and N. Zinner, “Quantum magnetism in strongly interacting one-dimensional spinor bose systems,” Scientific Reports **5**, 10675 (2015).

[34]J. Dubail, J.-M. Stéphan, J. Viti, and P. Calabrese, “Conformal field theory for inhomogeneous one-dimensional quantum systems: the example of non-interacting fermi gases,” SciPost Physics **2**, `10.21468/scipostphys.2.1.002` (2017).

[35]T. Giamarchi, “Luttinger liquids,” in *Quantum physics in one dimension* (Oxford university press, Oxford, 2003), pp. 70–94.

[36]M. A. Cazalilla, “Bosonizing one-dimensional cold atomic gases,” Journal of Physics B: Atomic, Molecular and Optical Physics **37**, S1–S47 (2004).

[37]E. Miranda, “Introduction to bosonization,” Braz. J. Phys. **33**, 3–35 (2003).

[38]D. Sénéchal, *An introduction to bosonization*, 1999, arXiv:`cond-mat/9908262 [cond-mat.str-el]`.

[39]K. Rodríguez, A. Argüelles, A. K. Kolezhuk, L. Santos, and T. Vekua, “Field-induced phase transitions of repulsive spin-1 bosons in optical lattices,” Phys. Rev. Lett. **106** (2011).

[40]S. Coleman, “Quantum sine-gordon equation as the massive thirring model,” Phys. Rev. D **11**, 2088–2097 (1975).

[41]S. I. Tomonaga, “Remarks on Bloch’s Method of Sound Waves applied to Many-Fermion Problems,” Prog. Theor. Phys. **5**, 544–569 (1950).

[42]J. M. Luttinger, “An exactly soluble model of a many-fermion system,” J. Math. Phys. **4**, 1154–1162 (1963).

[43]D. C. Mattis and E. H. Lieb, “Exact solution of a many-fermion system and its associated boson field,” J. Math. Phys. **6**, 304–312 (1965).

[44]A. Gogolin, A. Nersesyan, and A. Tsvelik, “Technical aspects of bosonization,” in *Bosonization and strongly correlated systems* (Cambridge University Press, Cambridge, 2003), pp. 1–129.

[45]G. Grosso and G. P. Parravicini, *Solid state physics* (Academic Press, London, 2000), pp. 1–36.

[46]J. Sólyom, “The fermi gas model of one-dimensional conductors,” Advances in Physics **28**, 201–303 (1979), eprint: https://doi.org/10.1080/00018737900101375.

[47]M. Peskin and D. Schroeder, “Interacting fields and feynman diagrams,” in *Introduction to quantum field theory* (Perseus Books, 1995), pp. 77–130.

[48]J. Novotny and M. Schnabl, “Point-splitting regularization of composite operators and anomalies,” Fortschritte der Physik **48**, 253–302 (2000), eprint: https://onlinelibrary.wiley.com/doi/pdf/10.1002/.

[49]G. Arfken, H. Weber, and F. Harris, “Integral transforms,” in *Mathematical methods for physicists*, Seventh Edition (Academic Press, Boston, 2013), pp. 963–1046.

[50]C. L. Kane, “Lectures on bosonization,” in ().

[51]G. Giuliani and G. Vignale, “Electrons in one dimension and the luttinger liquid,” in *Quantum theory of the electron liquid* (Cambridge University Press, 2005), pp. 501–549.

[52]J. von Delft and H. Schoeller, “Bosonization for beginners - refermionization for experts,” Annalen der Physik **7**, 225–305 (1998).

[53]M. Schwartz, “Lorentz invariance and second quantization,” in *Quantum field theory and the standard model* (Cambridge university press, 2013), pp. 10–27.

[54]N. N. Bogoljubov, “On a new method in the theory of superconductivity,” Il Nuovo Cimento (1955-1965) **7**, 794–805 (1958).

[55]P. Jordan and E. Wigner, “Über das paulische äquivalenzverbot,” Zeitschrift für Physik **47**, 631–651 (1928).

[56]I. Affleck, “Field theory methods and quantum critical phenomena,” in Les Houches Summer School in Theoretical Physics: Fields, Strings, Critical Phenomena (June 1988).

[57]H. Bethe, “Zur theorie der metalle,” Zeitschrift für Physik **71**, 205–226 (1931).

[58]S. Sachdev, “The ising chain in a transverse field,” in *Quantum phase transitions*, 2nd ed. (Cambridge University Press, 2011), pp. 135–170.

[59]H. J. Schulz, “Phase diagrams and correlation exponents for quantum spin chains of arbitrary spin quantum number,” Phys. Rev. B **34**, 6372–6385 (1986).

[60]B. I. Halperin, “On the hohenberg–mermin–wagner theorem and its limitations,” Journal of Statistical Physics **175**, 521–529 (2018).

[61]S. Stringari, “Dynamics of bose-einstein condensed gases in highly deformed traps,” Phys. Rev. A **58**, 2385–2388 (1998).

[62]C. Menotti and S. Stringari, “Collective oscillations of a one-dimensional trapped bose-einstein gas,” Phys. Rev. A **66**, 043610 (2002).

[63]P. Öhberg and L. Santos, "Dynamical transition from a quasi-one-dimensional bose-einstein condensate to a tonks-girardeau gas," Phys. Rev. Lett. **89**, 240402 (2002).

[64]A. S. Campbell, D. M. Gangardt, and K. V. Kheruntsyan, "Sudden expansion of a one-dimensional bose gas from power-law traps," Phys. Rev. Lett. **114**, 125302 (2015).

[65]K. Huang and C. N. Yang, "Quantum-mechanical many-body problem with hard-sphere interaction," Phys. Rev. **105**, 767–775 (1957).

[66]M. Girardeau, "Relationship between systems of impenetrable bosons and fermions in one dimension," Journal of Mathematical Physics **1**, 516–523 (1960), eprint: `https://doi.org/10.1063/1.1703687`.

[67]G. Lang, F. Hekking, and A. Minguzzi, "Ground-state energy and excitation spectrum of the lieb-liniger model: accurate analytical results and conjectures about the exact solution," SciPost Physics **3**, `10.21468/scipostphys.3.1.003` (2017).

[68]C. K. Law, H. Pu, and N. P. Bigelow, "Quantum spins mixing in spinor bose-einstein condensates," Phys. Rev. Lett. **81**, 5257–5261 (1998).

[69]T.-L. Ho, "Spinor bose condensates in optical traps," Phys. Rev. Lett. **81**, 742–745 (1998).

[70]F. Schwabl, "Scattering theory," in *Quantum mechanics* (Springer Berlin Heidelberg, Berlin, Heidelberg, 2007), pp. 325–352.

[71]M. Lewenstein and A. Sampera, "Ultracold spinor atomic gases," in *Ultracold atoms in optical lattices* (Oxford University Press, Oxford, 2013), pp. 205–237.

[72]C. C. Bradley, C. A. Sackett, and R. G. Hulet, "Bose-einstein condensation of lithium: observation of limited condensate number," Phys. Rev. Lett. **78**, 985–989 (1997).

[73]C. Warner, A. Z. Lam, N. Bigagli, H. C. Liu, I. Stevenson, and S. Will, "Overlapping bose-einstein condensates of ^{23}na and ^{133}cs," Phys. Rev. A **104**, 033302 (2021).

[74]G. Roati, M. Zaccanti, C. D'Errico, J. Catani, M. Modugno, A. Simoni, M. Inguscio, and G. Modugno, "^{39}k bose-einstein condensate with tunable interactions," Phys. Rev. Lett. **99**, 010403 (2007).

[75]G. Modugno, G. Ferrari, G. Roati, R. J. Brecha, A. Simoni, and M. Inguscio, "Bose-einstein condensation of potassium atoms by sympathetic cooling," Science **294**, 1320–1322 (2001).

[76]Y. Lim, J. Goo, H. Kwak, and Y. Shin, "Large-area ^{87}rb bose-einstein condensate in a clipped-gaussian optical dipole trap," Phys. Rev. A **103**, 063319 (2021).

[77]D. C. Aveline, J. R. Williams, E. R. Elliott, C. Dutenhoffer, J. R. Kellogg, J. M. Kohel, N. E. Lay, K. Oudrhiri, R. F. Shotwell, N. Yu, and R. J. Thompson, "Observation of bose–einstein condensates in an earth-orbiting research lab," Nature **582**, 193–197 (2020).

[78]G. H. Fuller, "Nuclear spins and moments," Journal of Physical and Chemical Reference Data **5**, 835–1092 (1976), eprint: `https://doi.org/10.1063/1.555544`.

[79]F. Deuretzbacher, "Spinor tonks-girardeau gases and ultracold molecules," PhD thesis (Staats- und Universitätsbibliothek Hamburg Carl von Ossietzky, 2008).

[80]J. Stenger, S. Inouye, D. M. Stamper-Kurn, H.-J. Miesner, A. P. Chikkatur, and W. Ketterle, "Spin domains in ground-state bose–einstein condensates," Nature **396**, 345–348 (1998).

[81]D. M. Stamper-Kurn and M. Ueda, "Spinor bose gases: symmetries, magnetism, and quantum dynamics," Rev. Mod. Phys. **85**, 1191–1244 (2013).

[82]F. Schwabl, "Second quantization," in *Advanced quantum mechanics* (Springer Berlin Heidelberg, Berlin, Heidelberg, 2004), pp. 3–31.

[83]F. Gerbier, A. Widera, S. Fölling, O. Mandel, and I. Bloch, "Resonant control of spin dynamics in ultracold quantum gases by microwave dressing," Phys. Rev. A **73**, 041602 (2006).

[84]S. R. Leslie, J. Guzman, M. Vengalattore, J. D. Sau, M. L. Cohen, and D. M. Stamper-Kurn, "Amplification of fluctuations in a spinor bose-einstein condensate," Phys. Rev. A **79**, 043631 (2009).

[85]Y. Kawaguchi and M. Ueda, "Spinor bose–einstein condensates," Physics Reports **520**, Spinor Bose–Einstein condensates, 253–381 (2012).

[86]E. Orignac, "Quantum Magnetism, Interacting Bosons, and Low Dimensionality," Habilitation à diriger des recherches (Ecole normale supérieure de lyon - ENS LYON, Feb. 2013).

[87]F. H. L. Essler and V. E. Korepin, "Scattering matrix and excitation spectrum of the hubbard model," Phys. Rev. Lett. **72**, 908–911 (1994).

[88]D. van Oosten, P. van der Straten, and H. T. C. Stoof, "Quantum phases in an optical lattice," Phys. Rev. A **63**, 053601 (2001).

[89]M. P. A. Fisher, P. B. Weichman, G. Grinstein, and D. S. Fisher, "Boson localization and the superfluid-insulator transition," Phys. Rev. B **40**, 546–570 (1989).

[90]J. K. Freericks and H. Monien, "Phase diagram of the bose-hubbard model," Europhysics Letters (EPL) **26**, 545–550 (1994).

[91]T. D. Kühner, S. R. White, and H. Monien, "One-dimensional bose-hubbard model with nearest-neighbor interaction," Phys. Rev. B **61**, 12474–12489 (2000).

[92]T. D. Kühner and H. Monien, "Phases of the one-dimensional bose-hubbard model," Phys. Rev. B **58**, R14741–R14744 (1998).

[93]C. Trefzger, C. Menotti, B. Capogrosso-Sansone, and M. Lewenstein, "Ultracold dipolar gases in optical lattices," Journal of Physics B: Atomic, Molecular and Optical Physics **44**, 193001 (2011).

[94]G. G. Batrouni, R. T. Scalettar, and G. T. Zimanyi, "Quantum critical phenomena in one-dimensional bose systems," Phys. Rev. Lett. **65**, 1765–1768 (1990).

[95]F. Alet, G. Misguich, V. Pasquier, R. Moessner, and J. L. Jacobsen, "Unconventional continuous phase transition in a three-dimensional dimer model," Phys. Rev. Lett. **97**, 030403 (2006).

[96]R. Winkler, "Quasi-degenerate perturbation theory," in *Spin–orbit coupling effects in 2d electron and hole systems* (Springer Berlin Heidelberg, Berlin, Heidelberg, 2003), pp. 201–206.

[97]R. Shankar, in *Principles of quantum mechanics* (Springer, New York, 1994), pp. 325–352.

[98]M. S. Bulakhov, A. S. Peletminskii, S. V. Peletminskii, and Y. V. Slyusarenko, "Magnetic phases and phase diagram of spin-1 condensate with quadrupole degrees of freedom," Journal of Physics A: Mathematical and Theoretical **54**, 165001 (2021).

[99]J. Van Kranendonk, "Relations between cartesian and sperical tensor components," in *Solid hydrogen* (Springer-Verlag US, Boston, MA, 1983), pp. 325–352.

[100]A. Peletminskii, S. Peletminskii, and Y. Slyusarenko, "Su(3) symmetry in theory of a weakly interacting gas of spin-1 atoms with bose-einstein condensate," Physics Letters A **384**, 126798 (2020).

[101]A. R. Moura and A. R. Pereira, "Study of the bilinear biquadratic heisenberg model on a honeycomb lattice via schwinger bosons," Journal of Magnetism and Magnetic Materials **342**, 11–16 (2013).

[102]J. Varela, "Matsubara green's function approach to study spin-1 lattice systems," Bachelor's Thesis (Universidad del Valle, 2022).

[103]M. Rizzi, D. Rossini, G. De Chiara, S. Montangero, and R. Fazio, "Phase diagram of spin-1 bosons on one-dimensional lattices," Physical Review Letters **95**, `10.1103/physrevlett.95.240404` (2005).

[104]T. A. Tóth, A. M. Läuchli, F. Mila, and K. Penc, "Competition between two- and three-sublattice ordering for $s = 1$ spins on the square lattice," Phys. Rev. B **85**, 140403 (2012).

[105]H.-Z. Xu, S.-Y. Zhang, G.-C. Guo, and M. Gong, "Exact dimer phase with anisotropic interaction for one dimensional magnets," Scientific Reports **11**, 6462 (2021).

[106]A. Luther and D. J. Scalapino, "Critical properties of a two-dimensional planar model," Phys. Rev. B **16**, 1153–1163 (1977).

[107]M. den Nijs, "The critical exponent η of the planar model from one-dimensional quantum field theory," Physica A: Statistical Mechanics and its Applications **111**, 273–287 (1982).

[108]J. Timonen and A. Luther, "Continuum-limit correlation functions for the spin-one anisotropic heisenberg chain," Journal of Physics C: Solid State Physics **18**, 1439–1454 (1985).

[109]H. Tschirhart, E. T. S. Ong, P. Sengupta, and T. L. Schmidt, "Phase diagram of spin-1 chains with dzyaloshinskii-moriya interaction," Phys. Rev. B **100**, 195111 (2019).

[110]J. I. Latorre, E. Rico, and G. Vidal, "Ground state entanglement in quantum spin chains," Quantum Info. Comput. **4**, 48–92 (2004).

[111]G. Vidal, J. I. Latorre, E. Rico, and A. Kitaev, “Entanglement in quantum critical phenomena,” Phys. Rev. Lett. **90**, 227902 (2003).

[112]W. Ding, A. Seidel, and K. Yang, “Entanglement entropy of fermi liquids via multidimensional bosonization,” Phys. Rev. X **2**, 011012 (2012).

[113]M. T. Tan and S. Ryu, “Particle number fluctuations, rényi entropy, and symmetry-resolved entanglement entropy in a two-dimensional fermi gas from multidimensional bosonization,” Physical Review B **101**, 10.1103/physrevb.101.235169 (2020).

[114]G. C. Levine, “Entanglement entropy in a boundary impurity model,” Physical Review Letters **93**, 10.1103/physrevlett.93.266402 (2004).

[115]X. Deng, R. Citro, E. Orignac, A. Minguzzi, and L. Santos, “Bosonization and entanglement spectrum for one-dimensional polar bosons on disordered lattices,” New Journal of Physics **15**, 045023 (2013).

[116]D. Green, L. Santos, and C. Chamon, “Isolated flat bands and spin-1 conical bands in two-dimensional lattices,” Phys. Rev. B **82**, 075104 (2010).

[117]R. M. Morra, W. J. L. Buyers, R. L. Armstrong, and K. Hirakawa, “Spin dynamics and the haldane gap in the spin-1 quasi-one-dimensional antiferromagnet csnicl$_3$,” Phys. Rev. B **38**, 543–555 (1988).

[118]T. Liu, W. Li, A. Weichselbaum, J. von Delft, and G. Su, “Simplex valence-bond crystal in the spin-1 kagome heisenberg antiferromagnet,” Physical Review B **91**, 10.1103/physrevb.91.060403 (2015).

[119]J.-X. Hou and X.-C. Yu, “Thermodynamic properties of a spin-1 model with long-range interactions,” Modern Physics Letters B **32**, 1850053 (2018), eprint: https://doi.org/10.1142/S0217984918500537.

[120]S. Takei, B. I. Halperin, A. Yacoby, and Y. Tserkovnyak, “Superfluid spin transport through antiferromagnetic insulators,” Phys. Rev. B **90**, 094408 (2014).

[121]S. Takei and Y. Tserkovnyak, “Superfluid spin transport through easy-plane ferromagnetic insulators,” Phys. Rev. Lett. **112**, 227201 (2014).

[122]S. K. Kim and Y. Tserkovnyak, “Topological effects on quantum phase slips in superfluid spin transport,” Physical Review Letters **116**, 10.1103/physrevlett.116.127201 (2016).

[123]S. K. Kim and Y. Tserkovnyak, “Magnetic domain walls as hosts of spin superfluids and generators of skyrmions,” Phys. Rev. Lett. **119**, 047202 (2017).

[124]P. Upadhyaya, S. K. Kim, and Y. Tserkovnyak, “Magnetic domain wall floating on a spin superfluid,” Phys. Rev. Lett. **118**, 097201 (2017).

[125]S. Hoffman, D. Loss, and Y. Tserkovnyak, *Superfluid transport in quantum spin chains*, 2018, arXiv:1810.11470 [cond-mat.mes-hall].

[126]E. B. Sonin, "Spin and mass superfluidity in a ferromagnetic spin-1 bose-einstein condensate," Phys. Rev. B **97**, 224517 (2018).

[127]E. B. Sonin, "Superfluid spin transport in ferro- and antiferromagnets," Phys. Rev. B **99**, 104423 (2019).

[128]E. B. Sonin, "Superfluid spin transport in magnetically ordered solids," Low Temperature Physics **46**, 436–447 (2020).

[129]T. Schneider, D. Hill, A. Kákay, K. Lenz, J. Lindner, J. Fassbender, P. Upadhyaya, Y. Liu, K. Wang, Y. Tserkovnyak, I. N. Krivorotov, and I. Barsukov, "Self-stabilizing exchange-mediated spin transport," Phys. Rev. B **103**, 144412 (2021).

[130]M. Evers and U. Nowak, "Transport properties of spin superfluids: comparing easy-plane ferromagnets and antiferromagnets," Phys. Rev. B **101**, 184415 (2020).

[131]A. Bedoya-Pinto, J.-R. Ji, A. K. Pandeya, P. Gargiani, M. Valvidares, P. Sessi, J. M. Taylor, F. Radu, K. Chang, and S. S. P. Parkin, "Intrinsic 2d-xy ferromagnetism in a van der waals monolayer," Science **374**, 616–620 (2021).

[132]A. Ruff, Z. Wang, S. Zherlitsyn, J. Wosnitza, S. Krohns, H.-A. Krug von Nidda, P. Lunkenheimer, V. Tsurkan, and A. Loidl, "Multiferroic spin-superfluid and spin-supersolid phases in $MnCr_2S_4$," Physical Review B **100**, `10.1103/physrevb.100.014404` (2019).

[133]W. Yuan, Q. Zhu, T. Su, Y. Yao, W. Xing, Y. Chen, Y. Ma, X. Lin, J. Shi, R. Shindou, X. C. Xie, and W. Han, "Experimental signatures of spin superfluid ground state in canted antiferromagnet Cr_2O_3 via nonlocal spin transport," Science Advances **4**, eaat1098 (2018), eprint: `https://www.science.org/doi/pdf/10.1126/sciadv.aat1098`.

[134]J. Rubinstein, "Sine-gordon equation," Journal of Mathematical Physics **11**, 258–266 (1970), eprint: `https://doi.org/10.1063/1.1665057`.

[135]R. Rajaraman, *Solitons and instantons: an introduction to solitons and instantons in quantum field theory*, North-Holland personal library (North-Holland Publishing Company, 1982).

[136]S. Takayoshi, S. C. Furuya, and T. Giamarchi, "Topological transition between competing orders in quantum spin chains," Phys. Rev. B **98**, 184429 (2018).

[137]Q. Faure, S. Takayoshi, S. Petit, V. Simonet, S. Raymond, L.-P. Regnault, M. Boehm, J. S. White, M. Månsson, C. Rüegg, P. Lejay, B. Canals, T. Lorenz, S. C. Furuya, T. Giamarchi, and B. Grenier, "Topological quantum phase transition in the ising-like antiferromagnetic spin chain baco2v2o8," Nature Physics **14**, 716–722 (2018).

[138]J. Zhang, H. Hu, X.-J. Liu, and H. Pu, "Fermi gases with synthetic spin–orbit coupling," Annual Review of Cold Atoms and Molecules, 81–143 (2014).

[139]G. Guarnaccia and C. Noce, "Hubbard model with spin-orbit coupling: lattice gauge theory approach," Phys. Rev. B **86**, 064409 (2012).

[140] H. Zhai, "Spin-orbit coupled quantum gases," International Journal of Modern Physics B **26**, 1230001 (2012).

[141] J. Ruhman, E. Berg, and E. Altman, "Topological states in a one-dimensional fermi gas with attractive interaction," Physical Review Letters **114**, `10.1103/physrevlett.114.100401` (2015).

[142] K. Björnson, S. S. Pershoguba, A. V. Balatsky, and A. M. Black-Schaffer, "Spin-polarized edge currents and majorana fermions in one- and two-dimensional topological superconductors," Phys. Rev. B **92**, 214501 (2015).

[143] K. Björnson and A. M. Black-Schaffer, "Vortex states and majorana fermions in spin-orbit coupled semiconductor-superconductor hybrid structures," Phys. Rev. B **88**, 024501 (2013).

[144] V. Kozii, J. Ruhman, L. Fu, and L. Radzihovsky, "Ferromagnetic transition in a one-dimensional spin-orbit-coupled metal and its mapping to a critical point in smectic liquid crystals," Physical Review B **96**, `10.1103/physrevb.96.094419` (2017).

[145] A. Iucci, "Correlation functions for one-dimensional interacting fermions with spin-orbit coupling," Physical Review B **68**, `10.1103/physrevb.68.075107` (2003).

[146] M. Rizzi, M. Polini, M. A. Cazalilla, M. R. Bakhtiari, M. P. Tosi, and R. Fazio, "Fulde-ferrell-larkin-ovchinnikov pairing in one-dimensional optical lattices," Physical Review B **77**, `10.1103/physrevb.77.245105` (2008).

[147] H. Shimahara, "Phase fluctuations and kosterlitz-thouless transition in two-dimensional fulde-ferrell-larkin-ovchinnikov superconductors," Journal of the Physical Society of Japan **67**, 1872–1875 (1998), eprint: `https://doi.org/10.1143/JPSJ.67.1872`.

[148] J. Lee and X. Guan, "Asymptotic correlation functions and fflo signature for the one-dimensional attractive spin-1/2 fermi gas," Nuclear Physics B **853**, 125–138 (2011).

[149] E. Witten, "Non-abelian bosonization in two dimensions," Communications in Mathematical Physics **92**, 455–472 (1984).

[150] I. Affleck, "Exact critical exponents for quantum spin chains, non-linear σ-models at $\theta = \pi$ and the quantum hall effect," Nuclear Physics B **265**, 409–447 (1986).

[151] A. J. A. James, R. M. Konik, P. Lecheminant, N. J. Robinson, and A. M. Tsvelik, "Non-perturbative methodologies for low-dimensional strongly-correlated systems: from non-abelian bosonization to truncated spectrum methods," Reports on Progress in Physics **81**, 046002 (2018).

[152] Y.-T. Huang and D.-H. Lee, "Non-abelian bosonization in two and three spatial dimensions and applications," Nuclear Physics B **972**, 115565 (2021).

[153] T. Inami and S. Odake, *Continuum limit of spin-1 chain*, 1992, arXiv:`hep-th/9209019 [hep-th]`.

[154] D. Allen and D. Sénéchal, "Spin-1 ladder: a bosonization study," Phys. Rev. B **61**, 12134–12142 (2000).

[155]E. J. König, P. Coleman, and A. M. Tsvelik, "Spin magnetometry as a probe of stripe superconductivity in twisted bilayer graphene," Phys. Rev. B **102**, 104514 (2020).

[156]A. Chew, Y. Wang, B. A. Bernevig, and Z.-D. Song, *Higher-order topological superconductivity in twisted bilayer graphene*, 2021, arXiv:2108.05373 [cond-mat.supr-con].

[157]G. Gorohovsky, R. G. Pereira, and E. Sela, "Chiral spin liquids in arrays of spin chains," Phys. Rev. B **91**, 245139 (2015).

[158]P.-H. Huang, J.-H. Chen, P. R. S. Gomes, T. Neupert, C. Chamon, and C. Mudry, "Non-abelian topological spin liquids from arrays of quantum wires or spin chains," Phys. Rev. B **93**, 205123 (2016).

[159]R. Wang, Y. Wang, Y. X. Zhao, and B. Wang, *Kondo signatures in dirac spin liquids: non-abelian bosonization after chern-simons fermionization*, 2020, arXiv:2010.05022 [cond-mat.str-el].

[160]A. Auerbach and D. P. Arovas, *Schwinger bosons approaches to quantum antiferromagnetism*, 2008, arXiv:0809.4836 [cond-mat.str-el].

[161]P. Coleman, C. Pépin, and A. M. Tsvelik, "Supersymmetric spin operators," Phys. Rev. B **62**, 3852–3868 (2000).

[162]D. P. Arovas and A. Auerbach, "Functional integral theories of low-dimensional quantum heisenberg models," Phys. Rev. B **38**, 316–332 (1988).

[163]A. A. Abrikosov, "Electron scattering on magnetic impurities in metals and anomalous resistivity effects," Physics Physique Fizika **2**, 5–20 (1965).

[164]J. J. Sakurai and J. Napolitano, "Theory of angular momentum," in *Modern quantum mechanics*, 2nd ed. (Cambridge University Press, 2017), pp. 157–261.

[165]J. Schwichtenberg, "Quantum mechanics," in *Physiscs from symmetry* (Springer Switzerland, Birkhauser, Cham, 2018), pp. 109–186.

[166]N. Jeevanjee, "Groups, lie groups, and lie algebras," in *An introduction to tensors and group theory for physicists* (Springer Switzerland, Birkhauser, Cham, 2015), pp. 109–186.

[167]W. H. Klink and S. Wickramasekara, "A simple method for calculating clebsch–gordan coefficients," Eur. J. Phys. **31**, 1021–1030 (2010).

[168]G. Tatara, H. Kohno, and J. Shibata, "Microscopic approach to current-driven domain wall dynamics," Physics Reports **468**, 213–301 (2008).

[169]G. Tatara, "Effective gauge field theory of spintronics," Physica E: Low-dimensional Systems and Nanostructures **106**, 208–238 (2019).

[170]O. Boulle, J. Kimling, P. Warnicke, M. Kläui, U. Rüdiger, G. Malinowski, H. J. M. Swagten, B. Koopmans, C. Ulysse, and G. Faini, "Nonadiabatic spin transfer torque in high anisotropy magnetic nanowires with narrow domain walls," Phys. Rev. Lett. **101**, 216601 (2008).

[171] C. Burrowes, A. P. Mihai, D. Ravelosona, J.-V. Kim, C. Chappert, L. Vila, A. Marty, Y. Samson, F. Garcia-Sanchez, L. D. Buda-Prejbeanu, I. Tudosa, E. E. Fullerton, and J.-P. Attané, "Non-adiabatic spin-torques in narrow magnetic domain walls," Nature Physics **6**, 17–21 (2010).

[172] C. A. Akosa, P. B. Ndiaye, and A. Manchon, "Intrinsic nonadiabatic topological torque in magnetic skyrmions and vortices," Phys. Rev. B **95**, 054434 (2017).

[173] L. Heyne, J. Rhensius, D. Ilgaz, A. Bisig, U. Rüdiger, M. Kläui, L. Joly, F. Nolting, L. J. Heyderman, J. U. Thiele, and F. Kronast, "Direct determination of large spin-torque nonadiabaticity in vortex core dynamics," Phys. Rev. Lett. **105**, 187203 (2010).

[174] S. D. Pollard, L. Huang, K. S. Buchanan, D. A. Arena, and Y. Zhu, "Direct dynamic imaging of non-adiabatic spin torque effects," Nature Communications **3**, 1028 (2012).

[175] K.-J. Kim, Y. Yoshimura, and T. Ono, "Current-driven magnetic domain wall motion and its real-time detection," Japanese Journal of Applied Physics **56**, 0802A4 (2017).

[176] S. Parkin and S.-H. Yang, "Memory on the racetrack," Nature Nanotechnology **10**, 195–198 (2015).

[177] D. A. Allwood, G. Xiong, M. D. Cooke, C. C. Faulkner, D. Atkinson, N. Vernier, and R. P. Cowburn, "Submicrometer ferromagnetic not gate and shift register," Science **296**, 2003–2006 (2002), eprint: `https://www.science.org/doi/pdf/10.1126/science.1070595`.

[178] J. Grollier, D. Querlioz, and M. D. Stiles, "Spintronic nanodevices for bioinspired computing," Proceedings of the IEEE **104**, 2024–2039 (2016).

[179] P. M. Levy and S. Zhang, "Resistivity due to domain wall scattering," Phys. Rev. Lett. **79**, 5110–5113 (1997).

[180] S. Zhang and Z. Li, "Roles of nonequilibrium conduction electrons on the magnetization dynamics of ferromagnets," Phys. Rev. Lett. **93**, 127204 (2004).

[181] S. E. Barnes and S. Maekawa, "Current-spin coupling for ferromagnetic domain walls in fine wires," Phys. Rev. Lett. **95**, 107204 (2005).

[182] J. Xiao, A. Zangwill, and M. D. Stiles, "Spin-transfer torque for continuously variable magnetization," Phys. Rev. B **73**, 054428 (2006).

[183] X. Waintal and M. Viret, "Current-induced distortion of a magnetic domain wall," Europhysics Letters (EPL) **65**, 427–433 (2004).

[184] R. L. Cooper and E. A. Uehling, "Ferromagnetic resonance and spin diffusion in supermalloy," Phys. Rev. **164**, 662–668 (1967).

[185] A. Thiaville, Y. Nakatani, J. Miltat, and Y. Suzuki, "Micromagnetic understanding of current-driven domain wall motion in patterned nanowires," Europhysics Letters (EPL) **69**, 990–996 (2005).

[186] R. A. Duine, A. S. Núñez, J. Sinova, and A. H. MacDonald, "Functional keldysh theory of spin torques," Phys. Rev. B **75**, 214420 (2007).

[187]J.-i. Kishine and A. S. Ovchinnikov, "Adiabatic and nonadiabatic spin-transfer torques in the current-driven magnetic domain wall motion," Phys. Rev. B **81**, 134405 (2010).

[188]R. Mondal, M. Berritta, and P. M. Oppeneer, "Unified theory of magnetization dynamics with relativistic and nonrelativistic spin torques," Phys. Rev. B **98**, 214429 (2018).

[189]R. Cheng and Q. Niu, "Microscopic derivation of spin-transfer torque in ferromagnets," Phys. Rev. B **88**, 024422 (2013).

[190]H. Kohno, G. Tatara, and J. Shibata, "Microscopic calculation of spin torques in disordered ferromagnets," Journal of the Physical Society of Japan **75**, 113706 (2006), eprint: `https://doi.org/10.1143/JPSJ.75.113706`.

[191]G. Tatara and P. Entel, "Calculation of current-induced torque from spin continuity equation," Phys. Rev. B **78**, 064429 (2008).

[192]G. Tatara and H. Kohno, "Theory of current-driven domain wall motion: spin transfer versus momentum transfer," Phys. Rev. Lett. **92**, 086601 (2004).

[193]R. F. L. Evans, W. J. Fan, P. Chureemart, T. A. Ostler, M. O. A. Ellis, and R. W. Chantrell, "Atomistic spin model simulations of magnetic nanomaterials," Journal of Physics: Condensed Matter **26**, 103202 (2014).

[194]T. Weindler, H. G. Bauer, R. Islinger, B. Boehm, J.-Y. Chauleau, and C. H. Back, "Magnetic damping: domain wall dynamics versus local ferromagnetic resonance," Phys. Rev. Lett. **113**, 237204 (2014).

[195]P. Mondal, A. Suresh, and B. K. Nikolić, "When can localized spins interacting with conduction electrons in ferro- or antiferromagnets be described classically via the landau-lifshitz equation: transition from quantum many-body entangled to quantum-classical nonequilibrium states," Phys. Rev. B **104**, 214401 (2021).

[196]U. Bajpai and B. K. Nikolić, "Spintronics meets nonadiabatic molecular dynamics: geometric spin torque and damping on dynamical classical magnetic texture due to an electronic open quantum system," Phys. Rev. Lett. **125**, 187202 (2020).

[197]N. Bode, S. V. Kusminskiy, R. Egger, and F. von Oppen, "Scattering theory of current-induced forces in mesoscopic systems," Phys. Rev. Lett. **107**, 036804 (2011).

[198]M. Thomas, T. Karzig, S. V. Kusminskiy, G. Zaránd, and F. von Oppen, "Scattering theory of adiabatic reaction forces due to out-of-equilibrium quantum environments," Phys. Rev. B **86**, 195419 (2012).

[199]G. Stefanucci and R. van Leeuwen, *Nonequilibrium many-body theory of quantum systems: a modern introduction* (Cambridge University Press, 2013).

[200]M. D. Petrović, B. S. Popescu, U. Bajpai, P. Plecháč, and B. K. Nikolić, "Spin and charge pumping by a steady or pulse-current-driven magnetic domain wall: a self-consistent multiscale time-dependent quantum-classical hybrid approach," Phys. Rev. Applied **10**, 054038 (2018).

[201] L. Berger, "Low-field magnetoresistance and domain drag in ferromagnets," Journal of Applied Physics **49**, 2156–2161 (1978), eprint: `https://doi.org/10.1063/1.324716`.

[202] Y. Aharonov and A. Stern, "Origin of the geometric forces accompanying berry's geometric potentials," Phys. Rev. Lett. **69**, 3593–3597 (1992).

[203] C. Stahl and M. Potthoff, "Anomalous spin precession under a geometrical torque," Phys. Rev. Lett. **119**, 227203 (2017).

[204] K. Capelle, G. Vignale, and B. L. Györffy, "Spin currents and spin dynamics in time-dependent density-functional theory," Phys. Rev. Lett. **87**, 206403 (2001).